Tunable Superlattice Amplifiers Based on Dynamics of Miniband Electrons in Electric and Magnetic Fields

TIMO HYART

Department of Physics
University of Oulu
Finland

Academic Dissertation to be presented with the assent of the Faculty of Science, University of Oulu, for public discussion in the Auditorium GO 101, on December 11th, 2009, at 12 o'clock noon.

REPORT SERIES IN PHYSICAL SCIENCES Report No. 62
OULU 2009 • UNIVERSITY OF OULU

Opponent
Prof. Andreas Wacker, Department of Physics,
University of Lund, Sweden

Reviewers
Prof. Antti-Pekka Jauho, Department of Micro- and Nanotechnology,
Technical University of Denmark, Denmark

Prof. Mark Fromhold, School of Physics and Astronomy,
University of Nottingham, United Kingdom

Custos
Prof. Erkki Thuneberg, Department of Physics,
University of Oulu, Finland

ISBN 978-951-42-6071-1
ISBN 978-951-42-6072-8 (PDF)
ISSN 0356-1852
OULU UNIVERSITY PRESS
Oulu 2009

Abstract

The most important paradigms in quantum mechanics are probably a two-level system, a harmonic oscillator and an ideal (infinite) periodic potential. The first two provide a starting point for understanding the phenomena in systems where the spectrum of energy levels is discrete, whereas the last one results in continuous energy bands. Here an attempt is made to study the dynamics of the electrons in a narrow miniband of a semiconductor superlattice under electric and magnetic fields.

Semiconductor superlattices are artificial periodic structures, where certain properties like the period and the energy band structure, defined in standard crystals by the nature, can be controlled. Electron dynamics in a single superlattice miniband is interesting both from the viewpoint of fundamental and applied physics. From the fundamental perspective superlattices serve as a model system for a wealth of phenomena resulting from the wave-nature of charge carriers. On the other hand, superlattices can potentially be utilized in oscillators and amplifiers operating at THz frequencies. They can, in principle, provide a reasonable THz Bloch gain under dc bias and parametric amplification in the presence of ac pump field. Because of numerous scientific and technological applications in different areas of science and technology, including astrophysics and atmospheric science, biological and medical sciences, and detection of concealed weapons and biosecurity, a construction of compact tunable THz amplifiers and generators that can operate at room temperature is an important - but so far unrealized - task.

This thesis focuses on the influence of electric and magnetic fields on small-signal absorption and gain in semiconductor superlattices in the presence of dissipation (scattering). We present several new ideas how the effects arising due to the wave nature of the electrons can be utilized in an operation of THz oscillators and amplifiers. In Papers I-V, we discuss the properties of superlattice sub-THz and THz parametric amplifiers, whereas the Papers VI-IX are devoted to the problem of domain instability in the realization of cw THz Bloch oscillator. In Paper IX we also establish a feasibility of new type of superlattice THz amplifier based on nonlinear cyclotron-like oscillations of the miniband electrons. The ideas presented in the Papers I-IX are supplemented here with a detailed discussion of the physical origin of the effects and more rigorous mathematical derivations of the main equations.

Key words: Semiconductor superlattices, Terahertz radiation, High-frequency effects, Semiclassical theories and applications, High-field and nonlinear effects

Acknowledgments

This work was carried out in the Theoretical Physics Division, Department of Physics, University of Oulu. I thank Prof. Erkki Thuneberg for introducing the topic of my thesis and for arranging the facilities for this work. Erkki's help in arranging the funding for this research is also appreciated. The financial support from Emil Aaltonen Foundation, Vilho, Yrjö and Kalle Väisälä Foundation, Magnus Ehrnrooth Foundation, University of Oulu, Yliopiston Apteekki Foundation and Oulu University Scholarship Foundation are gratefully acknowledged. I also had an opportunity to spend several months in Physics Department, Loughborough University, United Kingdom. I thank Prof. Feo Kusmartsev for hospitality during these visits, constant encouragement of this activity and the possibilities to participate in interesting conferences organized by the AQDJJ program of ESF. The considerations of magnetic-field-induced effects was partially stimulated by the interesting discussions with Feo.

I thank my supervisor Dr Kirill Alekseev for the guidance during the different stages of this work. Kirill has attracted my attention to a wide variety of different phenomena taking place in superlattices; It still surprises me that such a simple semiclassical approach can be used to describe so many interesting and still mostly unexplored regimes of electron motion. The debates and conversations with Kirill have aroused new questions and helped me to see the existing problems from different perspectives. Kirill's impressive knowledge of the physics of superlattices and Josephson junctions has provided new insights and connections to the existing literature. Moreover, Kirill's experience has been helpful in improving our papers to make them clearly organized, interesting for a broader community and accessible for non-specialists. All the results presented in this thesis are influenced by the discussions with Kirill.

I have been supported by several outstanding scientists during the preparation of the publications. I have been especially lucky to cooperate with Jussi Mattas. The early numerical simulations of Boltzmann equation and drift-diffusion model, performed by Jussi, have been the backbone in our considerations of the electric stability of superlattice amplifiers. Moreover, Jussi's help in the numerical simulations of the Boltzmann equation has helped us to find the temperature dependencies of the gain and absorption

in the presence of magnetic field. The collaboration of Aleksey Shorokhov, Natalia Alexeeva, Ahti Leppänen, Sergey Denisov, Natalia Demarina and Maxim Gorkunov is also appreciated. I thank Alvydas Lisauskas for discussions related to different approaches in realization of Bloch oscillator; Amalia Patane, Oleg Makarovsky and Gernot Fasching for useful discussions on the experimental feasibilities of the Bloch oscillator with modulated bias; Stephan Winnerl for discussions related to ac driven Bloch gain and Alexander Balanov for discussions related to magnetic field activity and electric stability of superlattice oscillators. I am also grateful to the reviewers, Prof. Antti-Pekka Jauho and Prof. Mark Fromhold, for careful reading of the manuscript and valuable comments.

I thank all the scientists at the theoretical physics department for creating such a carefree atmosphere and an excellent environment full of activities. I have learned a lot from Erkki Thuneberg, Kirill Alekseev, Mikko Saarela, Pekka Pietiläinen and Kari Rummukainen. On the other hand, the recreation days, conference trips and sport activities with Mikko Saarela, Jani Tuorila, Juha Leppäkangas, Timo Virtanen, Jussi Mattas, Heikki Laitala, Jukka Isohätälä, Lauri Kurki, Heikki Nykänen, Tauno Taipaleenmäki and Petri Mutka are unforgettable.

Finally, I want to thank my parents Tuula and Raimo for their support and my grandmother Anja for her wisdom. Very special thanks to my beloved Anna-Kaisa for always asking the most inspiring and intriguing questions.

Oulu, November 2009 Timo Hyart

LIST OF ORIGINAL PAPERS

The present thesis contains an introductory part and the following papers which will be referred in the text by their Roman numbers.

I. K. N. Alekseev, M. V. Gorkunov, N. V. Demarina, T. Hyart, N. V. Alexeeva and A. V. Shorokhov, *Suppressed absolute negative conductance and generation of high-frequency radiation in semiconductor superlattices*, Europhys. Lett., **73**, 934 (2006); Erratum, Europhys. Lett., **74**, 567 (2006).

II. T. Hyart, N. V. Alexeeva, A. Leppänen and K. N. Alekseev, *Terahertz parametric gain in semiconductor superlattices in the absence of electric domains*, Appl. Phys. Lett. **89**, 132105 (2006).

III. T. Hyart, A. V. Shorokhov and K. N. Alekseev, *Theory of Parametric Amplification in Superlattices*, Phys. Rev. Lett. **98**, 220404 (2007).

IV. T. Hyart, A. V. Shorokhov and K. N. Alekseev, *Terahertz Parametric Gain in Semiconductor Superlattices*, Conference Digest of the 2007 Joint 32nd International Conference on Infrared and Millimeter Waves and 15th International Conference on Terahertz Electronics, Vol. **1**, 472 (2007).

V. T. Hyart and K. N. Alekseev, *Nondegenerate parametric amplification in superlattices and the limits of strong and weak dissipation*, Int. J. Mod. Phys. B **23**, 4403 (2009).

VI. T. Hyart, K. N. Alekseev and E. V. Thuneberg, *Bloch gain in dc-ac-driven semiconductor superlattices in the absence of electric domains*, Phys. Rev. B **77**, 165330 (2008).

VII. T. Hyart, N. V. Alexeeva, J. Mattas and K. N. Alekseev, *Terahertz Bloch Oscillator with a Modulated Bias*, Phys. Rev. Lett. **102**, 140405 (2009).

VIII. T. Hyart, N. V. Alexeeva, J. Mattas and K. N. Alekseev, *Possible THz Bloch gain in dc-ac-driven superlattices*, Microelectronics Journal **40**, 719 (2009).

IX. T. Hyart, J. Mattas and K. N. Alekseev, *Model of the Influence of an External Magnetic Field on the Gain of Terahertz Radiation from Semiconductor Superlattices*, Phys. Rev. Lett. **103**, 117401 (2009).

The author had only a minor role in the original article I, but the Erratum is based on his results. The author has had a central role in all other articles presented in this thesis. He has developed the theory and computational tools around the phenomena, done all the simulations, and written the first versions of articles IV, V, VI, VII, VIII and IX.

Contents

Abstract i

Acknowledgments ii

List of original papers v

Contents vii

1 Introduction 1

2 Basics of superlattices 9
- 2.1 Energy band structure . . . 9
- 2.2 Semiclassical equations of motion . . . 13
- 2.3 Electron dynamics in the presence of scattering . . . 17
  - 2.3.1 Heuristic justification of Eqs. (2.36)-(2.40) . . . 20
  - 2.3.2 Mathematical proof of Eqs. (2.36)-(2.40) . . . 21
  - 2.3.3 Static fields and Esaki-Tsu approach . . . 24
- 2.4 Esaki-Tsu characteristic and Tucker relations . . . 25
  - 2.4.1 Esaki-Tsu characteristic . . . 25
  - 2.4.2 Tucker relations . . . 26
  - 2.4.3 Quasistatic limit . . . 29
  - 2.4.4 Photon-assisted transport . . . 29
  - 2.4.5 Coherent control of photon-assisted transport . . . 31
  - 2.4.6 Balance equations and effect of elastic scattering . . . 32
- 2.5 Domain instability in conditions of NDC . . . 33
  - 2.5.1 Limited space charge accumulation mode . . . 35
  - 2.5.2 Kroemer's criterion of electric stability . . . 36
- 2.6 The limits of miniband transport model . . . 37

3 New approaches to Bloch oscillator 39
- 3.1 Bloch gain . . . 39
- 3.2 Bloch gain in dc-ac driven superlattice . . . 43
- 3.3 Bloch gain in ac driven superlattice . . . 45
- 3.4 Bloch oscillator with modulated bias . . . 47

4 Parametric amplifiers and oscillators **51**
4.1 General equations 51
4.2 Generation of harmonics 52
4.3 Generation of half-harmonics 53
4.4 Generation of other commensurate frequencies? 54
4.5 Quasistatic limit 54
4.6 Manley-Rowe relations 56
4.7 Earlier works and main results 57
4.8 Comparison to experiments 60

5 Influence of magnetic field **61**
5.1 Cyclotron gain and Bloch gain in crossed fields 61
5.1.1 Ballistic electron dynamics in crossed fields 61
5.1.2 Dissipative electron dynamics in crossed fields 66
5.2 Stark-cyclotron resonances & stable THz gain 72

6 Conclusions and perspectives **77**

Bibliography **79**

Original papers **90**

Chapter 1

Introduction

The sub-terahertz (0.1-1 THz) and terahertz spectral ranges (1-10 THz) of electromagnetic radiation are known as a "THz gap", because historically they have been characterized by a lack of convenient radiation sources, amplifiers and detectors [1]. The construction of compact tunable solid-state sources of coherent THz radiation has been challenging, in large part because these frequency ranges span the transition between traditional electronics and photonics: Below 0.1 THz the devices are typically based on electron transport (transistors, Gunn oscillators, Schottky diode multipliers), whereas above 10 THz solid-state lasers and other devices based on optical transitions are common. THz devices are currently in the core of scientific research due to their numerous applications in different areas of science and technology, including astrophysics and atmospheric science, biological and medical sciences, wideband communications, detection of concealed weapons and biosecurity, and ultrafast spectroscopy [1, 2]. In this work we have theoretically studied the possibilities of turning the rich science of semiconductor superlattices into THz technology.

Semiconductor superlattice (SL) is an artificial periodic heterostructure of repeating quantum wells and barriers. As proposed by L. Esaki and R. Tsu almost four decades ago [3, 4], SLs can be constructed by depositing thin layers of two different semiconductor materials alternately to each other. Here it is essential that the constituent materials have similar lattice constants but the conduction band edges are not aligned, so that essentially an artificial crystal with *controllable SL potential* along the growth axis is formed. The technological progress in growth techniques has made it possible to define the thicknesses of the layers with an interfacial smoothness on the atomic scale, whereas the height of the potential barriers is determined by the constituent materials. The pioneering works of L. Esaki, R. Tsu and L. L. Chang with SLs [3, 5] and double barrier structures [6] attracted a great interest to semiconductor quantum heterostructures and opened up a frontier field in semiconductor research [4, 7]. Because these artificial materials can

be designed with prescribed electronic and photonic properties, they provide a great technological potential for optoelectronic applications. One of the technological triumphs obtained so far are quantum cascade lasers (QCLs) that can emit in the mid- to far-infrared portion of the electromagnetic spectrum. The laser emission in QCLs is achieved due to a population inversion between quantized energy levels in a multiple quantum well structure, an idea first proposed by R. F. Kazarinov and R. A. Suris 1971 [8] and experimentally realized by J. Faist *et al.* 1994 [9]. Recently QCLs operating at THz and even sub-THz frequencies have been demonstrated [2, 10], but it seems difficult to establish a population inversion in these devices at room temperature [2]. This difficulty can be easily appreciated because in this case the thermal energy is larger than the energy level separation.

Some of the implications of the SL potential on the electron dynamics and transport are well-known from the theory of conventional periodic crystals, which have been a subject of interest since the early years of quantum mechanics [11, 12]. The electronic Bloch states occupy certain allowed energy intervals, energy bands, which are separated by forbidden intervals, bandgaps, in the energy spectrum. The Bloch states are characterized by band index n and quasimomentum $\hbar\mathbf{k}$, where the Bloch wavevector $\mathbf{k}$ is restricted to the first Brillouin zone. If an electric field $\mathbf{E}$ is applied, the Bloch states are no longer eigenstates of the Hamiltonian, but the quasimomentum along the electric field becomes time-dependent according to the Bloch acceleration theorem

$$\hbar\frac{d\mathbf{k}}{dt} = e\mathbf{E},$$

where $e < 0$ is the electron charge. If the electric field is large enough, the carriers reach higher parts of the bands before they are scattered, so that the quantum mechanical wave nature of electrons becomes essential and the electrons do not behave like free carriers anymore. In fact, if interband tunneling and scattering processes can be neglected the electron subjected to a static electric field E_{dc} returns repeatedly to its original state in the quasimomentum space. This oscillatory motion in quasimomentum and energy is accompanied by a periodic motion in real space, the so-called Bloch oscillations [12]. The frequency of these oscillations $\omega_B = eE_{dc}d/\hbar$ is proportional to the electric field E_{dc} and lattice period d. However, for typical materials and electric fields ω_B is much smaller than the scattering rate. Therefore, Bloch oscillations have never been observed in standard crystals, but instead the electron motion there is characterized by Drude drift transport [13]. This restriction can be easily circumvented in SLs, where the SL period d can be orders of magnitude larger than the lattice constants of the host crystals. Moreover, the energy band widths in SLs are typically much smaller than in bulk semiconductors reducing the scattering probability with e.g. optical phonons. Bloch oscillations in SLs with photoexcited carriers have been

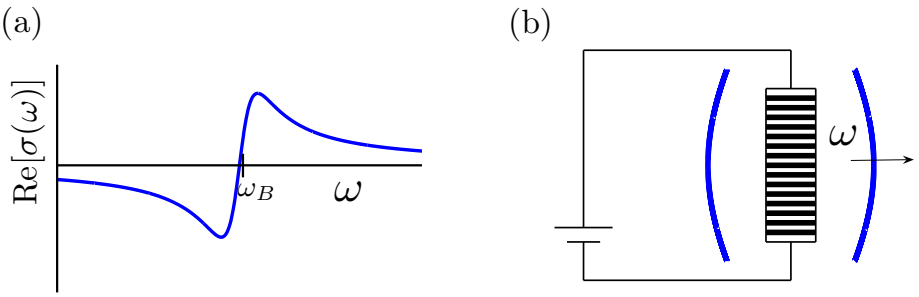

Figure 1.1: (a) Dispersive gain profile of a Bloch oscillator. Negative real part of the dynamical conductivity, $\mathrm{Re}[\sigma(\omega)] < 0$, corresponds to gain. (b) Simplified picture showing the principle of the Bloch oscillator. Superlattice is connected to a static voltage and it generates radiation by stimulated emissions at frequency ω determined by the resonator.

observed using a number of different methods [14]: The first experiments used four-wave mixing technique [15] and later for example THz emission spectroscopy [16] and photorefractive experiments [17] have been employed. Importantly, Bloch oscillations exist also at room temperature [18].

The possibility of inversionless lasing in dc biased SL in the presence of dissipation was recognized already in 1972, when Ktitorov *et al.* calculated the response of the miniband electrons to a weak ac field by using a semiclassical theory [19]. The important prediction was a so-called Bloch gain profile. Namely, if electrons perform relatively many Bloch oscillations between the scattering events, the gain as a function of ac field frequency ω is shaped as a familiar dispersion curve [Fig. 1.1 (a)], where a crossover from gain to loss occurs approximately at the Bloch frequency. This theoretical work led to a suggestion of a Bloch oscillator [20]: a device where a dc biased SL is connected to a resonator whose resonance frequency is the desired alternating field frequency ω [Fig. 1.1 (b)]. The Bloch oscillator has become an old dream of the semiconductor community, because the Bloch frequency in SLs typically belongs to the THz frequency range and is tunable simply by changing the dc bias. Moreover, the estimates predict a reasonable THz gain also at room temperature at frequencies somewhat smaller than the Bloch frequency. The realization of THz Bloch oscillator would be a major scientific and technological breakthrough: It would be the first semiconductor THz source, which can operate at room temperature.

Despite the optimistic theoretical predictions, the Bloch oscillator operating in a cw mode has still not been realized almost four decades after the first proposition. The Bloch oscillations lead to localization of the electrons, which in the stationary transport regime manifests itself as a decrease of drift

velocity with an increase in electric field [3]. If the distribution of electrons is approximately homogeneous, the local electric field-drift velocity relation is connected to the global voltage-current (VI) characteristic of the device with simple geometrical factors, so that the decreasing drift velocity corresponds to a negative differential conductivity (NDC). The considerations of bulk materials with NDC can be traced back [21] to the works of H. Kroemer, W. Shockley, B. K. Ridley, T. B. Watkins and C. Hilsum [22, 23, 24, 25, 26] in 1950s and 1960s. It was realized that the NDC state in bulk materials is accompanied by an inherent instability of the homogeneous electric field, which results in formation of high-field domains inside a long sample [23, 26]. The same electric instability exists also in SLs in spite of the very different origin of the NDC [27] (for reviews of the non-linear domain dynamics, see [28, 29, 30]). From the perspective of the Bloch oscillator, these electric domains are a nuisance. The homogeneous electric field is a key ingredient in the Bloch gain, and therefore the electric domains are believed to be the main reason for the failure so far to realize a true cw Bloch oscillator. One possibility to suppress the formation of the electric domains might be to use a super-superlattice structure consisting of a stack of short SLs. Recently an increase in THz transmission with applied dc bias was observed in this system [31], but the effect is still too weak to be considered as a direct experimental evidence of net Bloch gain.

On the other hand, it is well-known from the theory of Gunn diodes that these space-charge inhomogeneities can be utilized in generation and amplification of radiation near the harmonics of the transit frequency $f_t = v/L$ either due to propagating dipole domains in Gunn oscillators [32] or due to growing space-charge waves in Thim amplifiers [33]. Here v is the propagation speed of the domains and L is the length of the sample. Both these effects have been observed also in SLs. The negative dynamical conductivity in SLs in the vicinity of the transit frequency, typical for Thim amplifiers, was reported already in Ref. [34] and later reflection gain up to 65 GHz has been obtained [35]. The first experimental observation of traveling electric domains was reported in photoexcited SLs [36]. Thereafter, Gunn oscillations have been observed in SLs up to a frequency 147 GHz [37]. Recently, it was shown theoretically that the magnetic field can induce multiple propagating charge domains in SLs, which result in current oscillations in the sub-THz frequency regime [38]. The influence of ac field on Gunn oscillations has been investigated both experimentally and theoretically [39, 40, 41].

A very active research directions in the generation of high-frequency radiation in SLs are also the frequency multipliers and parametric amplifiers. The basic idea in such kind of devices is that strong ac field pumps energy into the system, which is then converted to radiation at harmonics or half-harmonics of the pump frequency due to the nonlinearities of the SL. Suitable nonlinearities exist both in homogeneous SLs and due to the dynamics of the

electric domains. So far the latter has received more experimental attention. Low-efficiency frequency multiplication suitable for laboratory spectroscopy has been obtained even at THz frequencies [42], whereas significant enhancement of the generated power at certain threshold amplitude of the pump field, attributed to the onset of the parametric amplification, has been observed at the sub-THz frequency range [43].

In this work we consider the generation and amplification of THz radiation in SLs in the absence of electric domains. The topic is covered both from the applied and fundamental perspectives: Our novel ideas and approaches are based on the different phenomena resulting from the wave-nature of charge carriers, such as Bloch oscillations, photon-assisted transport [44] and parametric resonance in dc-ac-driven SLs, coherent Hall effect in crossed electric and magnetic fields [45] and Stark-cyclotron resonances in tilted magnetic field [46, 47, 48]. We will review the physics behind these phenomena and show that they can be utilized to obtain stable small-signal gain in SLs. We propose several new types of THz amplifiers and oscillators based on: (i) Parametric gain, (ii) Bloch gain and (iii) cyclotron gain.

(i) The parametric amplifiers and oscillators are considered in Papers I-V. The theoretical feasibility of significant phase-sensitive parametric gain in dc-ac-driven SLs at harmonics and half-harmonics of the pump frequency was established in Papers I-III. In Paper IV we particularly addressed the applied aspect of this suggestion by showing that parametric interaction enables both up- and down-conversion to sub-THz and THz frequency ranges using available sources of low- and high-frequency radiation. The origin of the parametric resonance in the limits of weak and strong dissipation was discussed in Paper V. We found that in the limit of weak dissipation the oscillations of the effective mass of the electrons plays an important role in the parametric amplification, whereas in the limit of strong dissipation the effect takes place due to oscillations of differential conductivity. We underline that the characteristic features of the predicted parametric amplification are quite different from those observed in the experiments [43]. In these experiments a heavily doped SL was used, and therefore we believe that electric domains played an important role in the observed effects (see Paper I).

(ii) The central idea in the suggestions of stable Bloch oscillators is that the electric instability can be circumvented if the sample exhibits positive dynamical conductivity at low frequencies, including dc, while the high-frequency conductivity is still negative giving rise to an amplification [49, 50]. In particular, it was suggested earlier in studies of weakly coupled SLs, that the high-frequency gain is not indispensably connected to the NDC, if an additional peak can appear in the voltage-current characteristic [50]. This idea is is easiest to explain with the help of a so-called Tucker formula [51], which connects the absorption and gain in different tunneling systems to VI

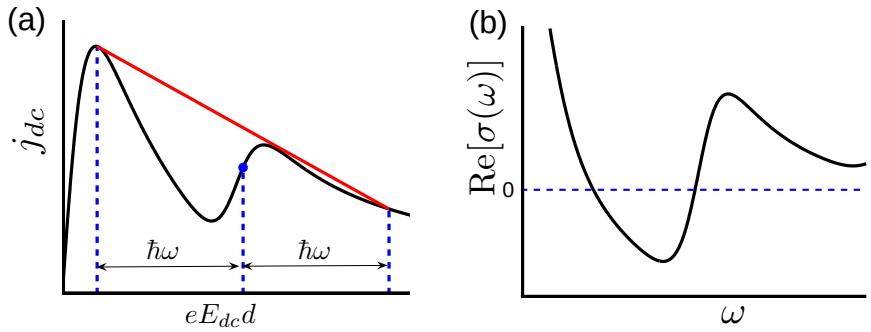

Figure 1.2: (a) Schematic figure illustrating the geometric meaning of the Tucker formula. The real part of the dynamical conductivity $\mathrm{Re}[\sigma(\omega)]$ at the operation point (marked) is proportional to slope of the inclined (red) segment. (b) Schematic figure showing that the structures in VI characteristic can be utilized to obtain stable high-frequency gain. By choosing the operation point at the PDC part of the additional peak in the VI characteristic, the Tucker formula results in positive dynamical conductivity at low frequencies and negative dynamical conductivity at higher frequencies.

characteristics as

$$\mathrm{Re}[\sigma(\omega)] = \frac{j_{dc}(eE_{dc}d + \hbar\omega) - j_{dc}(eE_{dc}d - \hbar\omega)}{2\hbar\omega} ed.$$

Here $j_{dc}(eE_{dc}d)$ is the current density and $\mathrm{Re}[\sigma(\omega)]$ is the real part of dynamical conductivity determining the absorption $\mathrm{Re}[\sigma(\omega)] > 0$ and gain $\mathrm{Re}[\sigma(\omega)] < 0$. The Tucker formula represents essentially a discrete derivative, where the step size is defined by the photon energy $\hbar\omega$. This geometric meaning is illustrated in Fig. 1.2 (a) for a particular VI characteristic. If now the VI characteristic contains structures such as shown in Fig. 1.2 (a), the operation point can be chosen from the positive differential conductivity (PDC) part of the additional peak, and by applying the Tucker formula we see that stable high-frequency gain can be obtained [Fig. 1.2 (b)]. We find that a similar approach works also in the case of strongly coupled SLs, where additional peak(s) can arise due to an action of auxiliary ac field (see Papers VI-VIII) or magnetic field (see Paper IX). In the first case the necessary structures can appear either due to photon-assisted transport [44] in the presence of high-frequency pump field (Paper VI) or due to reasonably fast switching between two electric field values in the presence of low-frequency polychromatic pump field (Papers VII and VIII). In Paper IX we demonstrate that although the Tucker formula is not in general valid in the presence of magnetic field, the structures induced by Stark-cyclotron resonances in tilted magnetic field [47] can still be utilized in the stabilization of the Bloch gain.

(iii) In Paper IX we also studied the small-signal absorption and gain in crossed electric and magnetic fields. We found that the magnetic field significantly alters the shapes of the gain profiles and the magnitude of THz gain in SLs. In particular, we predict a very large and tunable THz gain due to nonlinear cyclotron oscillations. In contrast to usual Bloch gain, here the SL is, as a rule, in an electrically stable state.

From the technological perspective the devices (i)-(iii) have different attractive features. The nonlinear cyclotron oscillations in crossed fields can provide very strong gain at low temperatures, whereas parametric amplification and Bloch oscillations still provide reasonable THz gain also at room temperature. On the other hand, Bloch and cyclotron oscillations are easily tunable with magnetic and electric fields and provide phase-insensitive gain, whereas the phase-sensitive parametric gain occurs only at harmonics and half-harmonics of the pump frequency. Finally, the device performance typically depends on the boundary conditions defined by the attached electric contacts. However, in the case of cyclotron oscillator the operation point can be chosen from the almost linearly increasing part of the static VI characteristic, and therefore we expect a very high electric stability independently on the boundary conditions.

In this thesis we concentrate on SLs, but it should be stressed that the results are applicable also to several other systems. The effects arising due to oscillations of the effective mass of the carriers can be observed in other crystals with reasonably narrow energy bands [52] or large band gaps [53]. On the other hand, the universality of the dynamics of quantum particles in periodic potentials brings together several different research communities. The Bloch oscillations have been observed in different systems such as optical lattices for ultracold atoms [54] and several types of structures for light beams [55], and the intrinsic periodicity in $\mathbf{k}$-space makes the single-band systems in many respects similar to the Josephson junctions [44, 56]. The studies of Bloch oscillations in different systems are motivated not only by the fundamental interest, but also far-reaching applications such as metrological tasks [57] and measurements of small spatial scale forces [58]. In comparison to SLs, these systems have advantages like possibility to control the dephasing time. Recently, long-lived Bloch oscillations (more than 20000 cycles) were demonstrated in optical lattices [59]. Although all these systems have similarities in the ballistic motion, the dynamics of the carriers is also affected by the environment. Surprisingly, it has been found that certain type of small Josephson junctions [60] and ultracold fermions in optical lattices [61] can show very similar dissipative dynamics as the electrons in SLs. In the case of optical lattices a *continuously tunable* dissipation is effectively induced by adding bosons to the system. The fermions can exchange energy with the bosons in a similar way as the electrons interact with phonons in SLs.

Our work addresses also a general issue of dispersive gain profile, which

has attracted a lot of attention recently. The existence of Bloch gain in SLs was under a hot debate for a long time, because it cannot be based on population inversion. The solution to this dilemma was obtained approximately 30 years after the prediction of Ktitorov *et al.* [19]. It was found that the dispersive Bloch gain can be understood in terms of scattering-assisted transitions between the Wannier-Stark states [62]. In this quantum mechanical picture, which is complementary to Bloch oscillations, the constant electric field splits the continuous energy band into discrete ladder of energy levels with spacing $\hbar\omega_B$ [63, 64]. The theoretical breakthrough achieved in the quantum mechanical understanding of the Bloch gain [62] sheds new light on the fundamental operation principles of the lasers. The frequency dependence of the Bloch gain can be interpreted as coexistence of gain and absorption in the same optical transition, thus generalizing the Einstein's famous thermodynamic consideration of the absorption and emission [65]. On the other hand, the consideration of the Bloch gain in terms of scattering-assisted transitions led to a prediction [62] and observation [66] of the dispersive gain profile in intersubband transitions of QCLs. In general, the dispersive gain profile is not limited to these two systems. Similar gain profile exists for example in the microwave responses of Josephson junctions [67] and Thim amplifiers [33].

This thesis is organized as follows. Chapter 2 introduces the basic mathematical formalism of miniband transport model, which is used in this thesis to describe the electron dynamics. As original results we present a derivation of the path-integral solution of the Boltzmann equation for arbitrary time-dependent electric and magnetic fields (Section 2.3) and discuss the similarity of the steady-state currents obtained as solutions of Tucker theory of sequential tunneling and the miniband transport model in the absence of magnetic field (Section 2.4.2). The Bloch gain and parametric amplification in dc-ac driven SLs are considered in Chapters 3 and 4, respectively. There in addition to the original results presented in the Papers, we briefly discuss the Bloch gain in ac driven SL (Section 3.3) and the mechanism of parametric amplification in particular limits (Sections 4.5 and 4.6). The influence of magnetic field on high-frequency gain is analyzed in Chapter 5. Additionally to the results presented in Paper IX, we describe the temperature dependencies of the cyclotron gain and Bloch gain, respectively. Finally, the conclusions and perspectives are presented in Chapter 6.

Chapter 2

Basics of superlattices

2.1 Energy band structure

Growing a periodic sequence of alternating thin layers of two different semiconductors forms a SL [3]. A lot of theoretical efforts have been devoted to realistic modelling of the electronic band structures in SLs [68]. However, here we are interested only about the qualitative understanding of the SL miniband engineering, and therefore we employ a simple Kronig-Penney model [69] scaled by appropriate effective masses [70]. We restrict the discussion to the so-called type I SLs [68], where the energy band gaps of the constituent materials are aligned, but the magnitudes of the band gaps are different. The materials with smaller and larger band gaps are called as quantum wells and quantum barriers, respectively. The direction perpendicular to the layers is called as the SL direction and chosen to be the x-direction in our coordinate system. We assume that the structure is translationally invariant in y and z directions. The lowest allowed energy in the conduction band, the conduction band edge $E_c(x)$, is therefore given by

$$E_c(x) = \begin{cases} E_{cw} & \text{at wells} \\ E_{cb} & \text{at barriers,} \end{cases} \tag{2.1}$$

where E_{cw} and E_{cb} are the conduction band edges of the materials forming the wells and barriers, respectively. Similarly the effective masses of the electrons in the conduction bands of the constituent materials are different (m_w and m_b at wells and barriers, respectively), so that also the effective mass of the electrons in the SL changes abruptly at the interfaces as

$$m_c(x) = \begin{cases} m_w & \text{at wells} \\ m_b & \text{at barriers.} \end{cases} \tag{2.2}$$

In the scaled Kronig-Penney model, the electrons see the changes of the conduction band edges $E_c(x)$ as an effective potential, and we obtain a

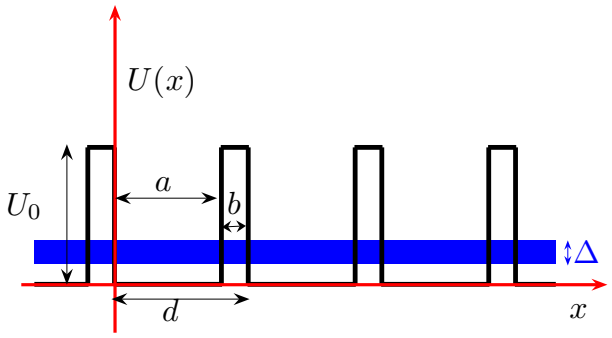

Figure 2.1: Schematic figure of the SL potential $U(x)$. The allowed energies in the case of an ideal infinite periodic potential form energy bands. The shaded (blue) region indicates the first miniband of width Δ.

Schrödinger-like equation for the envelope wave-function $\Psi(\mathbf{r})$

$$\left[E_c(x) - \frac{\hbar^2}{2m_c(x)}\nabla^2\right]\Psi(\mathbf{r}) = \varepsilon\Psi(\mathbf{r}). \tag{2.3}$$

In addition to the standard condition of the continuity of the wavefunction, we require that

$$\frac{1}{m(x)}\frac{\partial\Psi}{\partial x}$$

is continuous [70]. The latter condition ensures the continuity of particle flux. By defining $E_c(x) = E_{cw} + U(x)$, we effectively find a square-well potential $U(x)$ in the SL direction (see Fig. 2.1). This SL potential can be controlled during the growth process. The height of the potential barriers U_0 is determined by the choice of constituent materials $U_0 = E_{cb} - E_{cw}$, whereas the widths of the wells a and barriers b are defined by the thicknesses of the layers. The period of the SL, $d = a + b$, is typically substantially larger than the lattice constants of host crystals but shorter than the mean free path of the electrons. Therefore, we are exploring quantum effects at the mesoscopic scale.

The Schrödinger-like equation (2.3) can be solved by using the well-known quantum mechanical methods developed for periodic systems [30, 70]. Because the SL potential $U(x)$ does not exhibit (y, z)-dependence, the eigenstates $\Psi(\mathbf{r})$ are products of plane waves $e^{i\mathbf{k}_\perp\cdot\mathbf{r}_\perp}$ [$\mathbf{k}_\perp = (k_y, k_z)$, $\mathbf{r}_\perp = (y, z)$] and x-dependent functions $\psi(x)$, which satisfy an eigenvalue equation

$$\left[-\frac{\hbar^2}{2m_c(x)}\frac{\partial^2}{\partial x^2} + U(x)\right]\psi(x) = \varepsilon_x\psi(x). \tag{2.4}$$

Here the total energy has been written in the form

$$\varepsilon = E_{cw} + \frac{\hbar^2(k_y^2 + k_z^2)}{2m} + \varepsilon_x, \tag{2.5}$$

and we have defined the effective mass m parallel to the SL layers by using a first-order perturbation theory $\langle\psi|\frac{\hbar^2(k_y^2+k_z^2)}{2m_c(x)}|\psi\rangle = \frac{\hbar^2(k_y^2+k_z^2)}{2m}$. The eigenfunctions ψ exhibit a larger probability in the wells, so that $m \approx m_w$ [28].

The eigenvalue equation (2.4) can be nicely solved using the Bloch theorem [11], which states that the wave function in perfect periodic potential differs from the plane wave only by a periodic modulation $\psi_{k_x}(x) = e^{ik_x x}u(x)$, $u(x+d) = u(x)$. Here k_x is called as Bloch wave vector and it defines the quasimomentum $p_x = \hbar k_x$. By a straightforward calculation we obtain [30, 70]

$$\begin{aligned} \psi &= Ae^{i\alpha x} + Be^{-i\alpha x}, \qquad 0 \le x \le a \\ \psi &= Ce^{\beta x} + De^{-\beta x}, \qquad -b \le x \le 0. \end{aligned}$$

with following connection rules at the boundaries between wells and barriers

$$\begin{aligned} \psi_{k_x}(x)|_{x\to 0^-} &= \psi_{k_x}(x)|_{x\to 0^+} && \text{(continuity of the wave function)}, \\ \frac{1}{m_b}\psi'_{k_x}(x)|_{x\to 0^-} &= \frac{1}{m_w}\psi'_{k_x}(x)|_{x\to 0^+} && \text{(continuity of particle flux)}, \\ \psi_{k_x}(x)|_{x\to a^-} &= e^{ik_x d}\psi_{k_x}(x)|_{x\to -b^+} && \text{(continuity of } \psi\text{, Bloch theor.)}, \\ \frac{1}{m_w}\psi'_{k_x}(x)|_{x\to a^-} &= \frac{e^{ik_x d}}{m_b}\psi'_{k_x}(x)|_{x\to -b^+} && \text{(cont. of part. flux, Bloch theor.)}. \end{aligned}$$

Here A, B, C, D are constants, $\alpha^2 = 2m_w\varepsilon_x/\hbar^2$ and $\beta^2 = 2m_b(U_0 - \varepsilon_x)/\hbar^2$. The connection rules define a set of linear equations for the constants A, B, C and D. These equations have a nontrivial solution if

$$\cos(k_x d) = \cosh(\beta b)\cos(\alpha a) + \frac{1}{2}\left(\zeta - \frac{1}{\zeta}\right)\sinh(\beta b)\sin(\alpha a), \tag{2.6}$$

where

$$\zeta = \frac{\beta m_w}{\alpha m_b} = \sqrt{\frac{(U_0 - \varepsilon_x)m_w}{\varepsilon_x m_b}}. \tag{2.7}$$

The condition (2.6) determines the allowed energy minibands and the energy-quasimomentum dispersion relations for each band [30, 70]. If the absolute value of the right-hand side of the equation (2.6) is larger than one, the corresponding energy value belongs to the forbidden energy gaps.

The parameters m_w, m_b, U_0, b and a determine the energy band structures of the SLs. Parameters b and a are determined by the thicknesses of the layers and are typically couple of nanometers, whereas the other parameters are determined by the chosen constituent materials and for example in the case of GaAs/AlAs SLs, they are $m_w = 0.067m_e$, $m_b = 0.11m_e$ and $U_0 = 1.06$ eV [30]. Although the whole band structure of the SL can be more or less controlled with the SL potential, from the perspective of this thesis

the important quantities are the width of the first miniband Δ, the bandgap between the first and second minibands Δ_g and energy-quasimomentum dispersion relation of the first miniband. In general the energy bands $\varepsilon_x^n(k_x)$ (n is the band index) can be represented as a Fourier series

$$\varepsilon_x^n(k_x) = C_n + \sum_{h=1}^{\infty} 2T_h^n \cos(hk_x d), \tag{2.8}$$

where C_n and T_h^n ($h = 1, 2, 3...$) are constants corresponding to nth band. The energy bands arise due to the coupling of the quantum mechanical states localized in the quantum wells, and therefore it seems natural to expect that the locations of the energy bands C_n are determined by the energy levels of the isolated quantum wells. In the limit of completely isolated quantum wells we get the famous one-dimensional "particle in a box problem", so that $C_n = n^2\pi^2\hbar^2/2m_w a^2$. Thus, an increase in a will decrease the energy gap Δ_g between the first and second minibands. On the other hand, the coefficients T_h^n in the Fourier series (2.8) can be interpreted as caused by tunneling between quantum wells, which are h-lattice sites apart from each other. These tunneling probabilities can be controlled with the width b and height U_0 of the barriers. By choosing the center of the first miniband as the zero energy ($C_1 = 0$), we can redefine the energy dispersion relation of the first band as (we omit the band index 1 from these expressions)

$$\varepsilon_x(k_x) = \sum_{h=1}^{\infty} 2T_h \cos(hk_x d). \tag{2.9}$$

For typical SL parameters one obtains that the nearest-neighbor coupling dominates the other terms [28, 30], and we get the so-called tight-binding dispersion relation

$$\varepsilon_x(k_x) \approx -\frac{\Delta}{2}\cos k_x d, \tag{2.10}$$

where $\Delta \approx 4|T_1|$ is the width of the first miniband. Moreover, the bandgap Δ_g between the first and second miniband can be significantly larger than the miniband width Δ – allowing consideration of electron dynamics in single energy band. Because the reference energy can be chosen arbitrarily, we can redefine the complete energy momentum dispersion relation [Eq. (2.5)] so that

$$\varepsilon(\mathbf{k}) = \sum_{h=1}^{\infty} 2T_h \cos(hk_x d) + \frac{\hbar^2(k_y^2 + k_z^2)}{2m}. \tag{2.11}$$

In the tight-binding approximation, it becomes

$$\varepsilon(\mathbf{k}) = -\frac{\Delta}{2}\cos k_x d + \frac{\hbar^2(k_y^2 + k_z^2)}{2m}. \tag{2.12}$$

Typical miniband width and SL period are $\Delta = 60$ meV and $d = 6$ nm, respectively. These parameters are used in Papers II, III, IV, VI, VII and IX. Since the work of Esaki and Tsu [3] it has been well-known that the narrow energy band and Brillouin zone of the SLs makes it possible to study previously undetected electrical phenomena, like Bloch oscillations and negative differential conductivity (NDC). We now turn to consideration of these effects.

2.2 Semiclassical equations of motion

Historically, the Bloch theorem [11] goes back to the early days of quantum mechanics, when one of the main problems in condensed matter physics was to explain the small resistances of the metals, which decrease with decreasing temperature [71, 72]. Such resistances demanded a mean free path of the electrons much longer than the atomic distances. By using the Bloch theorem it is easy to understand this observation qualitatively: In metals the electrons occupying the Bloch states at the bottom of the energy band can move like free particles, and therefore the scattering of the electrons is not caused by the lattice itself but by defects in the lattice due to thermal fluctuations or impurities. Interestingly, this same theorem which was originally developed to understand the small resistances of the metals, straightforwardly also results in localization of electrons due to Bloch oscillations at large applied dc bias in SLs. In this Section, we present the semiclassical equations of motion and apply them to understand two important concepts: Bloch oscillations and dynamic localization.

If electric and magnetic fields are applied, the Bloch states are no longer the eigenstates of the system, but the Bloch wave vector $\mathbf{k}$ becomes time-dependent obeying a few apparently classical dynamical rules, which are called semiclassical equations of motion [28, 72, 73, 74]

$$\begin{aligned} \hbar\frac{d\mathbf{k}}{dt} &= e\mathbf{E} + e\mathbf{v}\times\mathbf{B} \\ \mathbf{v}(\mathbf{k}) &= \frac{1}{\hbar}\frac{\partial\varepsilon(\mathbf{k})}{\partial\mathbf{k}}. \end{aligned} \tag{2.13}$$

Here $\mathbf{v}(\mathbf{k})$ is the velocity of an electron with quasimomentum $\mathbf{k}$. In particular by using the dispersion relation (2.11), we get for the velocity components

$$\begin{aligned} v_x(k_x) &= \sum_{h=1}^{\infty} v_h \sin(hk_x d), \\ v_y(k_y) &= \hbar k_y/m, \\ v_z(k_z) &= \hbar k_z/m, \end{aligned} \tag{2.14}$$

where $v_h = -2hT_h d/\hbar$ ($h = 1, 2, 3...$). The velocity in the SL direction can be understood as a sum of the contributions caused by the tunneling over the different number of SL periods h. The effective mass of the electrons in the SL direction $m_{x,\mathbf{k}}$ is defined by the curvature of the energy band

$$m_{x,\mathbf{k}}^{-1} = \frac{1}{\hbar^2}\frac{\partial^2 \varepsilon}{\partial k_x^2}. \tag{2.15}$$

For the tight-binding miniband (2.12), we get

$$v_x(k_x) = v_1 \sin k_x d \tag{2.16}$$

and

$$m_{x,\mathbf{k}}^{-1} = -\frac{d^2}{\hbar^2}\varepsilon(\mathbf{k}) = m_x^{-1}\cos k_x d, \tag{2.17}$$

where $v_1 = \Delta d/2\hbar$ is the maximum miniband velocity and $m_x = 2\hbar^2/\Delta d^2$ is the effective mass at the bottom of the miniband. We see that in the upper part of the miniband the effective mass is negative, essentially meaning that there the applied force decelerates the electrons. The validity of the semiclassical dynamics in single energy band requires that the magnitudes and frequencies of the electric and magnetic fields are not too large, so that the electrons see the external potential as slowly varying and the transitions between the energy bands are suppressed [28, 72, 74]. Assuming a typical situation considered in this thesis, where a time-dependent electric field $\mathbf{E} = (E_{dc} + E_\omega \cos\omega t, 0, 0)$ is applied in the SL direction and a constant magnetic field is applied in an arbitrary direction $\mathbf{B} = (B_x, 0, B_z)$, these conditions are roughly equivalent with the requirement that the energy quanta associated with the fields are smaller than the miniband width and energy gap i.e. $\hbar\omega_B, eE_\omega d, \hbar\omega_c, \hbar\omega_{c\perp}, \hbar\omega \ll \Delta, \Delta_g$. Here $\hbar\omega_B$ is the Wannier-Stark spacing, $\omega_B = eE_{dc}d/\hbar$ is the Bloch frequency and $\hbar\omega_c$ and $\hbar\omega_{c\perp}$ are the Landau level spacings corresponding to cyclotron frequencies $\omega_c = eB_z/\sqrt{mm_x}$ and $\omega_{c\perp} = eB_x/m$, respectively. The meaning of these frequencies will be clarified in the following Chapters. Next we consider the dynamics of miniband electrons in an electric field. The discussion of the magnetic field induced effects is postponed to Chapter 5.

In the absence of magnetic field ($\mathbf{B} = \mathbf{0}$) the Eqs. (2.13) can be easily solved for arbitrary electric field. Here we are interested on the situation, where the electric field

$$E(t) = E_{dc} + \sum_{k=1}^{N} E_{\omega_k}\cos(\omega_k t + \alpha_k)$$

is applied along the SL direction $\mathbf{E} = (E(t), 0, 0)$. If the initial wave vector of the electron is $k_x(0) = k_x^0$, we get

$$k_x(t)d = k_x^0 d + \int_0^t dt' eE(t')d/\hbar = \phi + \omega_B t + \sum_{k=1}^{N}\beta_k \sin(\omega_k t + \alpha_k), \tag{2.18}$$

where $\phi = k_x^0 d - \sum_{k=1}^{N} \beta_k \sin\alpha_k$ and $\beta_k = eE_{\omega_k} d/\hbar\omega_k$. This means that the time-dependent velocity of the electron satisfies

$$v_x(t) = \sum_{h=1}^{\infty} v_x^h(t), \tag{2.19}$$

where $v_x^h(t)$ are the contributions caused by tunneling over h periods and they are given by

$$\begin{aligned} v_x^h(t) &= v_h \sin\left[hk_x(t)d\right] = v_h \mathrm{Im}\left\{ e^{ih\phi + ih\omega_B t} \prod_{k=1}^{N} e^{ih\beta_k \sin(\omega_k t + \alpha_k)} \right\} \\ &= v_h \mathrm{Im}\left\{ e^{ih\phi + ih\omega_B t} \sum_{n_1,\ldots,n_N} \prod_{k=1}^{N} J_{n_k}(h\beta_k) e^{in_k(\omega_k t + \alpha_k)} \right\} \\ &= v_h \sum_{n_1,\ldots,n_N} \left[\prod_{k=1}^{N} J_{n_k}(h\beta_k) \right] \sin\left[h\phi + h\omega_B t + \sum_{k=1}^{N} n_k(\omega_k t + \alpha_k) \right]. \end{aligned} \tag{2.20}$$

Here $J_n(\beta)$ are the Bessel functions of the first kind, the summation limits are $\pm\infty$ and we have used the relation [75]

$$e^{i\alpha \sin x} = \sum_{n=-\infty}^{\infty} J_n(\alpha) e^{inx}. \tag{2.21}$$

In the case of static electric field $E = E_{dc}$, we obtain

$$\begin{aligned} k_x(t)d &= k_x^0 d + \omega_B t \\ v_x(t) &= \sum_{h=1}^{\infty} v_h \sin\left[hk_x^0 d + h\omega_B t \right]. \end{aligned} \tag{2.22}$$

Because the Bloch vectors can be restricted to the first Brillouin zone $-\pi/d \leq k_x \leq \pi/d$, we see that a special feature has to arise, when the boundary of the Brillouin zone is reached. Since the electron stays within the same miniband and Bloch wave vectors k_x and $k_x + 2\pi/d$ are physically indistinguishable, the crossing of the Brillouin zone boundary is equivalent to the change of electrons quasimomentum from $k_x = \pi/d$ to $k_x = -\pi/d$ in the way that the trajectory continues there. This process is called Bragg reflection. Therefore, after a single Bloch period

$$T_B = \frac{2\pi}{\omega_B} \tag{2.23}$$

the electron has returned to the same state in the quasimomentum space. This periodic motion in k_x-space is accompanied by periodic oscillations in

real space

$$x(t) = x(0) + \int_0^t dt' v(t') = x(0) + \frac{1}{eE_{dc}} \sum_{h=1}^{\infty} 2T_h \Big[\cos(hk_x^0 d + h\omega_B t) - \cos(hk_x^0 d) \Big]. \tag{2.24}$$

The total spatial extension of the oscillations δx corresponds to the potential drop equivalent with the miniband width

$$eE_{dc}\delta x = \Delta. \tag{2.25}$$

The discussion above holds for a wave packet of Bloch states initially localized around k_x^0. In general, the motion of the wave packet in real space, including the spatial amplitude of the Bloch oscillations, depends also on the initial conditions determined in undoped SLs by the optical excitation [14, 76].

The Bloch oscillations were originally predicted a long time ago by Zener [12] based on the work of Bloch [11], but this counterintuitive effect, where static force results in localized oscillations of the carriers, has never been observed in standard crystals. The reason is that for typical materials and electric fields the Bloch frequency ω_B is much smaller than the scattering rate, and therefore the electron motion is characterized by Drude drift transport [13]. On the other hand, in SLs the period d can be substantially larger and Bloch oscillations with photoexcited carriers have been observed using several different methods [14]. Also in SLs the scattering destroys the coherence of the oscillations in a time scale of few picoseconds, so that only transient oscillations (decaying signals) have been detected.

Alternatively to the dc bias, the electrons in SL miniband can also be localized with the help of ac field. Illustrative examples are the dynamic localization with the help of square wave field and monochromatic field $E(t) = E_{\omega_1} \cos \omega_1 t$ [77]. In the case of square wave field it is immediately clear, that the dynamic localization occurs if one or more complete Bloch oscillations take place in exactly half the period of the field [77]. On the other hand, in the case of monochromatic field and tight-binding SL (2.12), we obtain from Eqs. (2.18)-(2.20)

$$\begin{aligned} k_x(t)d &= k_x^0 d + \beta_1 \sin(\omega_1 t), \\ v_x(t) &= v_1 \sum_{n_1} J_{n_1}(\beta_1) \sin \Big[k_x^0 d + n_1 \omega_1 t \Big]. \end{aligned} \tag{2.26}$$

Therefore, it is clear that the electron periodically return to the initial state both in the quasimomentum space and in real space, if $J_0(\beta_1) = 0$ [77]. Alternatively to the semiclassical picture, the dynamic localization can be understood as a collapse of the miniband [78]. A number of investigations of dynamic localization for different miniband structures in dc-ac-driven SLs have been made (see [79], and references therein). For example, in the case

of tight-binding SL and electric field $E(t) = E_{dc} + E_{\omega_1} \cos \omega_1 t$, $\omega_B = n\omega_1$, the condition for dynamic localization becomes $J_n(\beta_1) = 0$.

2.3 Electron dynamics in the presence of scattering

The problem of electron dynamics in SLs has been separated in two parts. The periodic potential of the SL is taken into account in the dispersion relation $\varepsilon(\mathbf{k})$. On the other hand, the electric and magnetic fields act like a force, which changes the quasimomentum of the electron. So far we have only considered the dynamics of single electron in perfect periodic potential without any impurities or thermal fluctuations. Next we study the dissipative electron dynamics in time-dependent electric and magnetic fields by using a well-established miniband transport model based on Boltzmann transport equation [28, 72].

We restrict the analysis to the first SL miniband and suppose that the number of electrons with Bloch wave vector $\mathbf{k}$ at position $\mathbf{r}$ is

$$\frac{2}{(2\pi)^3} f(\mathbf{k}, \mathbf{r}, t) d\mathbf{k} d\mathbf{r},$$

where $2/(2\pi)^3$ is the density of states (including the spin degeneracy). By assuming that electron positions and wave vectors change according to semiclassical equations of motion (2.13), we get with the help of continuity equation in $(\mathbf{k}, \mathbf{r})$-space [72]

$$\frac{\partial f(\mathbf{k}, \mathbf{r}, t)}{\partial t} + \frac{e\mathbf{E} + e\mathbf{v} \times \mathbf{B}}{\hbar} \cdot \frac{\partial f(\mathbf{k}, \mathbf{r}, t)}{\partial \mathbf{k}} + \mathbf{v}(\mathbf{k}) \cdot \frac{\partial f(\mathbf{k}, \mathbf{r}, t)}{\partial \mathbf{r}} = \left(\frac{\partial f(\mathbf{k}, \mathbf{r}, t)}{\partial t} \right)_s, \tag{2.27}$$

where a weak scattering has been taken into account with a scattering integral (right-hand side of the equation). The current density $\mathbf{j}(\mathbf{r}, t)$, the average miniband energy $W(\mathbf{r}, t)$ and the density of electrons $N_e(\mathbf{r}, t)$ are determined by the distribution function $f(\mathbf{k}, \mathbf{r}, t)$ as

$$\begin{aligned}
\mathbf{j}(\mathbf{r}, t) &= \frac{2e}{(2\pi)^3} \int_{-\infty}^{\infty} \int_{-\infty}^{\infty} dk_y dk_z \int_{-\pi/d}^{\pi/d} dk_x \ \mathbf{v}(\mathbf{k}) f(\mathbf{k}, \mathbf{r}, t), \\
W(\mathbf{r}, t) &= \frac{2}{(2\pi)^3 N_e} \int_{-\infty}^{\infty} \int_{-\infty}^{\infty} dk_y dk_z \int_{-\pi/d}^{\pi/d} dk_x \ \varepsilon_x(\mathbf{k}) f(\mathbf{k}, \mathbf{r}, t), \\
N_e(\mathbf{r}, t) &= \frac{2}{(2\pi)^3} \int_{-\infty}^{\infty} \int_{-\infty}^{\infty} dk_y dk_z \int_{-\pi/d}^{\pi/d} dk_x \ f(\mathbf{k}, \mathbf{r}, t).
\end{aligned} \tag{2.28}$$

Here $\mathbf{v}$ is defined by semiclassical equations of motion (2.13) and ε_x is given

by (2.9) and (2.10) for general and tight-binding dispersion relations, respectively. For spatially homogeneous SLs $N_e(\mathbf{r},t) = N_0$, we get

$$\frac{\partial f(\mathbf{k},t)}{\partial t} + \frac{1}{\hbar}\left[e\mathbf{E} + e\mathbf{v}\times\mathbf{B}\right]\cdot\frac{\partial f(\mathbf{k},t)}{\partial \mathbf{k}} = \left(\frac{\partial f(\mathbf{k},t)}{\partial t}\right)_{\mathrm{s}}. \tag{2.29}$$

The scattering probabilities for all different processes can be approximated using the Fermi's golden rule (see Ref. [28] p. 20-25 and references therein), but the resulting equation can then only be solved numerically using Monte-Carlo methods. Here we are more interested in tractable analytic calculations, and therefore we use phenomenological scattering terms. In many phenomena in SLs, these so-called relaxation time approximations have been found qualitatively equivalent with the full-scale Monte Carlo simulations (see Ref. [80] and Paper I).

In thermal equilibrium in the absence of the fields $f(\mathbf{k})$ is equal to the Fermi distribution

$$f_{eq}(\mathbf{k}) = \frac{1}{e^{[\varepsilon(\mathbf{k})-\mu]/k_BT_e}+1}, \tag{2.30}$$

where μ is the chemical potential and T_e is the temperature. In the non-degenerate limit the Fermi function becomes the Maxwell-Boltzmann distribution $f_{eq}(\mathbf{k}) = e^{-[\varepsilon(\mathbf{k})-\mu]/k_BT_e}$, and we get for the tight-binding SL (2.12) that $N_e = mk_BT_e e^{\mu/k_BT_e} I_0(\Delta/2k_BT_e)/d\pi\hbar^2$ [28]. Here we have used the relation

$$e^{z\cos\theta} = I_0(z) + 2\sum_{k=1}^{\infty} I_k(z)\cos k\theta, \tag{2.31}$$

where $I_k(z)$ are the modified bessel functions of the first kind. Thus, the equilibrium distribution in this limit can be written as

$$f_{eq}(\mathbf{k}) = \frac{N_e d\pi\hbar^2}{mk_BT_eI_0(\Delta/2k_BT_e)} e^{\frac{\Delta}{2k_BT_e}\cos k_x d} e^{-\hbar^2(k_y^2+k_z^2)/2mk_BT_e}. \tag{2.32}$$

This non-degenerate equilibrium distribution [Eq. (2.32)] is mostly used in the literature. It is valid if $e^{(-\Delta/2-\mu)/k_BT_e} \gg 1$ i.e.

$$\frac{N_e d\pi\hbar^2}{mk_BT_eI_0(\Delta/2k_BT_e)} e^{\Delta/2k_BT_e} \ll 1.$$

The underlying assumption in the relaxation time approximation is that the scattering processes try to restore the thermal equilibrium. In single (constant) scattering time τ approximation, the scattering term is

$$\left(\frac{\partial f(\mathbf{k},t)}{\partial t}\right)_{\mathrm{s}} = \frac{f_{eq}(\mathbf{k}) - f(\mathbf{k},t)}{\tau}. \tag{2.33}$$

However, elastic impurity scattering does not restore thermal equilibrium. Therefore a scattering term with two relaxation times is often used

$$\left(\frac{\partial f(\mathbf{k},t)}{\partial t}\right)_{\mathrm{s}} = \frac{f_{eq}(\mathbf{k}) - f(\mathbf{k},t)}{\tau_{\mathrm{in}}} + \frac{f(-k_x,k_y,k_z,t) - f(k_x,k_y,k_z,t)}{2\tau_{\mathrm{el}}}. \quad (2.34)$$

Here τ_{in} and τ_{el} can be interpreted as inelastic and elastic scattering times, respectively. The latter approximation makes the analytical considerations difficult, but it does not have large impact on the qualitative results as long as the inelastic scattering dominates. The scattering term (2.34) has been used extensively in the literature, because it results in simple superlattice balance equations in the absence of magnetic field (see Section 2.4.6). However, it is obvious that Eq. (2.34) does not describe correctly the possible energy transfer between the miniband energy and kinetic energy in the lateral directions: In a more reasonable description used in Ref. [81], the impurity scattering tends to drive the distribution function $f(\mathbf{k},t)$ at different quasimomentums $\mathbf{k}$ towards the corresponding average values

$$\Phi_f(\mathbf{k},t) = \frac{\int_{-\infty}^{\infty}\int_{-\infty}^{\infty} dk_y' dk_z' \int_{-\pi/d}^{\pi/d} dk_x'\ f(\mathbf{k}',t)\delta[\varepsilon(\mathbf{k}) - \varepsilon(\mathbf{k}')]}{\int_{-\infty}^{\infty}\int_{-\infty}^{\infty} dk_y' dk_z' \int_{-\pi/d}^{\pi/d} dk_x'\ \delta[\varepsilon(\mathbf{k}) - \varepsilon(\mathbf{k}')]}$$

taken over the constant energy surfaces. Such kind of elastic scattering makes the problem truly three dimensional and may result, depending on the ratio of elastic and inelastic scattering rates, in qualitative changes in the VI characteristic [81].

In this thesis, we mainly use the single relaxation time approximation (2.33). In this case the Boltzmann equation (2.29) can be written as

$$\frac{\partial f(\mathbf{k},t)}{\partial t} + \frac{1}{\hbar}\left[e\mathbf{E} + e\mathbf{v}\times\mathbf{B}\right]\cdot\frac{\partial f(\mathbf{k},t)}{\partial \mathbf{k}} = \frac{f_{eq}(\mathbf{k}) - f(\mathbf{k},t)}{\tau}. \quad (2.35)$$

Equation (2.35) has an exact formal solution in the form of a path-integral

$$f(\mathbf{k},t) = e^{-(t-t_0)/\tau} f_0(\mathbf{k}_t^{t_0}) + \frac{1}{\tau}\int_{t_0}^{t} ds\ e^{-(t-s)/\tau} f_{eq}(\mathbf{k}_t^s), \quad (2.36)$$

where the first term describes the transient defined by the initial distribution $f_0(\mathbf{k}) = f(\mathbf{k},t_0)$. By assuming that $t_0 \to -\infty$, we obtain the equation describing the steady-state dynamics

$$f(\mathbf{k},t) = \frac{1}{\tau}\int_{-\infty}^{t} ds\ e^{-(t-s)/\tau} f_{eq}(\mathbf{k}_t^s). \quad (2.37)$$

In these formulas, $\mathbf{k}_t^s$ is a ballistic trajectory governed by equations

$$\frac{d\mathbf{k}_t^s}{ds} = \frac{1}{\hbar}\left[e\mathbf{E}(s) + e\mathbf{v}(\mathbf{k}_t^s)\times\mathbf{B}(s)\right], \quad \mathbf{k}_t^t = \mathbf{k}. \quad (2.38)$$

The current density defined by Eq. (2.28) is given by

$$\begin{aligned}\mathbf{j}(t) &= \frac{2e}{(2\pi)^3}e^{-(t-t_0)/\tau}\int d^3k\ f_0(\mathbf{k})\mathbf{v}(\mathbf{k}^t_{t_0}) \\ &\quad +\frac{2e}{(2\pi)^3\tau}\int d^3k\ f_{eq}(\mathbf{k})\int_{t_0}^{t} ds\ e^{-(t-s)/\tau}\mathbf{v}(\mathbf{k}^t_s). \qquad (2.39)\end{aligned}$$

The first term again describes the transient dynamics such as the Bloch oscillations. The steady-state time-dependent current is given by

$$\mathbf{j}(t) = \frac{2e}{(2\pi)^3\tau}\int d^3k\ f_{eq}(\mathbf{k})\int_{-\infty}^{t} ds\ e^{-(t-s)/\tau}\mathbf{v}(\mathbf{k}^t_s). \qquad (2.40)$$

In Eqs. (2.39) and (2.40) k_x is integrated over the Brillouin zone and the integration limits for k_y and k_z are $\pm\infty$. Here we derive the solution (2.36)-(2.40) by using a generalization of the technique based on time-evolution operator [82, 83]. The same results can be obtained also with the method of characteristics [84, 85]. In the derivation of the formulas (2.39) and (2.40) we do not make any assumptions about the function $\mathbf{v}(\mathbf{k})$. Therefore, similar equations can be derived also for the average miniband energy $W(t)$. In particular, the steady-state miniband energy satisfies

$$W(t) = \frac{2}{(2\pi)^3 N_0\tau}\int d^3k\ f_{eq}(\mathbf{k})\int_{-\infty}^{t} ds\ e^{-(t-s)/\tau}\varepsilon_x(\mathbf{k}^t_s). \qquad (2.41)$$

Before going to the tedious mathematical proof of Eqs. (2.36)-(2.40), we start with a simple heuristic justification.

2.3.1 Heuristic justification of Eqs. (2.36)-(2.40)

The Eq. (2.36) can be heuristically justified as follows. First, we assume that the duration of scattering-free motion is larger than Δt with a probability $e^{-\Delta t/\tau}$. The probability that a particle has an initial quasimomentum $\mathbf{k}'$ at time t_0 is proportional to $f_0(\mathbf{k}')$. At time t the probability that no scattering event has yet occurred is therefore $e^{-(t-t_0)/\tau}$, and the probability distribution that last scattering event happened at time s is

$$p(s) = \frac{1}{\tau}e^{-(t-s)/\tau}, \qquad t_0 \le s \le t \qquad (2.42)$$

Now we also assume that in a scattering event the final state $\mathbf{k}'$ occurs with a probability proportional to $f_{eq}(\mathbf{k}')$. Thus the probability of finding an electron at momentum $\mathbf{k}$ at time t, $\mathcal{P}(\mathbf{k},t)$, satisfies

$$\begin{aligned}\mathcal{P}(\mathbf{k},t) &\propto e^{-(t-t_0)/\tau}\int d^3k' f_0(\mathbf{k}')\delta(\mathbf{k}'^t_{t_0}-\mathbf{k}) \\ &\quad +\int_{t_0}^{t} ds\ \frac{1}{\tau}e^{-(t-s)/\tau}\int d^3k' f_{eq}(\mathbf{k}')\delta(\mathbf{k}'^t_s-\mathbf{k}), \qquad (2.43)\end{aligned}$$

where $\mathbf{k'}_s^t$ is the quasimomentum of an electron at time t assuming that it follows a ballistic trajectory starting from $\mathbf{k'}$ at time s. If we have a ballistic trajectory $\mathbf{k'} \to \mathbf{k}$ as time goes $s \to t$, the integration backwards gives a ballistic trajectory $\mathbf{k} \to \mathbf{k'}$ as time goes $t \to s$. Therefore, we get from Eq. (2.43)

$$\begin{aligned}\mathcal{P}(\mathbf{k},t) \;\propto\; & e^{-(t-t_0)/\tau}\int d^3k' f_0(\mathbf{k'})\delta(\mathbf{k'}-\mathbf{k}_t^{t_0}) \\ & + \int_{t_0}^{t} ds\; \frac{1}{\tau} e^{-(t-s)/\tau}\int d^3k' f_{eq}(\mathbf{k'})\delta(\mathbf{k'}-\mathbf{k}_t^{s}). \qquad (2.44)\end{aligned}$$

By requiring that the density of the electrons is conserved we get Eq. (2.36).

Eq. (2.39) for the current can now be found using Eq. (2.28) and similar reasoning

$$\begin{aligned}\mathbf{j}(t) &= \frac{2e}{(2\pi)^3}e^{-(t-t_0)/\tau}\int d^3k\; \mathbf{v}(\mathbf{k}) f_0(\mathbf{k}_t^{t_0}) \\ &\quad + \frac{2e}{(2\pi)^3\tau}\int d^3k\; \mathbf{v}(\mathbf{k})\int_{t_0}^{t} ds\; e^{-(t-s)/\tau} f_{eq}(\mathbf{k}_t^{s}) \\ &= \frac{2e}{(2\pi)^3}e^{-(t-t_0)/\tau}\int d^3k \int d^3k'\; \mathbf{v}(\mathbf{k}) f_0(\mathbf{k'})\delta(\mathbf{k'}-\mathbf{k}_t^{t_0}) \\ &\quad + \frac{2e}{(2\pi)^3\tau}\int_{t_0}^{t} ds\; e^{-(t-s)/\tau}\int d^3k \int d^3k'\; \mathbf{v}(\mathbf{k}) f_{eq}(\mathbf{k'})\delta(\mathbf{k'}-\mathbf{k}_t^{s}) \\ &= \frac{2e}{(2\pi)^3}e^{-(t-t_0)/\tau}\int d^3k \int d^3k'\; \mathbf{v}(\mathbf{k}) f_0(\mathbf{k'})\delta(\mathbf{k'}_{t_0}^{t}-\mathbf{k}) \\ &\quad + \frac{2e}{(2\pi)^3\tau}\int_{t_0}^{t} ds\; e^{-(t-s)/\tau}\int d^3k \int d^3k'\; \mathbf{v}(\mathbf{k}) f_{eq}(\mathbf{k'})\delta(\mathbf{k'}_{s}^{t}-\mathbf{k}) \\ &= \frac{2e}{(2\pi)^3}e^{-(t-t_0)/\tau}\int d^3k'\; \mathbf{v}(\mathbf{k'}_{t_0}^{t}) f_0(\mathbf{k'}) \\ &\quad + \frac{2e}{(2\pi)^3\tau}\int_{t_0}^{t} ds\; e^{-(t-s)/\tau}\int d^3k'\; \mathbf{v}(\mathbf{k'}_{s}^{t}) f_{eq}(\mathbf{k'}). \qquad (2.45)\end{aligned}$$

2.3.2 Mathematical proof of Eqs. (2.36)-(2.40)

To prove Eqs. (2.36)-(2.40), we first notice that the Boltzmann equation (2.35) can be written as

$$\frac{\partial f(\mathbf{k},t)}{\partial t} + i\hat{\mathcal{L}}(t) f(\mathbf{k},t) = \frac{f_{eq}(\mathbf{k}) - f(\mathbf{k},t)}{\tau}, \qquad (2.46)$$

where we have defined an operator

$$i\hat{\mathcal{L}}(t) = \frac{1}{\hbar}\Big[e\mathbf{E}(t) + e\mathbf{v}(\mathbf{k})\times\mathbf{B}(t)\Big]\cdot\frac{\partial}{\partial\mathbf{k}}. \qquad (2.47)$$

In the absence of scattering Eq. (2.46) bears a strong analogy to the familiar time-dependent Schrödinger equation. Because in general, the operators $\hat{\mathcal{L}}(t)$ at different times do not commute $[\hat{\mathcal{L}}(t), \hat{\mathcal{L}}(t')] \neq 0$, the time-evolution operator $U(t,s)$ has to be written as a Dyson series

$$U(t,s) = 1 + \sum_{n=1}^{\infty} (-i)^n \int_s^t dt_1 \int_s^{t_1} dt_2 \cdots \int_s^{t_{n-1}} dt_n \hat{\mathcal{L}}(t_1)\hat{\mathcal{L}}(t_2)\cdots\hat{\mathcal{L}}(t_n). \tag{2.48}$$

To prove that $U(t,s)$ is a time-evolution operator, we need to show for arbitrary analytic function $F(\mathbf{k})$ that

$$U(t,s)F(\mathbf{k}) = F(\mathbf{k}_t^s). \tag{2.49}$$

Here we assume that $\mathbf{k}_t^s$, determined by Eq. (2.38), is an analytic function of s and denote $G_1^{\mathbf{k}}(s) = U(t,s)F(\mathbf{k})$ and $G_2^{\mathbf{k}}(s) = F(\mathbf{k}_t^s)$. We immediately see that

$$G_1^{\mathbf{k}}(t) = F(\mathbf{k}) = G_2^{\mathbf{k}}(t),$$

and after calculating couple of first derivatives we notice from the structure of the resulting equations that also

$$\left.\frac{d^n G_1^{\mathbf{k}}(s)}{ds^n}\right|_{s=t} = \left.\frac{d^n G_2^{\mathbf{k}}(s)}{ds^n}\right|_{s=t} \qquad n = 1, 2, 3, ...$$

Therefore, Eq. (2.49) is satisfied. Similarly, we also obtain

$$\frac{\partial}{\partial t} U(t,s)F(\mathbf{k}) \;\; = \;\; -i\hat{\mathcal{L}}(t)U(t,s)F(\mathbf{k}), \tag{2.50}$$

so that $f(\mathbf{k},t) = U(t,t_0)f_0(\mathbf{k}) = f_0(\mathbf{k}_t^{t_0})$ is the solution of the Boltzmann equation in the absence of scattering for the initial condition $f(\mathbf{k},t_0) = f_0(\mathbf{k})$. To prove that Eq. (2.36) is the solution of the Boltzmann equation in the presence of scattering, we first rewrite it with the help of time-evolution operator as

$$f(\mathbf{k},t) = e^{-(t-t_0)/\tau} U(t,t_0) f_0(\mathbf{k}) + \frac{1}{\tau}\int_{t_0}^{t} ds\; e^{-(t-s)/\tau} U(t,s) f_{eq}(\mathbf{k}), \tag{2.51}$$

and then find using Eq. (2.50)

$$\left[\frac{\partial}{\partial t} + i\hat{\mathcal{L}}(t)\right] f(\mathbf{k},t) \;\; = \;\; -\frac{f(\mathbf{k},t) - f_{eq}(\mathbf{k})}{\tau}.$$

Finally, we need to show Eq. (2.39) for the current density. We assume that the dispersion relation is periodic in all directions. This means that we take into account the band structure of the host crystals in y- and z-directions. In particular, we assume periods d_y and d_z in y- and z-directions,

respectively, which means that in the following equations the integration limits in k_y and k_z are $\pm\pi/d_y$ and $\pm\pi/d_z$, respectively. Because the periods can be arbitrarily small and the distribution function vanishes at large values of k_y and k_z, our approach is valid also for the dispersion relation given by Eq. (2.11). We can now expand all the functions in the Fourier basis $e^{i\mathbf{k}\cdot\mathbf{a_n}}$, where $\mathbf{a_n} = (n_1 d, n_2 d_y, n_3 d_z)$. By straightforward calculation we obtain

$$\int d^3k e^{-i\mathbf{k}\cdot\mathbf{a_n}} i\hat{\mathcal{L}}(t) e^{i\mathbf{k}\cdot\mathbf{a_{n'}}} = \int d^3k \Big[-i\hat{\mathcal{L}}(t) e^{i\mathbf{k}\cdot\mathbf{a_n}} \Big]^* e^{i\mathbf{k}\cdot\mathbf{a_{n'}}}, \tag{2.52}$$

which means that arbitrary real-valued functions $F(\mathbf{k},t) = \sum_{\mathbf{n}} F_n(t) e^{i\mathbf{k}\cdot\mathbf{a_n}}$ and $G(\mathbf{k},t) = \sum_{\mathbf{n}} G_n(t) e^{i\mathbf{k}\cdot\mathbf{a_n}}$ satisfy

$$\int d^3k \; F(\mathbf{k},t) i\hat{\mathcal{L}}(t) G(\mathbf{k},t) \;\; = \;\; \int d^3k \Big[-i\hat{\mathcal{L}}(t) F(\mathbf{k},t) \Big] G(\mathbf{k},t).$$

By using this result, we get

$$F(\mathbf{k})\hat{\mathcal{L}}(t_1)\hat{\mathcal{L}}(t_2)\cdots\hat{\mathcal{L}}(t_n)G(\mathbf{k}) = (-1)^n G(\mathbf{k})\hat{\mathcal{L}}(t_n)\cdots\hat{\mathcal{L}}(t_2)\hat{\mathcal{L}}(t_1)F(\mathbf{k}).$$

Therefore, if we define a new operator $U_2(t,s)$ as

$$U_2(t,s) = 1 + \sum_{n=1}^{\infty} i^n \int_t^s dt_1 \int_t^{t_1} dt_2 \cdots \int_t^{t_{n-1}} dt_n \hat{\mathcal{L}}(t_n)\cdots\hat{\mathcal{L}}(t_2)\hat{\mathcal{L}}(t_1), \tag{2.53}$$

we get

$$\int d^3k \; F(\mathbf{k}) U(t,s) G(\mathbf{k}) \;\; = \;\; \int d^3k \; G(\mathbf{k}) U_2(s,t) F(\mathbf{k}). \tag{2.54}$$

It turns out that

$$U_2(t,s) = U(t,s), \tag{2.55}$$

which can be easily checked by noticing that

$$\begin{aligned} U_2(t,t)F(\mathbf{k}) &= U(t,t)F(\mathbf{k}), \\ \frac{d^n}{ds^n} U_2(t,s)F(\mathbf{k})\Big|_{s=t} &= \frac{d^n}{ds^n} U(t,s)F(\mathbf{k})\Big|_{s=t} \qquad n = 1,2,3... \end{aligned}$$

Finally, the Eq. (2.39) follows from Eqs. (2.28) and (2.51) by using Eqs. (2.54)

and (2.55)

$$\begin{aligned}
\mathbf{j}(t) &= \frac{2e}{(2\pi)^3} e^{-(t-t_0)/\tau} \int d^3k\ \mathbf{v}(\mathbf{k}) U(t,t_0) f_0(\mathbf{k}) \\
&\quad + \frac{2e}{(2\pi)^3 \tau} \int d^3k\ \mathbf{v}(\mathbf{k}) \int_{t_0}^{t} ds\ e^{-(t-s)/\tau} U(t,s) f_{eq}(\mathbf{k}) \\
&= \frac{2e}{(2\pi)^3} e^{-(t-t_0)/\tau} \int d^3k\ f_0(\mathbf{k}) U(t_0,t) \mathbf{v}(\mathbf{k}) \\
&\quad + \frac{2e}{(2\pi)^3 \tau} \int d^3k\ f_{eq}(\mathbf{k}) \int_{t_0}^{t} ds\ e^{-(t-s)/\tau} U(s,t) \mathbf{v}(\mathbf{k}) \\
&= \frac{2e}{(2\pi)^3} e^{-(t-t_0)/\tau} \int d^3k\ f_0(\mathbf{k}) \mathbf{v}(\mathbf{k}^t_{t_0}) \\
&\quad + \frac{2e}{(2\pi)^3 \tau} \int d^3k\ f_{eq}(\mathbf{k}) \int_{t_0}^{t} ds\ e^{-(t-s)/\tau} \mathbf{v}(\mathbf{k}^t_s).
\end{aligned}$$

2.3.3 Static fields and Esaki-Tsu approach

In the case of static electric and magnetic fields, the stationary current $\mathbf{j}$ [Eq. (2.40)] and average miniband energy W [Eq. (2.41)] can be written as

$$\mathbf{j} = \frac{2e}{(2\pi)^3 \tau} \int d^3k\ f_{eq}(\mathbf{k}) \int_0^{\infty} ds\ e^{-s/\tau} \mathbf{v}(\mathbf{k}^s_0) \tag{2.56}$$

and

$$W = \frac{2}{(2\pi)^3 N_0 \tau} \int d^3k\ f_{eq}(\mathbf{k}) \int_0^{\infty} ds\ e^{-s/\tau} \varepsilon_x(\mathbf{k}^s_0) \tag{2.57}$$

In the limit of low temperature $T_e \to 0$ and low carrier density $N_0 \to 0$,

$$f_{eq} \approx 4 N_0 \pi^3 \delta(\mathbf{k}) \tag{2.58}$$

and the equations are equivalent with the approach used by Esaki and Tsu in their pioneering work [3]. Since then, Eq. (2.56) has been used frequently in the modelling of the electron dynamics in SLs. In the presence of magnetic field, the equation (2.56) was proven to be a solution of the Boltzmann equation by Bass *et al.* [82] using a time-evolution operator

$$U(0,s) = e^{i\hat{\mathcal{L}}s}.$$

This operator can be obtained as a special case of time-evolution operator (2.48), because for stationary fields the operator $\hat{\mathcal{L}}$ does not depend on time.

2.4 Esaki-Tsu characteristic and Tucker relations

In the absence of magnetic field ($\mathbf{B} = \mathbf{0}$), we obtain

$$\hbar\frac{d\mathbf{k}}{dt} = e\mathbf{E}(t) \qquad \text{i.e.} \qquad \mathbf{k}_s^t = \mathbf{k} + \frac{1}{\hbar}\int_s^t e\mathbf{E}(t')dt'. \tag{2.59}$$

Thus the steady-state current (2.40) is given by

$$\mathbf{j}(t) = \frac{2e}{(2\pi)^3\tau}\int d^3k\ f_{eq}(\mathbf{k})\int_{-\infty}^{t} ds\ e^{-(t-s)/\tau}\mathbf{v}\left(\mathbf{k} + \frac{1}{\hbar}\int_s^t e\mathbf{E}(t')dt'\right). \tag{2.60}$$

2.4.1 Esaki-Tsu characteristic

If a static electric field $E(t) = E_{dc}$ is applied along the SL direction, we get by assuming tight-binding SL [Eq. (2.12)] and using Eq. (2.60)

$$j_{dc}(eE_{dc}d) = j_p\frac{2eE_{dc}d/\Gamma}{1 + (eE_{dc}d)^2/\Gamma^2}. \tag{2.61}$$

Here $\Gamma = \hbar/\tau$ is the scattering induced broadening and

$$j_p = e\frac{\Delta d}{4\hbar}\frac{2}{(2\pi)^3}\int d^3k\ f_{eq}(\mathbf{k})\cos(k_x d) \tag{2.62}$$

is the peak current corresponding to the critical field $E_{dc} = E_{cr} \equiv \hbar/ed\tau$. Similarly, we get for the average miniband energy [Eq. (2.57)]

$$W_{dc} = -W_0\frac{1}{1 + (eE_{dc}d)^2/\Gamma^2}, \tag{2.63}$$

where

$$W_0 = \frac{1}{N_0}\frac{\Delta}{2}\frac{2}{(2\pi)^3}\int d^3k\ f_{eq}(\mathbf{k})\cos k_x d. \tag{2.64}$$

The Esaki-Tsu VI characteristic is plotted in Fig. 2.2 (a). The existence of the maximum current can be interpreted with the help of Bloch oscillations. If electric field is large enough $E_{dc} > E_{cr}$ ($\omega_B\tau > 1$), electrons reach the boundary of the Brillouin zone before scattering, and the current decreases with increasing electric field. On the other hand, the average miniband energy increases with increasing electric field [Fig. 2.2 (b)]. In the limit $E_{dc} \gg E_{cr}$, the electrons are uniformly distributed throughout the Brillouin zone, and therefore both the current j_{dc} and the miniband energy W_{dc} vanish. ($\varepsilon_x = 0$ at the center of the miniband.) The negative differential conductivity $dj_{dc}/dE_{dc} < 0$ makes SL inherently unstable with respect to space-charge

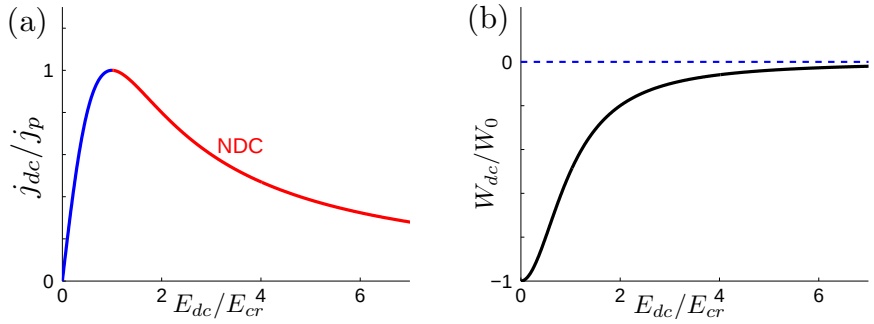

Figure 2.2: (a) Esaki-Tsu VI characteristic. (b) The average miniband energy W_{dc} as a function of E_{dc}.

fluctuations, resulting in formation of high-field electric domains [26, 27] (see Section 2.5). Although the formation of electric domains usually prevents the direct observation of Esaki-Tsu characteristic, a number of experiments (see e.g. [34, 35, 86, 87, 88, 89, 90, 91]) indicate that the Esaki-Tsu characteristic gives excellent approximation for the local electric field-drift velocity characteristic. Therefore, it is well-established that in the absence of electric domains the VI characteristic can be described with Eq. (2.61).

If we assume the nondegenerate equilibrium distribution (2.32), which is valid in typical experimental conditions, we obtain

$$j_p = eN_0 \frac{\Delta d}{4\hbar} \frac{I_1(\Delta/2k_BT_e)}{I_0(\Delta/2k_BT_e)} \tag{2.65}$$

and

$$W_0 = \frac{\Delta}{2} \frac{I_1(\Delta/2k_BT_e)}{I_0(\Delta/2k_BT_e)}. \tag{2.66}$$

The temperature dependence of the current [Eq. (2.65)] is in agreement with the experiment [92].

2.4.2 Tucker relations

In the case of time-dependent electric fields Eq. (2.60) has been frequently used to describe the dissipative electron dynamics in SLs since the works of Ignatov and Romanov [93]. The response to a general electric field considered here was found by Romanov *et al.* [94].

In the following, we consider the current density in the SL direction under an electric field

$$E(t) = E_{dc} + \sum_{k=1}^{N} E_{\omega_k} \cos(\omega_k t + \alpha_k) \tag{2.67}$$

applied along the SL direction $\mathbf{E} = (E(t), 0, 0)$. Assuming the dispersion relation (2.11), the semiclassical velocity [Eq. (2.14)] satisfies

$$v_x\left(k_x + \frac{1}{\hbar}\int_s^t eE(t')dt'\right) = \sum_{h=1}^{\infty} v_h\Big\{\sin(hk_xd)\cos\left(h\int_s^t \frac{eE(t')d}{\hbar}dt'\right) + \cos(hk_xd)\sin\left(h\int_s^t \frac{eE(t')d}{\hbar}dt'\right)\Big\}. \quad (2.68)$$

Because the equilibrium distribution is symmetric with respect to k_x, we obtain

$$\int d^3k\ f_{eq}(\mathbf{k})\sin(hk_xd) = 0. \quad (2.69)$$

By denoting

$$j_h = \frac{2e}{(2\pi)^3}\int d^3k\ f_{eq}(\mathbf{k})v_h\cos(hk_zd), \quad (2.70)$$

we can write the current density (2.60) as

$$j_x(t) = \sum_{h=1}^{\infty} j_h\int_{-\infty}^{t} ds\ \frac{1}{\tau}e^{-(t-s)/\tau}\sin\left(h\int_s^t \frac{eE(t')d}{\hbar}dt'\right). \quad (2.71)$$

By using similar tricks as in the derivation of Eqs. (2.19) and (2.20), we get

$$j_x(t) = \sum_{h=1}^{\infty} j_x^h(t), \quad (2.72)$$

where j_x^h is the component of the current caused by tunneling over h periods and is given by

$$j_x^h(t) = \sum_{n_1,\ldots,n_N=-\infty}^{\infty}\sum_{m_1,\ldots,m_N=-\infty}^{\infty}\Big[\prod_{k=1}^{N} J_{n_k}(h\beta_k)J_{n_k+m_k}(h\beta_k)\Big] \times\Big\{j_{dc}^h\big(eE_{dc}hd + \sum_{k=1}^{N} n_k\hbar\omega_k\big)\cos\big[\sum_{k=1}^{N} m_k(\omega_kt+\alpha_k)\big] + K^h\big(eE_{dc}hd + \sum_{k=1}^{N} n_k\hbar\omega_k\big)\sin\big[\sum_{k=1}^{N} m_k(\omega_kt+\alpha_k)\big]\Big\}. \quad (2.73)$$

Here $\beta_k = eE_{\omega_k}d/\hbar\omega_k$,

$$j_{dc}^h\big(eE_{dc}hd\big) = j_h\frac{eE_{dc}hd/\Gamma}{1+(eE_{dc}hd/\Gamma)^2} \quad (2.74)$$

and

$$K^h\big(eE_{dc}hd\big) = j_h\frac{1}{1+(eE_{dc}hd/\Gamma)^2}. \quad (2.75)$$

Eqs. (2.72) and (2.73) are equivalent with the expressions in Refs. [74, 83, 94].

In particular, for the tight-binding miniband (2.12) $v_1 = \Delta d/2\hbar$ and $v_h = 0$ $(h = 2, 3, 4....)$, we obtain

$$\begin{aligned} j_x(t) &= \sum_{n_1,...,n_N=-\infty}^{\infty} \sum_{m_1,...,m_N=-\infty}^{\infty} \Big[\prod_{k=1}^{N} J_{n_k}(\beta_k) J_{n_k+m_k}(\beta_k) \Big] \\ &\times \Big\{ j_{dc}\big(eE_{dc}d + \sum_{k=1}^{N} n_k \hbar\omega_k\big) \cos\big[\sum_{k=1}^{N} m_k(\omega_k t + \alpha_k)\big] \\ &+ K\big(eE_{dc}d + \sum_{k=1}^{N} n_k \hbar\omega_k\big) \sin\big[\sum_{k=1}^{N} m_k(\omega_k t + \alpha_k)\big] \Big\}, \quad (2.76) \end{aligned}$$

where $j_{dc}(eE_{dc}d) = j^1_{dc}(eE_{dc}d)$ is equivalent with the expression (2.61) and

$$K(eE_{dc}d) = K^1\big(eE_{dc}d) = j_1 \frac{1}{1 + (eE_{dc}d/\Gamma)^2} = j_p \frac{2}{1 + (eE_{dc}d/\Gamma)^2}. \quad (2.77)$$

In the case of tight-binding SLs, the relation (2.76) can also be derived with the approach based on SL balance equations [28] (see Section 2.4.6). The functions $K(eE_{dc}d)$ and $j_{dc}(eE_{dc}d)$ can be connected to each other with the help of Kramers-Kronig relation [28], and therefore the time-dependent current (2.76) is completely determined by the static VI characteristic $j_{dc}(eE_{dc}d)$. We find [95, 96] that exactly same relation (2.76) between the time-dependent current and the static VI characteristic can be derived using the Tucker theory [51] of sequential tunneling. Therefore, we call the relations obtained from Eq. (2.76) as Tucker relations. In the Tucker theory we should use instead of electric fields E_{dc} and E_{ω_k} the potential drop over the corresponding number of SL periods $eE_{dc}hd$ and $eE_{\omega_k}hd$. Therefore, we see that in the general case the total current [Eqs. (2.72) and (2.73)] is a sum of current components caused by tunneling over different number of SL periods, and each of these components [Eq. (2.73)] satisfies the Tucker relation separately.

It is important to notice that the transport mechanism in SLs depends on the relation of the relevant energy scales [28] (see Section 2.6). In the weakly coupled SLs $\Delta \ll \Gamma$ the miniband transport model is not valid, but instead the mechanism of transport is the sequential tunneling. However, as described above the same Tucker relation between the time-dependent current and static VI characteristic holds also in this case. Moreover, at least in particular limits the static VI characteristic in weakly coupled SLs can be approximated with the Esaki-Tsu characteristic with suitably chosen critical field and peak velocity [28]. Therefore, the steady-state time-dependent current in SLs under arbitrary homogeneous electric field $E(t)$ is qualitatively similar both in weakly and strongly coupled SLs.

2.4.3 Quasistatic limit

If the electric field varies slowly with respect to the scattering time $dE/dt \ll E_{cr}/\tau$, we can write

$$\begin{aligned} j_x(t) &= \sum_{h=1}^{\infty} j_h \int_{-\infty}^{t} ds\ \frac{1}{\tau} e^{-(t-s)/\tau} \sin\left(h \int_s^t \frac{eE(t')d}{\hbar} dt' \right) \\ &\approx \sum_{h=1}^{\infty} j_h \int_{-\infty}^{t} ds\ \frac{1}{\tau} e^{-(t-s)/\tau} \sin\left(h \frac{eE(t)d}{\hbar} (t-s) \right) \\ &= j_{dc}\big(eE(t)d\big), \end{aligned} \tag{2.78}$$

where $j_{dc}(eE_{dc}d)$ is the static VI characteristic for the appropriate dispersion relation. In the case of tight-binding SLs, $j_{dc}(eE_{dc}d)$ is given by Eq. (2.61). Therefore, we see that in the quasistatic limit the current adiabatically follows the instantaneous value of the electric field via the static VI characteristic. Other proofs of this very intuitive result for particular time-dependent field can be found e.g. from Refs. [51, 93, 97].

2.4.4 Photon-assisted transport

From now on we concentrate on the current (2.76) in the case of tight-binding dispersion relation. The generalization to arbitrary band structure is straightforward.

In the case of monochromatic field $E(t) = E_{dc} + E_\omega \cos\omega t$, we get from Eq. (2.76) [28, 93, 98, 99]

$$j_x^\omega(t) = j_{dc}^\omega + \sum_{n=1}^{\infty} [j_n^{\omega,\cos} \cos(n\omega t) + j_n^{\omega,\sin} \sin(n\omega t)], \tag{2.79}$$

$$j_{dc}^\omega = \sum_{l=-\infty}^{\infty} J_l^2(\beta) j_{dc}(eE_{dc}d + l\hbar\omega), \tag{2.80}$$

$$j_n^{\omega,\cos} = \sum_{l=-\infty}^{\infty} J_l(\beta)[J_{l+n}(\beta) + J_{l-n}(\beta)] j_{dc}(eE_{dc}d + l\hbar\omega), \tag{2.81}$$

$$j_n^{\omega,\sin} = \sum_{l=-\infty}^{\infty} J_l(\beta)[J_{l+n}(\beta) - J_{l-n}(\beta)] K(eE_{dc}d + l\hbar\omega). \tag{2.82}$$

Here we discuss only the dc current given by Eq. (2.80). The other Fourier components, determining the absorption and the harmonic generation, will be considered in Chapters 3 and 4. It can be seen from Eq. (2.80) that the VI characteristic in the presence of ac field is given by a sum of shifted Esaki-Tsu characteristics. The shifts correspond to a potential drop $eE_{dc}d$ equal to integer number of photon quanta $l\hbar\omega$, and therefore the functions $j_{dc}(eE_{dc}d + l\hbar\omega)$

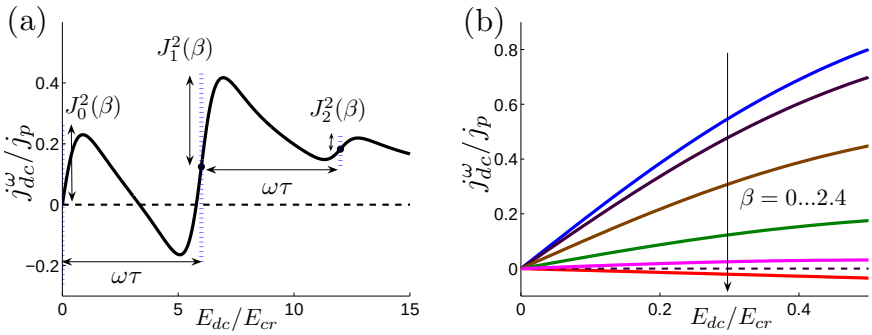

Figure 2.3: (a) VI characteristic for $\omega\tau = 6$ and $E_\omega = 9E_{cr}$ revealing two photon-assisted peaks at $E_{dc}/E_{cr} = l\omega\tau + 1$ ($l = 1, 2$). (b) VI characteristic for $\omega\tau = 4$ and $E_\omega/E_{cr} =: 0, 2, 4, 6, 7.5, 9.6$. The last amplitude ($\beta = 2.4$) corresponds approximately to the condition of dynamic localization $J_0(\beta) \approx 0$.

are called photon replicas [100]. The expression (2.80) for the VI characteristic is well-known from the so-called Tien-Gordon model [101, 102], where one considers tunneling over a single potential barrier. There, the coefficients $J_l(\beta)$ define the probability amplitudes of net l photon transitions to virtual states [56, 103]. After absorption of l photons the electrons effectively experience a potential difference $eE_{dc}d + l\hbar\omega$ across the barrier instead of the bare potential drop due to the dc bias.

In the case of SLs with Esaki-Tsu static VI relation (2.61), the opening of new transport channels involving the absorption and emission of photons [Eq. (2.80)] results in photon-assisted peaks in the VI characteristic at dc bias values $eE_{dc}d = l\hbar\omega + \Gamma$ ($E_{dc}/E_{cr} = l\omega\tau + 1$). The magnitudes of these peaks are proportional to $J_l^2(\beta)$. Such kind of structures are illustrated in Fig. 2.3 (a). One of the peculiar features resulting from Eq. (2.80) is the existence of absolute negative conductance (ANC) i.e. the direction of the current is opposite to the direction of the static force. This effect occurs typically at dc bias values $eE_{dc}d \approx l\hbar\omega - \Gamma$ as illustrated in Fig. 2.3 (a). Near the Bessel roots $J_0(\beta) \approx 0$ the ANC can exist also at small values of dc bias as illustrated in Fig. 2.3 (b). The suppression of the dc current and the ANC at small dc bias in the vicinity of $J_0(\beta) \approx 0$ can be attributed to the collapse of the main transport channel ($l = 0$) so that only the transport channels involving absorption/emission of photons contribute to the current.

The Tien-Gordon picture gives natural explanation for the Eq. (2.80) in the case of sequential tunneling. However, we underline that the same equation is valid also for coherent miniband transport in the presence of weak scattering. In this picture the effect has nice analogy with the Shapiro-like steps occurring in Josephson junctions [44, 56]. It has been found, by

studying the distribution function $f(\mathbf{k}, t)$, that in the vicinity of resonances $\omega_B = n\omega$ ($\omega_B\tau \gg 1$) the electrons bunch together in the quasimomentum space [104]. This electron bunch performs Bloch oscillations, which are synchronized with the ac field. The phase of the oscillations of the bunch in the quasimomentum space is controlled by $\omega_B - n\omega$, resulting in peaks in the VI characteristic proportional to $J_n(\beta)$ [104, 105] [see Fig. 2.3 (a)]. If $J_n(\beta) = 0$, the current at dc bias $\omega_B \approx n\omega$ vanishes due to the dynamic localization (see Section 2.2). The strong suppression of the current and ANC at small dc bias values in the vicinity of $J_0(\beta) \approx 0$ [see Fig. 2.3 (b)] also result from the dynamic localization. It should be noticed that the dynamic localization only works if $\omega\tau \gtrsim 1$. In the quasistatic limit $\omega\tau \ll 1$ [Eq. (2.78)], we also find suppression of the low field current, but with different characteristic features [106] [see Fig. 2.5 (b)]. In particular, the location of peak current in the VI characteristic just shifts towards larger applied dc bias with increasing E_ω and ANC does not occur for any ac field amplitude.

In the above discussion one should bear in mind that in conditions of NDC, the space-charge fluctuations tend to grow resulting in formation of electric domains (see Section 2.5). Therefore, the observation of the structures described above is difficult, and it is expected that space-charge inhomogeneities play at least some role in almost all typical experimental conditions. The photon-assisted transport, dynamic localization and ANC have been subjects of intensive investigations both theoretically and experimentally. Some of the theoretical studies, including prediction of photon-assisted transport and ANC, using the miniband transport model can be found from Refs. [28, 93, 98, 100, 107]. The photon-assisted tunneling and ANC, including multi-photon processes, have been experimentally observed in weakly coupled SLs [108] nicely in agreement with the theory [28, 109]. The photon-assisted peaks in the miniband transport regime have also been observed [44], but in this case the results are less clear probably due to more important role of the space-charge inhomogeneities. The suppression of low-field current by using both quasistatic and high-frequency fields has been reported in excellent agreement with the theory [106].

2.4.5 Coherent control of photon-assisted transport

In the case of polychromatic field (2.67), where the frequencies satisfy a resonance condition

$$\sum_{k=1}^{N} l_k \omega_k = 0, \tag{2.83}$$

also a phase-dependent dc current arises [95]. Such kind of current appears due to harmonic mixing, and exists also in unbiased symmetric SL. In the Tien-Gordon model the probability amplitudes for transitions to vir-

tual states should be calculated as a sum of all optical pathways leading to absorption/emission of same amount of energy, and it turns out that the dc current appears due to asymmetry between absorption and emission processes caused by quantum interference [95]. In addition to SLs [95, 110] the dc current due to harmonic mixing has been studied in many other systems (see e.g. Refs. [111]). In general, the possibility of directed transport without directed force is known as a ratchet effect [112] and requires that relevant spatiotemporal symmetries of the system are violated [113].

2.4.6 Balance equations and effect of elastic scattering

Alternatively to the path-integral approach (2.60), the current density in a homogeneous SL in the tight-binding approximation (2.12) for $\mathbf{B} = \mathbf{0}$ and $\mathbf{E} = (E(t), 0, 0)$ can be calculated from the so-called SL balance equations [93]. These balance equations are differential equations for the average electron velocity

$$V(t) = \frac{2}{(2\pi)^3 N_0} \int_{-\infty}^{\infty}\int_{-\infty}^{\infty} dk_y dk_z \int_{-\pi/d}^{\pi/d} dk_x \; v_x(k_x) f(\mathbf{k}, t) \tag{2.84}$$

and average miniband energy $W(t)$ [Eq. (2.28)]. By a direct calculation using the Boltzmann equation (2.29) and relaxation time approximation with two relaxation rates (2.34), one obtains [28, 93]

$$\begin{aligned} \frac{dV}{dt} &= -\frac{d^2 eE(t)}{\hbar^2} W(t) - \gamma_v V(t) \\ \frac{dW}{dt} &= eE(t)V(t) - \gamma_w (W + W_0), \end{aligned} \tag{2.85}$$

where $\gamma_v = \tau_{\mathrm{in}}^{-1} + \tau_{\mathrm{el}}^{-1}$, $\gamma_w = \tau_{\mathrm{in}}^{-1}$ and W_0 is defined as (2.64). The miniband energy in thermal equilibrium in the absence of electric field is $W_{eq} = -W_0$. By defining the effective mass of the electrons as

$$M^{-1}(t) = \frac{2}{(2\pi)^3 N_0} \int_{-\infty}^{\infty}\int_{-\infty}^{\infty} dk_y dk_z \int_{-\pi/d}^{\pi/d} dk_x \; m_{x,\mathbf{k}}^{-1} f(\mathbf{k}, t) = -\frac{d^2}{\hbar^2} W(t), \tag{2.86}$$

we see that Eqs. (2.85) can be written in the form of standard Newton equations, but with time-dependent mass. However, one should keep in mind that these equations really describe the dynamics of quantum particles in tight-binding miniband, where Bragg reflections are also included with an assumption that $f(-\pi/d, k_y, k_z) = f(\pi/d, k_y, k_z)$. Moreover, this kind of balance equations are equivalent with the Boltzmann equation only in the absence of magnetic field.

If static electric field $E = E_{dc}$ is applied, the current density $j_{dc} = eN_0V$ is still described by Esaki-Tsu characteristic [Eq. (2.61)] [93, 114], where $\Gamma = \hbar/\tau$, $\tau = 1/\sqrt{\gamma_v\gamma_w}$ and

$$j_p = eN_0\sqrt{\frac{\gamma_w}{\gamma_v}}\frac{W_0 d}{2\hbar}. \tag{2.87}$$

The magnitude of the peak current is decreased by the additional factor $\sqrt{\frac{\gamma_w}{\gamma_v}}$ in comparison with Eq. (2.62). In the limit $\tau_{\rm el} \to \infty$, the definitions of j_p and τ reduce to the results obtained in the case of single scattering time. In general, the elastic scattering tends to distribute the carriers uniformly in the Brillouin zone resulting in suppression of both dc current and current oscillations [115].

2.5 Domain instability in conditions of NDC

If the electron distribution is not spatially homogeneous, the semiclassical miniband dynamics in the mean field approximation can be described with Boltzmann transport equation (2.27) and Poisson equation. If the electric field is slowly varying in both space and time, the so-called drift-diffusion model can be derived from these equations by using the relaxation time approximation for the scattering [29, 30, 116]

$$\begin{aligned} j(x,t) &= eN_eV(E) - eD(E)\frac{\partial N_e}{\partial x}, \\ e\frac{\partial N_e}{\partial t} &= -\frac{\partial j}{\partial x}, \\ \frac{\partial E}{\partial x} &= \frac{e}{\epsilon\epsilon_0}(N_e - N_0). \end{aligned} \tag{2.88}$$

Here the first equation describes a current due to drift and diffusion. The average drift velocity $V(E)$ is given by the Esaki-Tsu relation

$$V(E) = V_p\frac{2E/E_{cr}}{1+(E/E_{cr})^2}, \qquad V_p = j_p/N_0e \tag{2.89}$$

and the diffusion coefficient $D(E)$ has quite complicated field dependence [29, 30, 116]. In particular limits $D(E)$ reduces to the Einstein relation [29, 30, 116]

$$D(E) = \frac{k_BT}{e}\frac{V(E)}{E}. \tag{2.90}$$

The second and third equation in (2.88) are the standard continuity and Poisson equation, respectively. The electric field in all equations is the local value at a given time $E = E(x,t)$.

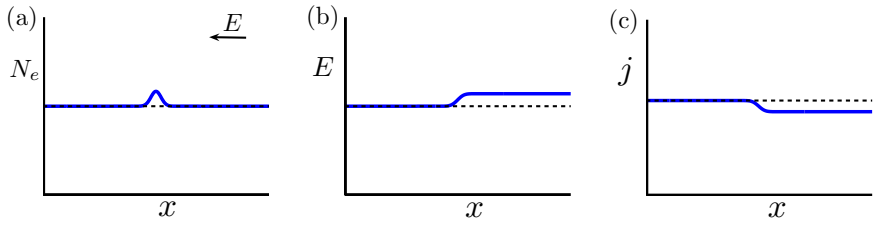

Figure 2.4: The principle of the growth of the inhomogeneties in NDC materials.

Let's start with a consideration of the dc biased SL, which now corresponds to a constant voltage applied over the SL so that the average electric field is $E = E_{dc}$. By linearizing these equations with a substitution $N_e = N_0 + \delta N e^{-i(\omega t - kx)}$, $E = E_{dc} + \delta E e^{-i(\omega t - kx)}$, $V = V(E_{dc}) + \delta V e^{-i(\omega t - kx)}$ and $j = eN_0 V(E_{dc}) + \delta j e^{-i(\omega t - kx)}$, one obtains a dispersion relation for drift-diffusion instability (convective space-charge wave) [27, 29, 30, 116]

$$\omega = kV(E_{dc}) + i\left[- \frac{\sigma_{dc}(E_{dc})}{\epsilon\epsilon_0} - D(E_{dc})k^2 \right], \tag{2.91}$$

where

$$\sigma_{dc}(E_{dc}) = eN_0 \frac{\partial V(E_{dc})}{\partial E_{dc}} \tag{2.92}$$

is the dc differential conductivity. The system is obviously stable against the formation of the high field domains if dc differential conductivity is positive. However, in conditions of NDC the long wavelength $k \approx 2\pi/L$ (L is the length of the SL) fluctuations tend to grow, resulting in formation of electric domains. The time scale for domain formation is

$$\tau_d = \frac{\epsilon\epsilon_0}{|\sigma_{dc}(E_{dc})|}. \tag{2.93}$$

The formation of the electric domains can be understood with the help of schematic picture shown in Fig. 2.4. Consider a small fluctuation (accumulation) in the carrier density depicted in Fig. 2.4 (a). The electric field grows at the accumulation layer according to the Poisson equation [see Fig. 2.4 (b)], resulting in decrease of current due to NDC [see Fig. 2.4 (c)]. This means that more electrons are flowing into the accumulation than coming out of it, so that the accumulation tends to grow up in time. The growth of the fluctuations finally leads to formation of electric domains i.e. regions with different internal fields [27, 29, 30, 116].

Much of the research efforts in this thesis is concentrated in trying to find schemes and regimes where the domains do not form (see Chapters 3, 4 and 5). One very useful concept in our suggestions for the suppression of the domain formation is the limited space charge accumulation mode, which will be considered next.

2.5.1 Limited space charge accumulation mode

We now turn to the consideration of electric stability in the presence of time-dependent periodic electric field $E_p(t)$. We first assume that the electric field is quasistatic, so that the drift velocity follows adiabatically the instantaneous value of the electric field via the Esaki-Tsu characteristic as described in Eq. (2.78). Since the field changes slowly, the drift-diffusion model can be used to calculate the growth factor at each given moment of time. Therefore, the amplitude A of the long wavelength fluctuations ($k \to 0$) is determined by equation

$$\frac{dA(t)}{dt} = -\frac{\sigma_{dc}(E_p(t))}{\epsilon\epsilon_0} A(t). \tag{2.94}$$

During a single period T of the electric field $E_p(t)$, the amplitude changes as

$$A(T) = A(0) \exp\left[-\int_0^T dt' \, \frac{\sigma_{dc}(E_p(t'))}{\epsilon\epsilon_0} \right]. \tag{2.95}$$

Thus in the presence of electric field $E_p(t) = E_{dc} + E_{ac}(t)$, where $E_{ac}(t)$ is a low-frequency ac field, the growth of the space-charge fluctuations is still controlled by the dc differential conductivity

$$\sigma^p_{dc}(E_{dc}) = \int_0^T dt' \, \sigma_{dc}(E_p(t')) = \frac{d}{dE_{dc}} \int_0^T dt' \, eN_0 V_{dc}(E_p(t')) = \frac{dj^p_{dc}}{dE_{dc}}, \tag{2.96}$$

where j^p_{dc} is now the time-average of the current density over the period of the electric field. In addition to the condition $\sigma^p_{dc} > 0$ the suppression of the formation of electric domains requires that $T \ll \tau_d$. This means the accumulation of charge during a single period of the ac field is always weak, so that the linear stability analysis used above is well-justified. If both these conditions are satisfied, the device operates in the so-called limited space charge accumulation (LSA) mode introduced by J. A. Copeland [117].

The principle of the Copeland's LSA mode becomes apparent by considering an electric field $E(t) = E_{dc} + E_\omega \cos \omega t$, where $\omega\tau \ll 1$ [Fig. 2.5 (a)]. If we now assume that $E_\omega > E_{dc} - E_{cr}$ the field dips during each cycle to the low values, where the current-field characteristic has a positive slope. The strong ac field modifies the VI characteristic $j^\omega_{dc}(eE_{dc}d)$, determined by Eq. (2.80), by shifting the peak current towards larger E_{dc} [Fig. 2.5 (b)]. Therefore, if E_{dc} is fixed and the amplitude of the ac field is sufficiently strong $E_\omega > E_{dc} - E_{cr}$ the dc differential conductivity dj^ω_{dc}/dE_{dc} at the operation point becomes positive. If significant fluctuations are not formed during the NDC part of the cycle, our linear stability analysis is valid, and the inhomogeneities will decay during the PDC part. From the practical viewpoint, the electric field can be considered homogeneous during the whole cycle.

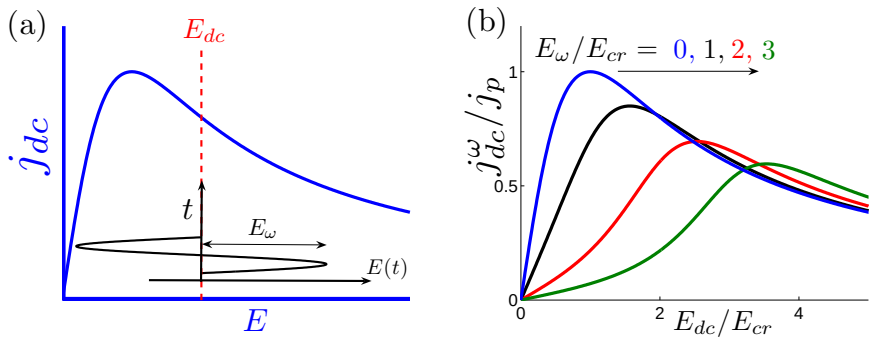

Figure 2.5: (a) Principle of Copeland's LSA operation mode. Strong quasistatic ac field ($\omega\tau \ll 1$) causes the total field to dip, during each cycle, to low values of electric field, where Esaki-Tsu characteristic has a positive slope. The domains formed at the NDC part of the cycle decay during the PDC part. (b) The ac field results in shift of the peak current towards larger E_{dc} in the VI characteristic. In conditions of LSA, the operation point is in the PDC part of the modified VI characteristic.

2.5.2 Kroemer's criterion of electric stability

Although the drift-diffusion model and the LSA condition derived above are valid only if the electric field is slowly varying, the physical picture shown in Fig. 2.4 suggest that the domain formation is controlled by the slope of the time-average VI characteristic also at frequencies $\omega\tau > 1$. This generalized assumption was proposed by Kroemer [100], and although the rigorous analytical treatment of the linear stability in the presence of high-frequency electric field $\omega\tau > 1$ is rather difficult problem, the numerical simulations with Boltzmann equation confirm the Kroemer's hypothesis [30, 118]. Therefore, throughout this thesis, we assume that the conditions of LSA at a given operation point are

$$\frac{dj^p_{dc}}{dE_{dc}} > 0 \qquad \text{and} \qquad T \ll \tau_d, \tag{2.97}$$

where j^p_{dc} is the VI characteristic in the presence of electric field $E_p(t) = E_{dc} + E_{ac}(t)$ and $E_{ac}(t)$ is ac field with period T.

The Kroemer's generalization of the LSA conditions allow a new mechanism for domain suppression based on photon-assisted transport [100]. As was discussed in Section 2.4.4 the strong high-frequency ac field $E_\omega \cos\omega t$ ($\omega\tau \gtrsim 1$) results in photon-assisted peaks in the VI characteristic, so that PDC ($dj^\omega_{dc}/dE_{dc} > 0$) can exist for a range of dc bias values, where the Wannier-Stark spacing approximately equals an integer number of photon quanta $|eE_{dc}d - l\hbar\omega| < \Gamma$ ($l = 1, 2, 3...$).

It should be emphasized that in the above analysis we have assumed a spatially homogeneous electric field throughout the SL, and considered only the instability with respect to small fluctuations. However, to ensure the current continuity through the interface of the SL and contact, the electric field values inside the contacts are typically much smaller than inside the SL. Therefore, there must be a SL-to-contact transition region, where the field changes from these low values inside the contacts to the large values inside the SL. Importantly, the linear stability analysis presented above is obviously not valid in this transition region. As pointed out by Kroemer [100], this is typically a relatively inconsequential problem in PDC material, but in the case of Kroemer's LSA mode the VI characteristic at the electric field values below the operation point E_{dc} contains structures, including regions of NDC, which may potentially cause problems from the viewpoint of domain suppression [30, 100] (see Chapter 6 for further discussion).

2.6 The limits of miniband transport model

Historically three different approaches have been used to describe electron transport in dc biased SLs: miniband conduction, sequential tunneling and Wannier-Stark hopping [28]. The appropriate transport mechanism is determined by the relations of the energy scales Γ, $eE_{dc}d$ and Δ [28]. The miniband conduction and sequential tunneling have clearly distinct regimes of validity. The semiclassical miniband transport requires that the miniband width is much larger than the other energy scales $\Delta \gg eE_{dc}d$ and $\Delta \gg \Gamma$, whereas the sequential tunneling is applicable if $\Delta \ll eE_{dc}d$ or $\Delta \ll \Gamma$. The Wannier-Stark hopping provides a complementary picture to these other approaches in the NDC part of the VI characteristic $eE_{dc}d \gg \Gamma$. Recently, it was shown that a quantum transport model based on nonequilibrium Green functions reproduces the results of all three conventional theories in the appropriate limits [28, 119]. Another theoretical achievement in the unification of the different transport mechanisms was already discussed in Section 2.4.2. Namely, the different approaches give qualitatively similar results for the steady-state current under time-dependent spatially homogeneous electric field [28, 95, 96]. For both miniband transport and sequential tunneling models, the static VI characteristic is approximately described by the Esaki-Tsu relation and the dependence of the time-dependent current on the static VI characteristic is described by the Tucker relation (2.76).

In this thesis only the miniband transport model is used in calculations. Because we are using simple phenomenological scattering terms, we do not expect a complete quantitative agreement between the theory and possible experiments. However, reasonable agreement may be obtained if the time-dependent electric field $E(t) = E_{dc} + E_\omega \cos \omega t$ and magnetic fields

$\mathbf{B} = (B_x, 0, B_z)$ satisfy the requirements of the semiclassical dynamics given in Section 2.2, $eE_{dc}d, eE_{\omega}d, \hbar\omega_c, \hbar\omega_{c\perp}, \hbar\omega \ll \Delta, \Delta_g$, and the scattering can be considered as a weak perturbation $\Gamma \ll \Delta$. Also the length of the SL should be large compared to the SL period. We proceed by studying in the next Chapter the parametric amplification and Bloch gain in spatially homogeneous SLs. In these considerations we utilize the Tucker relations, and therefore our results are qualitatively applicable also to weakly coupled SLs. On the other hand, it is expected that the weakly and strongly coupled SLs behave in a qualitatively different way in the presence of space-charge inhomogeneities [29] or magnetic field [120]. Therefore, the validity of the results obtained in presence of magnetic field in Chapter 5 probably requires that all the conditions discussed above are at least approximately satisfied.

Chapter 3

New approaches to Bloch oscillator

3.1 Bloch gain

The idea of a THz Bloch oscillator is as old as the concept of SL itself: The patent for SL Bloch oscillator was in fact applied already before the first paper about SLs was published (see [4] p. 977). The small-signal gain resulting from the Bloch oscillations of the miniband electrons in homogeneous SL in the presence of weak scattering was first calculated using the semiclassical approach by Ktitorov *et al.* [19]. Later, the problem has been revisited in a number of papers including also the investigations of large-signal Bloch gain (see e.g. [56, 80, 93, 94, 98, 100, 104]). In general, to find the gain or absorption of a probe field $E_\omega \cos \omega t$ in the presence of some arbitrary pump field $E_p(t)$, we need to calculate the steady-state time-dependent current under the electric field $E(t) = E_p(t) + E_\omega \cos \omega t$. In the case of oscillator, the frequency ω is fixed by an external circuit (external cavity). The gain and absorption are determined by the real part of the dynamical conductivity

$$\mathrm{Re}[\sigma(\omega)] = \frac{2\langle j_x(t) \cos \omega t \rangle}{E_\omega}, \tag{3.1}$$

where $\langle ... \rangle$ denotes the time-average. Gain corresponds to $\mathrm{Re}[\sigma(\omega)] < 0$. In the figures presented in this thesis we always scale the dynamical conductivity with the Drude conductivity $\sigma_0 = 2j_p/E_{cr}$. The magnitude of the gain α (in units cm^{-1}) is related to the scaled dynamical conductivity as [62]

$$\alpha(\omega) = \alpha_0 \frac{\mathrm{Re}[\sigma(\omega)]}{\sigma_0}, \tag{3.2}$$

where

$$\alpha_0 = \frac{1}{\epsilon_0 \epsilon^{1/2} c} \frac{2j_p}{E_{cr}}, \tag{3.3}$$

ϵ is the relative permittivity, ϵ_0 is the permittivity of the vacuum and c is the speed of light in the vacuum. Assuming that j_p is determined by Eq. (2.65), we get by using typical SL parameters $\epsilon \approx 13$ (GaAs), $d = 6$ nm, $\Delta = 60$ meV, $\tau = 2 \cdot 10^{-13}$ s and moderate doping $N_0 = 10^{16}$ cm^{-3}, that $\alpha_0 \approx 417$ cm^{-1} at room temperature ($T_e = 300$ K) and $\alpha_0 \approx 833.5$ cm^{-1} at low temperatures ($T_e = 0$ K). These values can be used to estimate the magnitudes of the gain in all the figures. Larger magnitudes of the gain can be obtained by using more heavily doped SLs.

Although the original result for the Bloch gain in dc biased SL, $E(t) = E_{dc} + E_\omega \cos \omega t$, in Ref. [19] was derived using the relaxation time approximation with two relaxation rates [Eq. (2.34)], all the main features can already be described using the single relaxation time approximation [Eq. (2.33)]. In this case we obtain using Eq. (2.81)

$$\mathrm{Re}[\sigma(\omega)] = \frac{1}{E_\omega} \sum_{l=-\infty}^{\infty} J_l(\beta)[J_{l+1}(\beta) + J_{l-1}(\beta)] j_{dc}(eE_{dc}d + l\hbar\omega), \tag{3.4}$$

where $\beta = eE_\omega d/\hbar\omega$. In the limit of weak probe field $\beta \ll 1$, we get the Tucker formula [28, 50, 51, 121]

$$\mathrm{Re}[\sigma(\omega)] = \frac{j_{dc}(eE_{dc}d + \hbar\omega) - j_{dc}(eE_{dc}d - \hbar\omega)}{2\hbar\omega} ed. \tag{3.5}$$

In the limit of low-frequency $\omega\tau \ll 1$, we see that the dynamical conductivity reduces to the dc differential conductivity at the given operation point $\mathrm{Re}[\sigma(\omega)] = \sigma_{dc}(E_{dc})$. Fig. 3.1 (a) shows the Esaki-Tsu VI characteristic and illustrates the geometric meaning of the Tucker formula for an operation point $\omega_B\tau = 6$ and high-frequency probe field $\omega\tau = 4.8$. By utilizing this kind of graphical interpretation of Eq. (3.5), it is easy to figure out the shapes of the gain profiles also at other operation points marked in Fig. 3.1 (a). In the limit of weak dc bias $\omega_B\tau \ll 1$, one obtains from Eq. (3.5) the standard free-electron absorption

$$\mathrm{Re}[\sigma^{\mathrm{free}}(\omega)] = \sigma_0 \frac{1}{1 + \omega^2\tau^2}, \tag{3.6}$$

which is plotted in Fig. 3.1 (b) [line (i)]. The free-electron absorption is always positive with a maximum at low frequencies $\mathrm{Re}[\sigma^{\mathrm{free}}(\omega)] = \sigma_0$ and power-like decay $\mathrm{Re}[\sigma^{\mathrm{free}}(\omega)] \approx \sigma_0/\omega^2\tau^2$ at large frequencies $\omega\tau \gg 1$. If the dc bias is increased so that $\omega_B\tau = 1$ ($E_{dc} = E_{cr}$), we see [Fig. 3.1 (b), line (ii)] that the absorption profile becomes modified. At low-frequencies $\omega\tau \to 0$, we have $\mathrm{Re}[\sigma(\omega)] = 0$, but still $\mathrm{Re}[\sigma(\omega)] \geq 0$ at all frequencies. If $\omega_B\tau > 1$, the gain start to appear. First the gain occurs at low-frequencies, and the upper limit of the gain

$$\min\{\mathrm{Re}[\sigma(\omega)]\} = -1/8$$

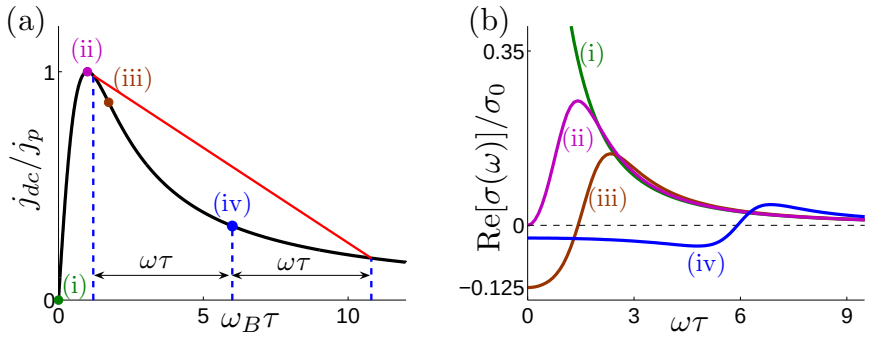

Figure 3.1: (a) Esaki Tsu VI characteristic and demonstration of the geometric meaning of the Tucker formula [Eq. (3.5)]. At the operation point $\omega_B\tau = 6$, the gain at frequency $\omega\tau = 4.8$ is proportional to the slope of the inclined (red) segment. (b) Absorption and gain profiles at the operation points (i) $\omega_B\tau = 0$, (ii) $\omega_B\tau = 1$, (iii) $\omega_B\tau = \sqrt{3}$ and (iv) $\omega_B\tau = 6$.

is achieved at $\omega_B\tau = \sqrt{3}$ [Fig. 3.1 (b), line (iii)], where the Esaki-Tsu characteristic has the steepest negative slope [Fig. 3.1 (a)]. With further increase of $\omega_B\tau$, the electrons perform several cycles of Bloch oscillations between the scattering events, and one obtains the so-called Bloch gain profile, which is shaped as a familiar dispersion curve [see Fig. 3.1 (b), line (iv)]. In the limit $\omega_B\tau \gg 1$, the crossover from gain to loss occurs at the Bloch frequency $\omega \approx \omega_B$ and the maximum of the Bloch gain $\mathrm{Re}[\sigma(\omega)] \approx -\sigma_0/4(\omega_B\tau - 1)$ is obtained at frequency $\omega \approx \omega_B - 1/\tau$. By studying the distribution function in the semiclassical picture, it has been shown that the dispersive Bloch gain profile near $\omega \approx \omega_B$ occurs because the electrons bunch together in the quasimomentum space forming a ballistic-like **k**-space wave, which performs Bloch oscillations at frequency ω synchronized with the ac field [80, 104]. Both scattering and the probe field play an important role in the formation of the electron bunches. Alternatively to the semiclassical picture, the Bloch gain has also been explained in terms of scattering-assisted transitions in the quantum mechanical Wannier-Stark picture [62]. The attractive properties of the Bloch gain are the tunability of the gain profile with the dc bias E_{dc} and smooth temperature dependence resulting in significant gain also at room temperature.

Despite the optimistic theoretical predictions and intensive experimental investigations a true cw Bloch oscillator has not yet been realized. The reason is that the Bloch gain occurs only if the operation point is in the NDC part of the VI characteristic [see Fig. 3.1 (a)]. In the gain profiles this means that the negative dynamical conductivity extends to the low frequencies [see Fig. 3.1 (b)]. Therefore, as discussed in Section 2.5, the homogeneous field profile is unstable with respect to small fluctuations in the space-charge distribution,

resulting in the formation of domains of high electric field inside the SL. These electric domains destroy the key ingredient of the Bloch gain, the homogeneous electric field resulting in synchronized Bloch oscillations, and they are probably one of the main reasons for the failure so far to observe net Bloch gain in SLs.

On the other hand, it is still potentially possible to avoid the formation of the electric domains in SL, if the amplified THz signal has large enough amplitude [100]. In this case, the gain can be obtained in conditions of PDC, because the ac field induces photon-assisted peaks in the VI characteristic as discussed in Section 2.4.4. This possibility is illustrated in Paper VI in Fig. 4 using Eqs. (2.80) and (3.4), and in Fig. 11 using the relaxation time approximation with two scattering rates [Eq. (2.34)]. Because the probe frequency is in THz range, the other LSA condition $\omega\tau_d \gg 1$ is also satisfied even for relatively large doping, in principle enabling large values of THz gain. This finding can potentially be used for the construction of large-signal amplifier. However, to realize a THz oscillator, it is still necessary to understand how to avoid the destructive electric domains at small amplitudes in order to reach the large-amplitude regime supporting the stable operation of the device. This is known as the device-turn-on problem for THz Bloch oscillator [100].

In recent years, a number of interesting suggestions to avoid the electric instability have been put forward. One possibility is to investigate the Bloch gain during a short time window after an optical excitation of carriers to the SL miniband, so that the domains do not have enough time to build up. Recently, the THz radiation emitted during the transient Bloch oscillations in this type of experiment was interpreted as an experimental evidence of the Bloch gain [122]. This observation is in excellent agreement [123] with the analysis of transient oscillations using the Boltzmann equation with two scattering rates [Eq. (2.34)] [114]. However, several groups [124, 125] have independently questioned the possibility of determining the small-signal dynamic conductivity from the analysis of the emitted coherent THz pulse. In Ref. [124] the authors demonstrated both in the semiclassical picture and in the full quantum mechanical picture that the transient Bloch oscillations do not provide convincing information about the steady-state Bloch gain. Thus, there is still no clear experimental proof of terahertz Bloch gain in optically excited SLs. Such kind of evidence could, however, be obtained by measuring the transmission of an externally applied THz field. In contrast to the usual Bloch gain discussed above, it has been predicted that the Bloch gain in undoped optically excited SLs arises due to exciton-induced asymmetry between the absorption and emission events [126].

Another interesting approach to obtain Bloch gain in the absence of electric domains is to use short SLs, where the domains do not have enough space to build up. Recently, a so-called super-superlattices, consisting of

a stack of short SLs interrupted by heavily doped AlAs regions, have been constructed for this purpose [31]. Although, an increase in THz transmission with applied bias has been observed in this system [31], the effect is still too weak to be considered as a direct experimental evidence of *net* Bloch gain. Moreover, although it is well-known that the electric field profile in a short SL can be stable, the electric field is also necessarily rather inhomogeneous: the electric field must have small values near the boundaries of the SL to ensure the current continuity at the interfaces. Therefore, a detailed modelling of the effect of the inhomogeneities on the THz gain is needed in order to understand, whether net gain can be achieved in this kind of system.

Another approach considered experimentally for suppression of the electric instability is to work with two-dimensional structures, where the domain instability is effectively more suppressed in comparison with the case of three-dimensional structures [127]. With this aim a lateral surface SL shunted by another SL has been introduced as an active material for future realization of the Bloch oscillator [90, 120]. It has been theoretically predicted that also the use of a shunt can stabilize the SL against the formation of the electric domains [128]. At least theoretically, it is possible to obtain a high-frequency gain in conditions of PDC also by engineering the miniband dispersion relations in SLs [129], using a hot electron injection into a miniband [130], or utilizing the interminiband tunneling in SLs with narrow energy gaps [131].

In Papers VI-VIII we have studied the possibility to stabilize the Bloch gain using an auxiliary ac field. Our approaches to the problem of THz Bloch oscillator are inspired by the investigations of THz gain in weakly-coupled SLs [50], where it was found that an additional peak appearing in the VI characteristics can be utilized to obtain stable high-frequency gain (see Chapter 1). In Sections 3.2 and 3.4 we discuss the main results of the Papers VI-VIII and slightly extend the analysis where appropriate. In Section 3.3 we consider the Bloch gain in unbiased SL driven by high-frequency auxiliary ac field.

3.2 Bloch gain in dc-ac driven superlattice

In Paper VI, we have analyzed the Bloch gain in the presence of high-frequency pump field $E_p(t) = E_{dc} + E_\Omega \cos \Omega t$, where the pump and probe frequencies, Ω and ω, are incommensurate. In this case, the total electric field is bichromatic, and we obtain the steady-state time-dependent current

using Eq. (2.76)

$$\begin{aligned} j_x(t) &= \sum_{n_1,n_2=-\infty}^{\infty} \sum_{m_1,m_2=-\infty}^{\infty} J_{n_1}(\beta_1) J_{n_1+m_1}(\beta_1) J_{n_2}(\beta) J_{n_2+m_2}(\beta) \\ &\times \Big\{ j_{dc}\big(eE_{dc}d + n_1\hbar\Omega + n_2\hbar\omega\big) \cos\big[m_1\Omega t + m_2\omega t\big] \\ &+ K\big(eE_{dc}d + n_1\hbar\Omega + n_2\hbar\omega\big) \sin\big[m_1\Omega t + m_2\omega t\big] \Big\}, \end{aligned} \tag{3.7}$$

where $\beta_1 = eE_\Omega d/\hbar\Omega$ and $\beta = eE_\omega d/\hbar\omega$. Now, both the electric field and the current are quasiperiodic, and therefore to find the dc current $j_{dc}^{\Omega,\omega}$ and the real part of the dynamic conductivity $\mathrm{Re}[\sigma(\omega)]$ [Eq. (3.1)] we formally take the time-average over infinite time-interval. We get

$$j_{dc}^{\Omega,\omega}(eE_{dc}d) = \sum_n J_n^2(\beta) j_{dc}^{\Omega}\big(eE_{dc}d + n\hbar\omega\big) \tag{3.8}$$

and

$$\mathrm{Re}[\sigma(\omega)] = \frac{1}{E_\omega} \sum_n J_n(\beta)\big[J_{n+1}(\beta) + J_{n-1}(\beta)\big] j_{dc}^{\Omega}\big(eE_{dc}d + n\hbar\omega\big), \tag{3.9}$$

where the summations are in infinite limits and

$$j_{dc}^{\Omega}(eE_{dc}d) = \sum_{n_1} J_{n_1}^2(\beta_1) j_{dc}\big(eE_{dc}d + n_1\hbar\Omega\big). \tag{3.10}$$

We emphasize that the assumptions of incommensurate frequencies and time-averaging over infinite time-interval are only simplifications, and the main results are valid also for most of the commensurate frequencies and finite time-averaging. If the frequencies are commensurate $\omega = l\Omega/q$ (l and q are relatively primes), the time-average can be taken over the common period of the fields, and for reasonable amplitudes of the pump and probe fields the coherent effects arising from the commensurability of the frequencies are important only if l and q are relatively small integers (see Chapter 4).

It is easy to notice that Eqs. (3.8) and (3.9) have exactly the same structure as Eqs. (2.80) and (3.4). Now the Esaki-Tsu characteristic $j_{dc}(eE_{dc}d)$ is just replaced by the VI characteristic modified by the pump field $j_{dc}^{\Omega}(eE_{dc}d)$. Therefore, in the limit of weak probe field, we obtain the Tucker formula

$$\mathrm{Re}[\sigma(\omega)] = \frac{j_{dc}^{\Omega}(eE_{dc}d + \hbar\omega) - j_{dc}^{\Omega}(eE_{dc}d - \hbar\omega)}{2\hbar\omega} ed. \tag{3.11}$$

The basic idea to obtain stable THz Bloch gain, introduced in the Paper VI, is now easy to understand. The pump field introduces additional peaks in the

VI characteristic, which can be controlled with the frequency and amplitude of the ac field as illustrated in Fig. 2.3. Now, we put the operation point in the PDC part of the additional peak, and by applying the Tucker formula we see that stable high-frequency gain can be obtained [for illustrations, see Fig. 1.2 and Paper VI Fig. 5]. Importantly, we find that although at low-frequencies the dynamical conductivity changes from negative to positive with applied ac pump field, the magnitude of the gain in the vicinity of Bloch gain maximum stays almost unaltered (see Paper VI Fig. 6). Therefore, relatively strong and stable THz gain can be obtained at room temperature with the help of high-frequency auxiliary pump field.

The necessity to use a high-frequency pump field in order to induce photon-assisted peaks limits the applied aspect of this suggestion. Therefore, we should ask the questions: Why this kind of stabilization of the Bloch gain is still interesting and what can be achieved? We have addressed these questions in Paper VI. Our main suggestions are to use this effect for a proof-of-the-principle demonstration of Bloch gain and in a starter for THz Bloch oscillator. From the perspective of Bloch gain, we underline, that the use of a high-frequency auxiliary ac field still enables the variation of dc bias within an interval $|eE_{dc}d - n\hbar\Omega| < \Gamma$ in conditions of PDC. Therefore, the tunability of the gain profile with dc bias can be demonstrated in the absence of electric domains. On the other hand, our analysis demonstrates that an application of a short THz pulse to a SL allows the suppression of the undesirable formation of electric domains and the achievement of a sustained stable large-amplitude operation of the dc biased Bloch oscillator. Therefore, our research contributes to the device-turn-on problem of THz Bloch oscillator. In a chain of SL Bloch oscillators the frequency of the generated signal can be tuned *continuously* over a wide frequency range.

In Paper VI we also briefly discussed the analogy of tilted magnetic field and high-frequency ac pump field. Later, in Paper IX, we found that indeed it is possible to obtain stable Bloch gain also by replacing the auxiliary ac pump field with a tilted magnetic field. This result will be discussed in more detail in Chapter 5.

3.3 Bloch gain in ac driven superlattice

One interesting peculiar consequence resulting from the analysis of Bloch gain in the presence of high-frequency pump field is that small-signal dispersive gain profile can in fact also be obtained in the absence of dc bias [132]. Interestingly, we have found that this kind of Bloch gain can be obtained also in conditions of PDC [105]. The basic idea how the stable high-frequency gain in unbiased SL arises from the Tucker relations is demonstrated in Fig. 3.2. If a pump field with suitable amplitude and frequency is applied, the VI

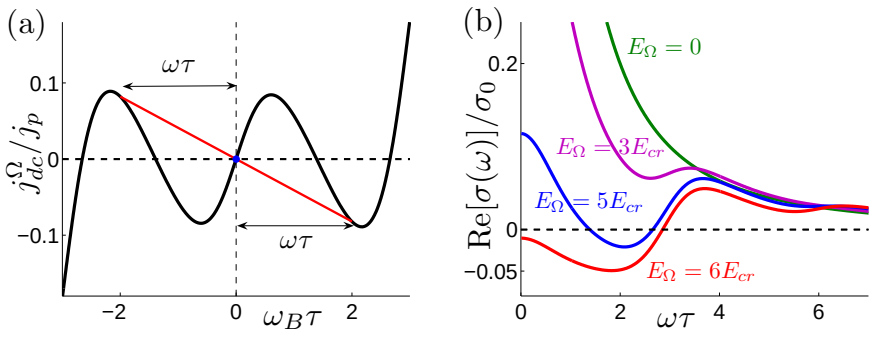

Figure 3.2: (a) VI characteristic in the presence of pump field $E_\Omega = 5E_{cr}$ and $\Omega\tau = 3$. (b) Absorption and gain profiles for $\Omega\tau = 3$ and different values of the pump amplitude $E_\Omega/E_{cr} =: 0, 3, 5, 6$.

characteristic shows positive slope at the small dc bias, but ANC exists for large values of E_{dc} [Fig. 3.2 (a)]. If we now apply the Tucker formula (3.11) at the operation point $E_{dc} = 0$, we see that the dynamical conductivity at small frequencies is positive but at the same time the high-frequency dynamical conductivity is negative in the vicinity of the gain resonance at $\omega = \Omega - 1/\tau$ [Fig. 3.2 (b), line marked $E_\Omega = 5E_{cr}$].

Fig. 3.2 (b) shows also how the gain profiles are modified as the amplitude of high-frequency pump field ($\Omega\tau = 3$) is varied from small to reasonably large values. For weak pump field $E_\Omega \ll E_{cr}$, the absorption profile is the usual free-carrier absorption demonstrating the power-like decay with an increase in frequency [Eq. (3.6)]. If the pump amplitude is several times the critical field $E_{ac} \approx 3E_{cr}$, an additional structure, a dispersive sub-profile, arises near the pump field frequency $\omega \approx \Omega$ [Fig. 3.2 (b)]. With a further increase of the pump strength $E_{ac} = 5E_{cr}$ the dispersive profile becomes more sharp and gain can be obtained for some frequencies which are lower than the pump frequency. However, we still have positive absorption at very low frequencies indicating PDC. The important difference to the Bloch gain in dc biased SL is that the gain profiles are now tunable by changing the pump frequency Ω. If the pump amplitude is further increased also the low-frequency dynamical conductivity becomes negative, and electric instability appears. By analyzing the distribution function in the semiclassical picture, we have found that the underlying physical mechanism causing the dispersive gain profile in ac driven SL in the vicinity of $\omega \approx n\Omega$ is similar to the mechanism of Bloch gain in dc biased SL [105]. In particular, the high-frequency gain arises due to dynamics of the electron bunch in the quasimomentum space. The suppression of the low-frequency absorption [Fig. 3.2 (b)] reflects the dynamic localization of the miniband electrons [133].

3.4 Bloch oscillator with modulated bias

The need to use a strong high-frequency pump field in the approaches presented above limits the potential applications of those suggestions. Therefore, in Papers VII and VIII we have considered the possibility to stabilize the Bloch gain using a low-frequency auxiliary pump fields.

In Paper VII we proposed a new type of stable THz oscillator, which we termed as Bloch oscillator with a modulated bias. To explain the physics behind our idea, we considered two types of periodic pump field profiles

$$E_p^{\text{asym}}(t) = \begin{cases} E_0 & \text{if} \quad 0 < t \ (\text{mod } T) < T - T_0 \\ 0 & \text{if} \quad T - T_0 < t \ (\text{mod } T) < T \end{cases} \tag{3.12}$$

and

$$E_p^{\text{sym}}(t) = \begin{cases} E_0 & \text{if} \quad 0 < t \ (\text{mod } T) < T/2 - T_0/2 \\ 0 & \text{if} \quad T/2 - T_0/2 < t \ (\text{mod } T) < T/2 \\ -E_0 & \text{if} \quad T/2 < t \ (\text{mod } T) < T - T_0/2 \\ 0 & \text{if} \quad T - T_0/2 < t \ (\text{mod } T) < T \end{cases} \tag{3.13}$$

shown in Paper VII Fig. 1 (a) and (b), respectively. We also assumed that the switching happens fast, the amplitude E_0 is large enough to excite Bloch oscillations ($E_0 > E_{cr}$), transients after switching can be neglected $T - T_0, T_0 \gg \tau$ and the fundamental frequency of the pump field $\Omega = 2\pi/T$ is incommensurate with the probe frequency ω. The symmetric pump profile $E_p^{\text{sym}}(t)$ satisfies conditions $\langle E_p^{\text{sym}}(t)\rangle = 0$ and $E_p^{\text{sym}}(t + T/2) = -E_p^{\text{sym}}(t)$, ensuring that only odd harmonics are present in Fourier spectrum. Although, the general time-dependent currents induced by the pump fields $E_p^{\text{sym}}(t)$ and $E_p^{\text{asym}}(t)$ are different, we find that the small-signal dynamical conductivity at the probe frequency ω satisfies in both cases

$$\text{Re}[\sigma(\omega)] = \left(1 - \frac{T_0}{T}\right) \text{Re}[\sigma^{KSS}(\omega)] + \frac{T_0}{T} \text{Re}[\sigma^{\text{free}}(\omega)], \tag{3.14}$$

where $\text{Re}[\sigma^{KSS}(\omega)]$ is the dynamical conductivity of biased SL

$$\text{Re}[\sigma^{KSS}(\omega)] = \frac{j_{dc}(eE_0 d + \hbar\omega) - j_{dc}(eE_0 d - \hbar\omega)}{2\hbar\omega} ed \tag{3.15}$$

and $\text{Re}[\sigma^{\text{free}}(\omega)]$ is the free-electron absorption determined by Eq. (3.6). In the limit $T_0/T \to 0$, Eq. (3.14) describes the usual Bloch gain profile. With an increase of T_0/T SL spends more time in an unbiased state, therefore the gain at low frequencies decreases and eventually the dynamical conductivity becomes positive, whereas the high-frequency gain is still preserved [see Paper VII Fig. 1 (c)]. The physical origin of such behavior is quite intuitive: At high frequencies around $\omega \approx eE_0 d/\hbar - \tau^{-1}$, the Bloch gain $\text{Re}[\sigma^{KSS}(\omega)] \approx$

$-\sigma_0/4\omega\tau$ dominates the free-electron absorption $\mathrm{Re}[\sigma^{\mathrm{free}}(\omega)] \approx \sigma_0/\omega^2\tau^2$. On the other hand, at low frequencies $\omega\tau \ll 1$, the free-electron absorption $\mathrm{Re}[\sigma^{\mathrm{free}}(\omega)] \approx \sigma_0$ overcomes the Bloch gain $\mathrm{Re}[\sigma^{KSS}(\omega)] \approx -\sigma_0/(E_0/E_{cr})^2$.

Importantly, the stable gain in the Bloch oscillator with modulated bias can also be understood analogously to the dc-ac driven Bloch gain with the help of Tucker relations (see Papers VII and VIII). The periodic pump field can be approximated in arbitrary accuracy as a Fourier series with finite number of harmonics

$$E_p(t) = E_{dc} + \sum_{k=1}^{N} E_k \cos(k\Omega t + \alpha_k). \tag{3.16}$$

Therefore, by employing the Eq. (2.76) for total electric field $E(t) = E_p(t) + E_\omega \cos\omega t$, we get that the dc current $j_{dc}^{p,\omega}$ and the dynamical conductivity $\mathrm{Re}[\sigma(\omega)]$ are

$$j_{dc}^{p,\omega}(eE_{dc}d) = \sum_n J_n^2(\beta) j_{dc}^p\big(eE_{dc}d + n\hbar\omega\big), \tag{3.17}$$

$$\mathrm{Re}[\sigma(\omega)] = \frac{1}{E_\omega}\sum_n J_n(\beta)\big[J_{n+1}(\beta) + J_{n-1}(\beta)\big] j_{dc}^p\big(eE_{dc}d + n\hbar\omega\big). \tag{3.18}$$

Here $j_{dc}^p(eE_{dc}d)$ is the pump field modified dc current

$$\begin{aligned} j_{dc}^p(eE_{dc}d) \;=\; & \sum_{n_1,\ldots,n_N} \sum_{\substack{m_1,\ldots,m_N \\ \sum_{k=1}^N k m_k = 0}} \Big[\prod_{k=1}^{N} J_{n_k}(\beta_k) J_{n_k+m_k}(\beta_k)\Big] \\ & \times j_{dc}\big(eE_{dc}d + \sum_{k=1}^{N} n_k \hbar k\Omega\big) \cos\big[\sum_{k=1}^{N} m_k\alpha_k\big], \end{aligned} \tag{3.19}$$

where $\beta_k = eE_k d/\hbar k\Omega$ $(k = 1, 2, ..., N)$. We notice that Eqs. (3.17) and (3.18) still have the same structure as in the case of monochromatic field. Now the Esaki-Tsu VI characteristic $j_{dc}(eE_{dc}d)$ is just replaced with $j_{dc}^p(eE_{dc}d)$, which contains phase-dependent terms due to harmonic mixing as discussed in Section 2.4.5. In the limit of weak probe field, we obtain the Tucker formula

$$\mathrm{Re}[\sigma(\omega)] = \frac{j_{dc}^p(eE_{dc}d + \hbar\omega) - j_{dc}^p(eE_{dc}d - \hbar\omega)}{2\hbar\omega} ed. \tag{3.20}$$

In the quasistatic limit, we obtain using Eq. (2.78)

$$j_{dc}^p(eE_{dc}d) = \langle j_{dc}(eE_p(t)d)\rangle. \tag{3.21}$$

Because for typical pump field profiles the amplitudes E_k decrease quite fast with increasing k, the condition of quasistatic field can often be written as $\Omega\tau \ll 1$. By using the particular pump field profiles (3.12) and (3.13), we

obtain using Eqs. (3.20) and (3.21) that the small-signal dynamical conductivity $\mathrm{Re}[\sigma(\omega)]$ is determined by Eq. (3.14).

In Papers VII and VIII we also addressed several issues, which are very important from the perspective of the experimental realization of the proposed scheme. In general the requirements to obtain stable and reasonably strong Bloch gain using quasistatic periodic pump field is that the waveform should contain two distinct part: Time interval of almost constant bias responsible for the THz gain due to excitation of Bloch oscillations and a virtually unbiased interval during which the dominant free-carrier absorption effectively suppresses the undesirable low-frequency instability. We have found that already a bichromatic pump field can mimic this kind of fast switching necessary for the stabilization (see Papers VII and VIII). We have also investigated the influence of space-charge instabilities on the THz gain. Apart from the condition of PDC the LSA operation mode requires that $\Omega\tau_d > 1$ (see Section 2.5). We find that this imposes a lower limit on the modulation frequency Ω, which in the case of moderately doped SLs can still belong to the microwave frequency range (see Paper VII). On the other hand, for a fixed value of the modulation frequency, this inequality requires that the doping density should be smaller than certain critical value imposing a restriction to the maximal value of gain α. Nevertheless, our analysis in Paper VII shows that at least proof-of-the-principle demonstration should be possible using commercially available sources of electric pulses. Moreover, larger THz gain can probably be obtained in the case of lateral surface SLs, where the domain growth rate is suppressed in comparison to the three-dimensional systems [127]. To understand the dependence of device performance on the boundary conditions, we studied a system consisting of a SL placed between two Ohmic buffer regions using a drift-diffusion model [Eqs. (2.88)] [134, 135]. We found that for a range of buffer conductivities the spatially averaged gain profiles [136] were practically indistinguishable from the gain profiles calculated using the homogeneous field approximation. If larger mismatch between the conductivities of SL and buffer regions was used, smaller values of doping density had to be required to achieve the desirable homogeneity [see Paper VII, Fig. 3]. In Paper VIII we showed that the stable Bloch gain profile still exists in the case of sub-THz pump field $\Omega\tau = 0.3$, where the quasistatic approximation (3.21) is not valid anymore.

Chapter 4

Parametric amplifiers and oscillators

Superlattice frequency multipliers and parametric amplifiers are based on coherent interaction of alternating fields (nonlinear mixing of photons), which can take place if the frequencies of the fields satisfy certain resonance condition. To understand the basic ideas of parametric amplification in SLs, we consider a SL under an electric field

$$E(t) = E_{dc} + E_{\Omega} \cos \Omega t + E_{\omega} \cos(\omega t + \phi), \tag{4.1}$$

where the frequencies ω and Ω are commensurate $\omega = n\Omega/m$, and the integers n and m are relatively primes. (In contrast to the previous Chapter, the phase-difference ϕ is now a physically meaningful parameter also in the steady-state dynamics and cannot be neglected.) Here $E_p(t) = E_{dc} + E_{\Omega} \cos \Omega t$ is again the pump field and we are interested on the amplification of the probe field $E_{pr} = E_{\omega} \cos(\omega t + \phi)$. In this Chapter we show that the semianalytic model developed in Section 2.4.2 allows to obtain a number of interesting results concerning the parametric interaction of the fields. After introducing the mathematical approach in Sections 4.1-4.4, we study the mechanisms of parametric amplification in the limits of strong and weak dissipation in Sections 4.5-4.6 and show that stable amplification of even harmonics and half-harmonics, depending on the biasing conditions, can be achieved at sub-THz and THz frequencies (Section 4.7). Finally, we compare the predictions of the theory to the recent experiments in Section 4.8.

4.1 General equations

We define an absorption at frequency ω as

$$\mathcal{A}_{\omega} = \langle j_x(t) \cos(\omega t + \phi) \rangle. \tag{4.2}$$

The absorbed/generated power density is then $\mathcal{P}_\omega = \mathcal{A}_\omega E_\omega$. We may also try to define the dynamical conductivity in the usual way $\sigma_\omega = 2\mathcal{A}_\omega/E_\omega$. However, we will show below that if spontaneous frequency multiplication effect takes place, $\mathcal{A}_\omega$ has a term, which is independent on the probe amplitude E_ω, and therefore the weak signal dynamical conductivity diverges. Thus, this definition of dynamical conductivity makes sense only in the absence of spontaneous frequency multiplication. On the other hand, the parametric amplification acts like a phase-dependent dynamical conductivity [137]. We should keep in mind that σ_ω is a continuous function of ω only in the subset of incommensurate ω and Ω values. There we can denote $\sigma_\omega = \sigma(\omega)$ as we did in the previous Chapter.

We obtain from Eq. (2.76) that the absorption $\mathcal{A}_\omega$ in tight-binding SL under the electric field (4.1) is

$$\begin{aligned}\mathcal{A}_\omega &= \frac{1}{2}\sum_{l,k,j} J_l(\beta_1)J_{l-nj}(\beta_1)J_k(\beta)\Big[J_{k+mj+1}(\beta)+J_{k+mj-1}(\beta)\Big] \\ &\times\Big[j_{dc}(eE_{dc}d+l\hbar\Omega+k\hbar\omega)\cos(mj\phi)+K(eE_{dc}d+l\hbar\Omega+k\hbar\omega)\sin(mj\phi)\Big],\end{aligned} \tag{4.3}$$

where $\beta_1 = eE_\Omega d/\hbar\Omega$ and $\beta = eE_\omega d/\hbar\omega$.

Similarly, we define the absorption and the absorbed/generated power density at frequency Ω as $\mathcal{A}_\Omega = \langle j_x(t)\cos\Omega t\rangle$ and $\mathcal{P}_\Omega = \mathcal{A}_\Omega E_\Omega$. We obtain

$$\begin{aligned}\mathcal{A}_\Omega &= \frac{1}{2}\sum_{l,k,j} J_l(\beta_1)\Big[J_{l-nj+1}(\beta_1)+J_{l-nj-1}(\beta_1)\Big]J_k(\beta)J_{k+mj}(\beta) \\ &\times\Big[j_{dc}(eE_{dc}d+l\hbar\Omega+k\hbar\omega)\cos(mj\phi)+K(eE_{dc}d+l\hbar\Omega+k\hbar\omega)\sin(mj\phi)\Big].\end{aligned} \tag{4.4}$$

We are mainly interested in the weak signal absorption, which should be negative in order to have an oscillator. We consider separately, the weak signal absorption for harmonics $\omega = n\Omega$, half-harmonics $\omega = n\Omega/2$ (n is odd) and other commensurate frequencies $\omega = n\Omega/m$, $m \geq 3$.

4.2 Generation of harmonics

If $\omega = n\Omega$, we obtain from Eq. (4.3) that the weak signal ($\beta \ll 1$) absorption is

$$\mathcal{A}_\omega = \mathcal{A}_\omega^{\rm harm} + \mathcal{A}_\omega^{\rm coh} + \mathcal{A}_\omega^{\rm incoh}, \tag{4.5}$$

where

$$\mathcal{A}_\omega^{\rm harm} = \frac{1}{2}\cos\phi \sum_l J_l(\beta_1)[J_{l+n}(\beta_1) + J_{l-n}(\beta_1)] j_{dc}(eE_{dc}d + l\hbar\Omega) \\ -\frac{1}{2}\sin\phi \sum_l J_l(\beta_1)[J_{l+n}(\beta_1) - J_{l-n}(\beta_1)] K(eE_{dc}d + l\hbar\Omega), \quad (4.6)$$

$$\begin{aligned}\mathcal{A}_\omega^{\rm coh} &= \frac{\beta}{4}\cos(2\phi) \sum_l J_l(\beta_1)\big[J_{l-2n}(\beta_1) - J_{l+2n}(\beta_1)\big] j_{dc}(eE_{dc}d + l\hbar\Omega) \\ &+\frac{\beta}{4}\sin(2\phi) \sum_l J_l(\beta_1)\big[J_{l-2n}(\beta_1) + J_{l+2n}(\beta_1)\big] K(eE_{dc}d + l\hbar\Omega) \\ &-\frac{\beta}{2}\sin(2\phi) \sum_l J_l(\beta_1) J_{l-2n}(\beta_1) K(eE_{dc}d + l\hbar\Omega - \hbar\omega), \end{aligned} \quad (4.7)$$

$$\mathcal{A}_\omega^{\rm incoh} = \frac{\beta}{4}\sum_l J_l^2(\beta_1)[j_{dc}(eE_{dc}d + l\hbar\Omega + \hbar\omega) - j_{dc}(eE_{dc}d + l\hbar\Omega - \hbar\omega)]. \quad (4.8)$$

Here $\mathcal{A}_{\rm incoh}$ is equivalent to the expression we found in the previous Chapter for incommensurate Ω and ω [Eq. (3.11)]. In the case of unbiased or weakly biased SLs considered here, it mainly describes the free electron absorption modified by the pump field. However, it can also describe the ac driven Bloch gain discussed in Section 3.3. The harmonic term can be written as $\mathcal{A}_\omega^{\rm harm} = \langle j_x^\Omega(t)\cos(\omega t + \phi)\rangle$, where $j_x^\Omega(t)$ is the current density induced by the pump field [see Eqs. (2.79)-(2.82)]. Therefore, it clearly describes the spontaneous frequency multiplication effect. Only odd harmonics are generated in unbiased SL due to symmetry, whereas in biased SL both odd and even harmonics exist. The term $\mathcal{A}_\omega^{\rm coh} \propto \beta$ acts like dynamical conductivity and has a typical phase-dependence of parametric amplification [137]. The physical origin of this term in particular limits will be discussed below. Here we just notice that it can be nonzero for both even and odd harmonics also in unbiased SL. Therefore, generation of even harmonics due to parametric gain can take place in unbiased SL. If the spontaneous frequency multiplication exists, it blurs out the other weaker effects caused by the incoherent $\mathcal{A}_\omega^{\rm incoh}$ and parametric $\mathcal{A}_\omega^{\rm coh}$ absorption.

4.3 Generation of half-harmonics

If $\omega = n\Omega/2$ (n odd), the weak signal ($\beta \ll 1$) absorption is

$$\mathcal{A}_\omega = \mathcal{A}_\omega^{\rm coh} + \mathcal{A}_\omega^{\rm incoh}, \quad (4.9)$$

where $\mathcal{A}_\omega^{\rm incoh}$ is given by Eq. (4.8) and the parametric amplification is now

$$\begin{aligned}\mathcal{A}_\omega^{\rm coh} &= \frac{\beta}{4}\cos(2\phi)\sum_l J_l(\beta_1)\big[J_{l-n}(\beta_1)-J_{l+n}(\beta_1)\big]j_{dc}(eE_{dc}d+l\hbar\Omega)\\ &+\frac{\beta}{4}\sin(2\phi)\sum_l J_l(\beta_1)\big[J_{l-n}(\beta_1)+J_{l+n}(\beta_1)\big]K(eE_{dc}d+l\hbar\Omega)\\ &-\frac{\beta}{2}\sin(2\phi)\sum_l J_l(\beta_1)J_{l-n}(\beta_1)K(eE_{dc}d+l\hbar\Omega-\hbar\omega). \qquad (4.10)\end{aligned}$$

The parametric amplification of half-harmonics occurs only in biased SL.

4.4 Generation of other commensurate frequencies?

If $\omega = n\Omega/m$ (n, m relatively primes) and $m \geq 3$, the weak signal $\beta \ll 1$ absorption is determined by $\mathcal{A}_\omega^{\rm incoh}$ given by Eq. (4.8) [138]. Therefore, the weak signal parametric amplification is not possible, and gain can only take place due to the mechanisms described in Chapter 3.

4.5 Quasistatic limit

If $\omega = n\Omega$, we obtain in the quasistatic limit $\omega\tau \ll 1$ from Eqs. (4.6)-(4.8) using the result (2.78) [139]

$$\mathcal{A}_\omega^{\rm harm} = \cos\phi\ \langle j_{dc}\big(eE_p(t)d\big)\cos\omega t\rangle, \qquad (4.11)$$

$$\mathcal{A}_\omega^{\rm coh} = \frac{E_\omega}{2}\cos(2\phi)\frac{d}{dE_{\rm dc}}\langle j_{dc}\big(eE_p(t)d\big)\cos(2\omega t)\rangle, \qquad (4.12)$$

$$\mathcal{A}_\omega^{\rm incoh} = \frac{E_\omega}{2}\frac{d}{dE_{dc}}\langle j_{dc}\big(eE_p(t)d\big)\rangle = \frac{E_\omega}{2}\frac{dj_{dc}^{\Omega}(eE_{dc}d)}{dE_{dc}}. \qquad (4.13)$$

The incoherent absorption is negative only in conditions of NDC, where also the electric instabilities exist. The parametric amplification is determined by the oscillations of the differential conductivity at twice the frequency of the signal. By straightforward calculation, we get [140]

$$E_\omega(\mathcal{A}_\omega^{\rm incoh}+\mathcal{A}_\omega^{\rm coh}) = \langle\sigma_{dc}\big(E_p(t)\big)[E_{pr}(t)]^2\rangle. \qquad (4.14)$$

Therefore the parametric amplification can overcome the free electron absorption only if the electric field periodically reaches the values, where the Esaki-Tsu VI characteristic has NDC. The optimal phase is defined in the

way that it maximizes the gain. In the quasistatic limit the maximal values of gain are achieved if the maximum (minimum) absolute values of the probe field $|E_{pr}(t)|$ occur when the total electric field reaches the values in the NDC (PDC) portion of the Esaki-Tsu VI characteristic [140]. The optimal phases for even harmonics are $\{\pi/2, 3\pi/2\}$ and for odd harmonics $\{0, \pi\}$ [140].

In the case of half-harmonics, we obtain the same expressions (4.12) and (4.13) for $\mathcal{A}_\omega^{\rm coh}$ and $\mathcal{A}_\omega^{\rm incoh}$, respectively. Therefore the parametric amplification of half-harmonics has the same physical origin.

It is a general feature of all systems that, if the current follows the instantaneous value of the field adiabatically via the static VI characteristic, the oscillations of the differential conductivity at twice the frequency of the signal effectively act like negative dynamical conductivity at the signal frequency. This effect is analogous to the more typical parametric amplification, where the oscillations of reactance (e.g. inductance) at twice the frequency of the signal result effectively to negative resistance at the signal frequency [137]. Because in unbiased SL the differential conductivity oscillates at even harmonics of the pump frequency and in biased SL all harmonics are present, the parametric gain occurs only at the harmonics $\omega = n\Omega$ if $E_{dc} = 0$, whereas also the half-harmonics $\omega = n\Omega/2$ can be amplified if $E_{dc} \neq 0$.

It is clear from Eq. (4.14) that the parametric amplification due to oscillations of differential conductivity requires that the differential conductivity periodically takes on negative values. Therefore, we should ask the question: Why this kind of parametric interaction is of separate interest? The major advantage, as will be discussed in Section 4.7, is that strong gain can be obtained in conditions of suppressed electric instability. We should compare this type of parametric amplification also to the Bloch oscillator with quasistatically modulated bias. In both cases the average value of the oscillating dc differential conductivity should be positive to avoid the electric instability. However, in the latter case, a high-frequency phase-insensitive gain is obtained due to the Bloch gain, whereas in the case of parametric interaction large phase-sensitive gain is obtained at low-order harmonics and half-harmonics of the pump field. Therefore, the Bloch gain is more suitable for amplification of THz radiation, whereas this mechanism of parametric gain should work better at sub-THz frequencies.

4.6 Manley-Rowe relations

In the limit of weak dissipation $\tau \to \infty$, we obtain from Eqs. (4.3) and (4.4) for arbitrary amplitudes E_Ω and E_ω ($\omega = n\Omega/m$) in unbiased SL

$$\mathcal{A}_\omega = \sum_{k,j} J_{-kn}(\beta_1) J_{-kn-nj}(\beta_1) J_{km}(\beta) \Big[J_{km+mj+1}(\beta) + J_{km+mj-1}(\beta) \Big] \times j_p \sin(mj\phi), \tag{4.15}$$

$$\mathcal{A}_\Omega = \sum_{k,j} J_{-kn}(\beta_1) \Big[J_{-kn-nj+1}(\beta_1) + J_{-kn-nj-1}(\beta_1) \Big] J_{km}(\beta) J_{km+mj}(\beta) \times j_p \sin(mj\phi). \tag{4.16}$$

By using the Bessel function relation $J_{n-1}(x) + J_{n+1}(x) = 2nJ_n(x)/x$, we get

$$\mathcal{P}_\omega / m\omega = -\mathcal{P}_\Omega / n\Omega. \tag{4.17}$$

This simple connection between the generated/absorbed power at different frequencies is an example of Manley-Rowe relations, which are typical for parametric systems consisting of nonlinear inductors and capacitors [141]. The relation (4.17) corresponds to a parametric processes, where the miniband electrons absorb energy from the pump field in stacks of n photons and emit energy to the probe field in stacks of m photons.

In a dc biased tight-binding SL, the parametric processes in the limit of weak dissipation $\tau \to \infty$ can occur only if the Bloch frequency is an integer multiple of one of the ac field frequencies. For example in the case $eE_{dc}d = l\hbar\Omega$, we obtain

$$\mathcal{P}_\omega = \sum_{k,j} J_{-kn-l}(\beta_1) J_{-kn-l-nj}(\beta_1) J_{km}(\beta) J_{km+jm}(\beta) \times \Big[(k+j) m\hbar\omega \Big] \frac{2j_p}{ed} \sin(mj\phi), \tag{4.18}$$

$$\mathcal{P}_\Omega = -\sum_{k,j} J_{-kn-l}(\beta_1) J_{-kn-l-nj}(\beta_1) J_{km}(\beta) J_{km+mj}(\beta) \times \Big[l\hbar\Omega + (k+j) n\hbar\Omega \Big] \frac{2j_p}{ed} \sin(mj\phi). \tag{4.19}$$

Therefore we can write $\mathcal{P}_\omega = \sum_{k,j} \mathcal{P}_\omega^{k,j}$ and $\mathcal{P}_\Omega = \sum_{k,j} \mathcal{P}_\Omega^{k,j}$, where the terms in the summation satisfy Manley-Rowe relations

$$\mathcal{P}_\omega^{k,j} / [(k+j) m\hbar\omega] = -\mathcal{P}_\Omega^{k,j} / [l\hbar\Omega + (k+j) n\hbar\Omega]. \tag{4.20}$$

We attribute these terms to the processes involving $l+(k+j)n$ photons from the pump field and $(k+j)m$ photons from the probe field.

To understand the mechanism of the parametric amplification in the limit of weak dissipation in the semiclassical picture, we study the distribution function in the case of weak probe field $\beta \ll 1$ in unbiased SL for $\omega = n\Omega$. In this case the different components of the absorption can be written as

$$\begin{aligned} \mathcal{A}_\omega^{\rm harm} &= -j_p \sin\phi\big[1-(-1)^n\big] J_0(\beta_1) J_n(\beta_1) \\ \mathcal{A}_\omega^{\rm coh} &= j_p \beta \sin(2\phi) \Big[J_0(\beta_1) J_{2n}(\beta_1) - (-1)^n J_n^2(\beta_1) \Big], \\ \mathcal{A}_\omega^{\rm incoh} &= 0. \end{aligned} \tag{4.21}$$

The time-dependent steady-state current in this case is

$$j_x(t) = 2j_p\big[J_0(\beta_1)+\Lambda\big] \sin\big[\rho + \beta_1 \sin\Omega t + \beta\sin(\omega t+\phi)\big], \tag{4.22}$$

where $\Lambda = -[1-(-1)^n]\frac{\beta}{2} J_n(\beta_1)\cos\phi$ and $\rho = -[1+(-1)^n]\frac{\beta}{2}\frac{J_n(\beta_1)}{J_0(\beta_1)}\sin\phi$. The current oscillations arise, because the electrons are gathered together in quasimomentum space forming an electron bunch, which oscillates coherently along a ballistic trajectory $K_x(t)d \approx \rho + \beta_1 \sin\Omega t + \beta\sin(\omega t+\phi)$ [104, 105]. The amplitude of current oscillations ($\propto J_0(\beta_1)+\Lambda$) is determined by the number density of electrons involved in the bunch [105]. The absorption can now be written in an illustrative form $\mathcal{A}_\omega = \mathcal{A}_\omega^1 + \mathcal{A}_\omega^2$, where

$$\begin{aligned} \mathcal{A}_\omega^1 &= 2j_p\big[J_0(\beta_1)+\Lambda\big]\big\langle \sin\big(\rho+\beta_1\sin\Omega t\big)\cos(\omega t+\phi)\big\rangle \\ &= -[1-(-1)^n] j_p \sin\phi J_0(\beta_1) J_n(\beta_1) - (-1)^n j_p \beta J_n^2(\beta_1)\sin 2\phi \\ \mathcal{A}_\omega^2 &= j_p\beta J_0(\beta_1)\sin 2\phi \big\langle \cos\big(\beta_1\sin\Omega t\big)\cos(2\omega t)\big\rangle = j_p\beta\sin 2\phi J_0(\beta_1) J_{2n}(\beta_1). \end{aligned} \tag{4.23}$$

The first term corresponds to harmonic generation due to ballistic oscillations of the bunch, and the second term arises because the effective mass of the bunch oscillates at twice the frequency of the signal. We see that $\mathcal{A}_\omega^1 + \mathcal{A}_\omega^2 = \mathcal{A}_\omega^{\rm harm} + \mathcal{A}_\omega^{\rm coh}$. The parametric amplification $\mathcal{A}_\omega^{\rm coh}$ arises partly because of both contributions $\mathcal{A}_\omega^1$ and $\mathcal{A}_\omega^2$. The parametric amplification of half-harmonics can be interpreted similarly in terms of oscillations of electron bunch.

4.7 Earlier works and main results

Theoretical research devoted to frequency multiplication and parametric amplification in SLs has some history. The frequency multiplication in SLs using a perturbative approach was studied already by R. Tsu and L. Esaki [142]. This approach can be used to calculate the lowest order approximation for the harmonic generation given by Eq. (4.6). The expression of the frequency

multiplication for arbitrary amplitude of the pump field was obtained in Refs. [93], [98] and [143]. The possibility of parametric amplification of even harmonics and parametric generation of odd harmonics was pointed out in Refs. [144] and [145]. In Ref. [144] also the parametric effects occurring at half-harmonics were briefly mentioned. However, the phase-dependence of the gain was not taken into account in this pioneering work.

In Papers I-V we have considered the manifestations of the parametric resonance in the miniband transport regime. Here the following main questions arise: Can the parametric resonance provide high-frequency gain? What are the conditions for the parametric resonance? What is the physical mechanism of amplification? What is the role of relative phase? Is it possible to avoid the space-charge instability?

In Paper I, the generation of odd harmonics in SLs was studied in the limit of quasistatic frequencies $\Omega\tau \ll 1$. We derived the Eqs. (4.11)-(4.13) directly from Eq. (2.78), and checked that these expressions are still valid for pump frequencies of 100 GHz. Moreover, we demonstrated that if the pump amplitude is larger than a certain threshold value, the parametric term can overcome the free-electron absorption resulting in regenerative amplification of the probe field. Importantly, the numerical simulations showed an excellent agreement between the quasistatic approach [Eq. (2.78)] and 3D Monte-Carlo simulations. The conditions for suppression of the electric instability were studied numerically by using a drift-diffusion model. These numerical simulations essentially confirmed that if the LSA conditions (2.97) are satisfied, the electric field profile inside the SL stays approximately homogeneous, although the instantaneous electric field periodically reaches values, where the Esaki-Tsu characteristic has NDC. On the other hand, if the condition $\Omega\tau_d > 1$ is not completely satisfied, the space-charge inhomogeneities result in reduction of gain. However, it should be mentioned that the effects of realistic contact boundary conditions on the LSA mode were not studied in this work. The parametric amplification of weak probe field in the quasistatic limit has also been independently pointed out in Ref. [140]. In this work the authors neither studied the effects of large fields, nor considered the conditions (2.97) for suppression of domain instability.

In Papers II and III we examined the parametric amplification of even harmonics and half-harmonics in the absence of electric domains. We identified the important role of the oscillations of the electron's effective mass in the origin of the high-frequency parametric gain. Because SL is a strongly nonlinear medium the spontaneous frequency multiplication effect as a rule blurs out the parametric resonance. This problem is well-known for the parametric amplification in Josephson junctions, which also have strong nonlinearity [146]. Therefore, we suggested two schemes, where the parametric gain is the dominant mechanism of amplification: generation and amplification of even harmonics ($\omega/\Omega =: 2, 4, 6, 8...$) in unbiased SL and generation and amplifi-

cation of half-harmonics ($\omega/\Omega =: 1/2, 3/2, 5/2, ...$) in biased SL. In the case of unbiased SL, the weak signal parametric gain overcomes the free-electron absorption if the pump amplitude is large enough. The threshold amplitude depends on the generated harmonic and the frequency of the pump field. Moreover, if the frequency of the pump field is large enough $\Omega\tau_d > 1$, the electric instability exists only in conditions of absolute negative conductance (ANC). The high-frequency pump field can induce ANC, but it happens only if the amplitude is chosen in the vicinity of the roots of the Bessel function $J_0(\beta_1) \approx 0$ (see Section 2.4.4 and Paper III Fig. 2). Therefore, the electric instability exists only for specific amplitudes and frequencies of the pump field and there is plenty of room for the amplifier or oscillator to operate in the absence of electric domains. Additionally, we found that also the large-amplitude parametric gain as a rule occurs in the absence of the electric instability (see Paper II). In dc biased SL the stable parametric gain at half-harmonics can overcome the free-electron absorption also in the case of very weak pump amplitudes (see Paper III).

In Papers II, III and IV we have also addressed the important question of the magnitude of the gain at room temperature and considered the generation and amplification of desirable THz frequencies with the use of available sources of low- and high-frequency radiation. In the case of parametric up-conversion the largest magnitudes of the parametric gain occur typically at sub-THz frequencies. Nevertheless, the magnitude of parametric gain at frequencies of few THz can still be comparable to the estimated Bloch gain. In the case of down-conversion $\omega = \Omega/2$, we found strong gain if the pump frequency $\Omega\tau < 2$. Therefore, by employing a suitable pump field with frequency $1 - 2$ THz, a sub-THz probe field with frequency $0.5 - 1$ THz can be generated or amplified in a SL.

Finally, in Paper V we have re-examined the scheme of nondegenerate parametric amplification in SLs, which was initially suggested in Refs. [147]. In this case there are two resonator modes with incommensurate frequencies ω_1 and ω_2 satisfying $\omega_1 \pm \omega_2 = n\Omega$, where n is an integer and Ω is the pump frequency. In particular, we derived the formulas describing the parametric amplification for both weak and large signals and proved the corresponding Manley-Rowe relations in the limit of weak dissipation. We also discussed the different mechanism of parametric gain in the limits of quasistatic interaction and weak dissipation. In the case of nondegenerate parametric amplification, similarly as in the case of amplification of half-harmonics, there is no spontaneous frequency multiplication effect, and therefore the generation is always purely a parametric effect.

4.8 Comparison to experiments

The generation of harmonics in SLs due to the spontaneous frequency multiplication effect has been observed experimentally [148, 149]. On the other hand, to our knowledge, no clear experimental evidence of the parametric amplification in homogeneous SLs have been presented. The frequency multiplication and parametric amplification are, however, also possible in the presence of space-charge inhomogeneities. The frequency multiplication due to the periodic formation and annihilation of electric domains has been studied both theoretically [134] and experimentally [42, 150]. The parametric amplification has been observed in experiments in heavily doped SLs, where the LSA condition is not satisfied [43]. The experimental observation cannot be described using the model of homogeneous SL and therefore we expect that the electric domains are playing an important role in this effect. The frequency dependence of the generated power in the frequency multipliers and parametric amplifiers operating in the presence of electric domains most likely depends on the characteristic time of the domain build up τ_d, average scattering time τ and contact boundary conditions. The parametric interaction of high-frequency radiation with the electric domains is currently not theoretically well-understood. Theoretical modelling and new experiments with high-frequency radiation applied to heavily doped SLs [151] are required in order to understand the potential of domain mediated gain in amplifiers and oscillators operating at THz frequencies. Recently experiments have been performed also with resonators both for third and fifth harmonic of the pump field, and parametric processes in these double-resonance oscillators have been observed [152].

Chapter 5

Influence of magnetic field

In this Chapter we consider the electron dynamics in SLs in the presence of magnetic field. We discuss the results of the Paper IX and extend the analysis to describe the temperature dependence of the gain.

We assume a static magnetic field $\mathbf{B} = (B_x, 0, B_z)$ and an electric field $E(t) = E_{dc} + E_\omega \cos \omega t$ applied along the SL direction. In the presence of magnetic field, the Lorentz force acting on the miniband electrons depends on the electron's quasimomentum $\mathbf{k}$, and therefore the approach based on path-integral solution of the Boltzmann equation [Eq. (2.40)] is most powerful in the limits of low carrier density $N_0 \to 0$ and low temperature $T_e \to 0$, where the equilibrium distribution is given by Eq. (2.58) and the steady-state current is determined by the ballistic trajectories starting at $\mathbf{k} = \mathbf{0}$. We are particularly interested about the influence of magnetic field on absorption and gain. Since the dynamics of the electrons in perpendicular and tilted magnetic fields have quite different characteristic features, these two cases will be considered separately.

5.1 Cyclotron gain and Bloch gain in crossed fields

5.1.1 Ballistic electron dynamics in crossed fields

In the case of crossed electric and magnetic fields $\mathbf{B} = (0, 0, B_z)$ the ballistic electron dynamics in tight-binding SLs is determined by equations

$$\begin{aligned} \hbar \frac{dk_x}{dt} &= eE(t) + ev_y B_z = eE_{dc} + eE_\omega \cos \omega t + eB_z \frac{\hbar k_y}{m}, \\ \hbar \frac{dk_y}{dt} &= -ev_x B_z = -eB_z \frac{\Delta d}{2\hbar} \sin k_x d. \end{aligned} \tag{5.1}$$

The ballistic electron dynamics is equivalent with a driven pendulum [74, 153, 154, 155, 156]

$$\frac{d^2 k_x d}{dt} + \omega_c^2 \sin k_x d \;\; = \;\; -\beta\omega^2 \sin \omega t, \tag{5.2}$$

where $\beta = eE_\omega d/\hbar\omega$, $\omega_c = eB_z/\sqrt{m_x m}$ is the miniband cyclotron frequency and $m_x = 2\hbar^2/\Delta d^2$. We can now see that the magnetic field B_z determines the frequency of the linear oscillations of the pendulum near the stable equilibrium point and the dc field E_{dc} affects the initial velocity of the pendulum. In general the driven pendulum can show complicated nonlinear dynamics including chaos. However, in some limiting cases it is possible to derive analytic results. First, we will study the dynamics of the electrons in the absence of ac field. These insights will be used later in the interpretation of the numerical results concerning the small-signal absorption and gain.

In the absence of ac field the total energy of the pendulum is conserved

$$\frac{1}{2}\left(\frac{d}{dt} k_x d\right)^2 - \omega_c^2 \cos k_x d = 2\Omega_0^2 - \omega_c^2, \tag{5.3}$$

where $\Omega_0 > 0$ is constant. Using Eqs. (5.1) and denoting $\mu = m/m_x$, this can be rewritten as

$$\frac{1}{4}\left(\frac{\omega_B}{\omega_c} + \frac{k_y d}{\sqrt{\mu}}\right)^2 + \sin^2(k_x d/2) = \left(\frac{\Omega_0}{\omega_c}\right)^2. \tag{5.4}$$

If the pendulum has just enough kinetic energy to reach the unstable equilibrium point, it will approach it asymptotically and all oscillations are suppressed. In the case of smaller and larger kinetic energies, the pendulum will perform oscillations around the stable equilibrium point and full rotations, respectively. In the case of SLs, this means that for $\Omega_0 > \omega_c$ and $\Omega_0 < \omega_c$ the electrons perform full-miniband Bloch-like oscillations (rotations of pendulum) and cyclotron-like oscillations (oscillations of pendulum), respectively. These two oscillatory regimes of motion are set apart by separatrix at $\Omega_0 = \omega_c$.

The ballistic trajectories for different initial conditions $k_x(0) = k_x^0$ and $k_y(0) = k_y^0$ can be expressed in a very compact form by using the elliptic functions [74, 153, 154]

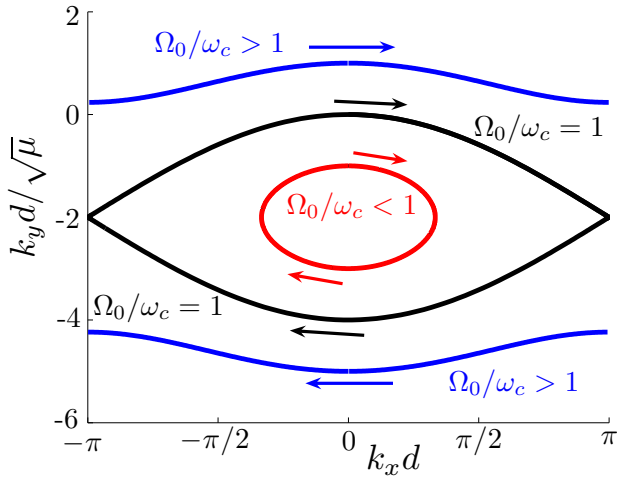

Figure 5.1: Ballistic trajectories in (k_x, k_y)-plane for $\omega_B/\omega_c = 2$. The open trajectories labeled $\Omega_0/\omega_c > 1$ correspond to Bloch-like oscillations, where electrons are periodically Bragg reflected at the Brillouin zone boundary. The closed trajectory labeled $\Omega_0/\omega_c < 1$ corresponds to cyclotron-like oscillations. At the separatrix $\Omega_0/\omega_c = 1$ the electrons are asymptotically approaching the boundary of the miniband and all oscillations are suppressed.

$$\begin{pmatrix} k_x d \\ \frac{k_y d}{\sqrt{\mu}} \end{pmatrix} = \begin{cases} \begin{pmatrix} 2\arcsin\left[\frac{\Omega_0}{\omega_c}\mathrm{sn}(\omega_c t+\phi, \Omega_0/\omega_c)\right] \\ -\omega_B/\omega_c + 2\frac{\Omega_0}{\omega_c}\mathrm{cn}(\omega_c t+\phi, \Omega_0/\omega_c) \end{pmatrix}, & \Omega_0 < \omega_c \\ \begin{pmatrix} 2\mathrm{am}(\Omega_0 t+\phi, \omega_c/\Omega_0) \\ -\omega_B/\omega_c + 2\frac{\Omega_0}{\omega_c}\mathrm{dn}(\Omega_0 t+\phi, \omega_c/\Omega_0) \end{pmatrix}, & \Omega_0 > \omega_c \\ & \frac{k_y^0 d}{\sqrt{\mu}} > -\frac{\omega_B}{\omega_c} \\ \begin{pmatrix} 2\mathrm{am}(-\Omega_0 t+\phi, \omega_c/\Omega_0) \\ -\frac{\omega_B}{\omega_c} - 2\frac{\Omega_0}{\omega_c}\mathrm{dn}(-\Omega_0 t+\phi, \omega_c/\Omega_0) \end{pmatrix}, & \Omega_0 > \omega_c \\ & \frac{k_y^0 d}{\sqrt{\mu}} < -\frac{\omega_B}{\omega_c} \\ \begin{pmatrix} 2\arcsin[\tanh(\omega_c t+\phi)] \\ -\omega_B/\omega_c + 2/\cosh(\omega_c t+\phi) \end{pmatrix}, & \Omega_0 = \omega_c \\ & \frac{k_y^0 d}{\sqrt{\mu}} > -\frac{\omega_B}{\omega_c} \\ \begin{pmatrix} 2\arcsin[\tanh(-\omega_c t+\phi)] \\ -\omega_B/\omega_c - 2/\cosh(-\omega_c t+\phi) \end{pmatrix}, & \Omega_0 = \omega_c \\ & \frac{k_y^0 d}{\sqrt{\mu}} < -\frac{\omega_B}{\omega_c}. \end{cases} \tag{5.5}$$

Here

$$\phi = \begin{cases} F\left(\text{atan2}\left[\frac{\omega_c}{\Omega_0}\sin(k_x^0 d/2), \frac{\omega_c k_y^0 d/\sqrt{\mu}+\omega_B}{2\Omega_0}\right], \Omega_0/\omega_c\right), & \Omega_0 < \omega_c \\ F\left(k_x^0 d/2, \omega_c/\Omega_0\right), & \Omega_0 > \omega_c \\ \text{arctanh}\left[\sin(k_x^0 d/2)\right], & \Omega_0 = \omega_c, \end{cases} \tag{5.6}$$

atan2$[Y, X]$ is the four-quadrant inverse tangent and

$$F(x,k) = \int_0^x \frac{dt}{\sqrt{1-k^2\sin^2 t}} \tag{5.7}$$

is the non-complete elliptic integral of the first kind. Here $k_x d$ should always be transferred to the first Brillouin zone. Typical trajectories described by Eqs. (5.5) and (5.6) are plotted in Fig. 5.1 in (k_x, k_y)-plane. The closed (open) trajectories correspond to cyclotron-like (Bloch-like) oscillations.

We notice that the effect of initial momentum in y-direction is the same as if the electric field would be transformed as $\omega_B' = \omega_B + \omega_c k_y d/\sqrt{\mu}$ [Eq. (5.4)]. This result can be understood as a Lorentz-transformation of the electric field $E_{dc}' = E_{dc} + Bv_y$ in the nonrelativistic limit [155]. Therefore, alternatively to applied dc bias in the SL direction, the oscillations can also be induced by injecting the electrons with an initial velocity in the y-direction [155] or by accelerating the electrons in y-direction with an electric field [157]. With this transformation it is easy to understand the symmetry of the electron trajectories in the quasimomentum space with respect to line $k_y d/\sqrt{\mu} = -\omega_B/\omega_c$ (Fig. 5.1).

From Eqs. (5.5), one obtains that the scaled velocities and miniband

energy ($v'_x = 2\hbar v_x/\Delta d$, $\varepsilon'_x = 2\varepsilon_x/\Delta$, $v'_y = \sqrt{\mu}2\hbar v_y/\Delta d$) are given by

$$\begin{pmatrix} v'_x \\ \varepsilon'_x \\ v'_y \end{pmatrix} = \begin{cases} \begin{pmatrix} 2\frac{\Omega_0}{\omega_c}\mathrm{sn}(\omega_c t+\phi,\frac{\Omega_0}{\omega_c})\mathrm{dn}(\omega_c t+\phi,\frac{\Omega_0}{\omega_c}) \\ -1+2\left(\frac{\Omega_0}{\omega_c}\right)^2\mathrm{sn}^2(\omega_c t+\phi,\Omega_0/\omega_c) \\ -\omega_B/\omega_c+2\frac{\Omega_0}{\omega_c}\mathrm{cn}(\omega_c t+\phi,\Omega_0/\omega_c). \end{pmatrix}, & \Omega_0<\omega_c \\ \begin{pmatrix} 2\mathrm{sn}(\Omega_0 t+\phi,\frac{\omega_c}{\Omega_0})\mathrm{cn}(\Omega_0 t+\phi,\frac{\omega_c}{\Omega_0}) \\ -1+2\mathrm{sn}^2(\Omega_0 t+\phi,\omega_c/\Omega_0) \\ -\omega_B/\omega_c+2\frac{\Omega_0}{\omega_c}\mathrm{dn}(\Omega_0 t+\phi,\omega_c/\Omega_0) \end{pmatrix}, & \Omega_0>\omega_c,\ \frac{k_y^0 d}{\sqrt{\mu}}>-\frac{\omega_B}{\omega_c} \\ \begin{pmatrix} 2\mathrm{sncn}(-\Omega_0 t+\phi,\omega_c/\Omega_0) \\ -1+2\mathrm{sn}^2(-\Omega_0 t+\phi,\omega_c/\Omega_0) \\ -\frac{\omega_B}{\omega_c}-2\frac{\Omega_0}{\omega_c}\mathrm{dn}(-\Omega_0 t+\phi,\omega_c/\Omega_0). \end{pmatrix}, & \Omega_0>\omega_c,\ \frac{k_y^0 d}{\sqrt{\mu}}<-\frac{\omega_B}{\omega_c} \\ \begin{pmatrix} 2\tanh(\omega_c t+\phi)/\cosh(\omega_c t+\phi) \\ -1+2\tanh^2(\omega_c t+\phi) \\ -\omega_B/\omega_c+2/\cosh(\omega_c t+\phi). \end{pmatrix}, & \Omega_0=\omega_c,\ \frac{k_y^0 d}{\sqrt{\mu}}>-\frac{\omega_B}{\omega_c} \\ \begin{pmatrix} 2\tanh(-\omega_c t+\phi)/\cosh(-\omega_c t+\phi) \\ -1+2\tanh^2(-\omega_c t+\phi) \\ -\omega_B/\omega_c-2/\cosh(-\omega_c t+\phi). \end{pmatrix}, & \Omega_0=\omega_c,\ \frac{k_y^0 d}{\sqrt{\mu}}<-\frac{\omega_B}{\omega_c}. \end{cases} \tag{5.8}$$

Here $\mathrm{sncn}(-\Omega_0 t+\phi,\omega_c/\Omega_0) = \mathrm{sn}(-\Omega_0 t+\phi,\omega_c/\Omega_0)\mathrm{cn}(-\Omega_0 t+\phi,\omega_c/\Omega_0)$. By using the properties of the elliptic functions [75], we obtain that the frequencies of the cyclotron-like and Bloch-like oscillations, respectively, are

$$\Omega = \begin{cases} \pi\omega_c/2K(\Omega_0/\omega_c), & \Omega_0<\omega_c \\ \pi\Omega_0/K(\omega_c/\Omega_0), & \Omega_0>\omega_c, \end{cases} \tag{5.9}$$

where $K(k) = F(\pi/2,k)$ is the complete elliptic integral of the first kind. By writing the elliptic functions as Fourier series [75], we notice that only odd harmonics of the fundamental frequency are present in the cyclotron-like regime, whereas all harmonics exist in the Bloch like regime. The higher harmonics are significant only in the vicinity of the separatrix [154].

The electrons in thermal equilibrium always have the largest probability to be at lowest possible energy. Especially at low temperatures and low carrier densities the equilibrium distribution $f_{eq}(\mathbf{k})$ peaks strongly at $\mathbf{k}=\mathbf{0}$ approaching the delta-function of Eq. (2.58) in the limit $T_e \to 0$ and $N_0 \to 0$. Therefore, we study in detail the effect of the electric and magnetic field on electrons starting at the bottom of the miniband. We obtain from Eq. (5.4) that $\Omega_0 = \omega_B/2$ meaning that cyclotron-like and Bloch-like oscillations occurs at electric fields $\omega_B < 2\omega_c$ and $\omega_B > 2\omega_c$, respectively. The frequency of the nonlinear oscillations of the electrons is now

$$\Omega = \begin{cases} \pi\omega_c/2K(\omega_B/2\omega_c), & \omega_B<2\omega_c \\ \pi\omega_B/2K(2\omega_c/\omega_B), & \omega_B>2\omega_c. \end{cases} \tag{5.10}$$

The frequency Ω is tunable by variation of the magnetic and electric fields. If $\omega_B \gg \omega_c$, the magnetic field only slightly perturbs the Bloch oscillations and we get $\Omega = \omega_B$. In the opposite limit $\omega_B \ll \omega_c$ we have $\Omega = \omega_c$. In this case the electron trajectories are restricted close to the bottom of the miniband and Eq. (5.2) describes a simple harmonic oscillator with a frequency ω_c.

The transient cyclotron-like and Bloch-like oscillations have been analyzed in detail both theoretically [154, 155] and experimentally [45], and they have been termed as coherent Hall-effect. The experimental observations are in qualitative agreement with the theory.

5.1.2 Dissipative electron dynamics in crossed fields

The dc current in the presence of static fields can be calculated using Eq. (2.56). In the limit of low temperatures and low carrier densities, where $f_{eq}(\mathbf{k})$ is given by (2.58), the problem was studied first by Polyanovskii [153].

Alternatively to the $\mathbf{k}$-space description, the ballistic dynamics of the miniband electrons in static fields can be described with variables v_x, v_y and ε_x

$$\begin{aligned} \frac{dv_x'}{dt} &= -\left[\omega_B + \omega_c v_y'\right]\varepsilon_x' \\ \frac{d\varepsilon_x'}{dt} &= \left[\omega_B + \omega_c v_y'\right]v_x' \\ \frac{dv_y'}{dt} &= -\omega_c v_x'. \end{aligned} \tag{5.11}$$

It is important to notice that in the presence of magnetic field this kind of balance equations are valid only in the absence of scattering. In the presence of scattering several different types of balance equations have been used [155, 158], but none of them is equivalent to the Boltzmann equation. By using the last relation in Eqs. (5.11) and Eq. (2.56), we get

$$j_y = -\frac{\omega_c \tau}{\sqrt{\mu}} j_x. \tag{5.12}$$

Therefore, we only need to calculate one of the current density components j_y or j_x. It turns out to be easier to calculate the j_y. By using the following series representations for the elliptic [75], cosh and $\psi(x) = \frac{d}{dx}\ln\Gamma(x)$-functions

$$\mathrm{cn}(x,k) = \frac{2\pi}{kK(k)} \sum_{n=0}^{\infty} \frac{q(k)^{n+1/2}}{1+q(k)^{2n+1}} \cos[(2n+1)\pi x/2K(k)], \tag{5.13}$$

$$\mathrm{dn}(x,k) = \frac{\pi}{2K(k)} + \frac{2\pi}{K(k)} \sum_{n=1}^{\infty} \frac{q(k)^{n}}{1+q(k)^{2n}} \cos[2n\pi x/2K(k)], \tag{5.14}$$

$$\frac{1}{\cosh x} = 2e^{-x}\frac{1}{1+e^{-2x}} = 2e^{-x}\sum_{n=0}^{\infty}(-1)^n e^{-2nx} = 2\sum_{n=0}^{\infty}(-1)^n e^{-(2n+1)x}, \tag{5.15}$$

and

$$\sum_{n=0}^{\infty}\frac{(-1)^n}{zn+1} = \frac{1}{2z}\left[\psi\left(\frac{z+1}{2z}\right) - \psi\left(\frac{1}{2z}\right)\right], \tag{5.16}$$

we get

$$j_x/j_p = \begin{cases} \frac{16\Omega\tau}{\omega_c^2\tau^2}\sum_{n=0}^{\infty}\frac{q(\omega_B/2\omega_c)^{n+1/2}}{1+q(\omega_B/2\omega_c)^{2n+1}}\frac{(2n+1)^2\Omega^2\tau^2}{1+(2n+1)^2\Omega^2\tau^2}, & \omega_B < 2\omega_c, \\ \frac{8\Omega\tau}{\omega_c^2\tau^2}\sum_{n=1}^{\infty}\frac{q(2\omega_c/\omega_B)^n}{1+q(2\omega_c/\omega_B)^{2n}}\frac{(n\Omega)^2\tau^2}{1+(n\Omega)^2\tau^2}, & \omega_B > 2\omega_c, \\ \frac{4}{\omega_c\tau}\left\{1-\frac{1}{2\omega_c\tau}\left[\psi\left(\frac{1}{4\omega_c\tau}+\frac{3}{4}\right)-\psi\left(\frac{1}{4\omega_c\tau}+\frac{1}{4}\right)\right]\right\}, & \omega_B = 2\omega_c. \end{cases} \tag{5.17}$$

Here $j_p = N_0 e\Delta d/4\hbar$ is given by Eq. (2.65) at $T_e = 0$, $q(k) = e^{-\pi K(k')/K(k)}$ and $k' = \sqrt{1-k^2}$.

In the limit of strong magnetic field $\omega_B \ll \omega_c$, the electrons are restricted close to the bottom of the miniband, and we get

$$j_x \approx j_p\frac{2\omega_B\tau}{1+\omega_c^2\tau^2}. \tag{5.18}$$

The current density is directly proportional to E_{dc} and the resistance $R \propto (1+\omega_c^2\tau^2)$. Therefore, we see that in the regime of Drude transport the magnetic field induces additional magnetoresistance proportional to B_z^2.

On the other hand, in the limit of weak magnetic field $\omega_c \ll \omega_B$, we get by straightforward calculation that

$$j_x \approx j_p\frac{2\omega_B\tau(1-\omega_c^2/\omega_B^2)}{1+\left[\omega_B\tau(1-\omega_c^2/\omega_B^2)\right]^2} + j_p\frac{\omega_c^2}{\omega_B^2}\frac{2\omega_B\tau}{1+4\omega_B^2\tau^2}. \tag{5.19}$$

We see that the magnetic field only slightly changes the Esaki-Tsu current density, which is obtained in the limit $\omega_c \to 0$.

The VI characteristics for different values of the magnetic field are shown in Fig. 5.2 (a). We see that reasonably weak magnetic fields $\omega_c\tau \approx 1$ result in significant enhancement of the dc current. For larger magnitudes $\omega_c\tau \gtrsim 3$, the transition from oscillatory to rotational motion at the separatrix $\omega_B = 2\omega_c$ manifests itself as a very abrupt and strong suppression of the dc current [120, 153, 154, 156]. In the cyclotron-like regime, there are no Bragg reflections and therefore it corresponds the PDC part of the VI characteristic. On the other hand, the Bragg reflections in the Bloch-like regime result in NDC at the operation point. We find that also the average

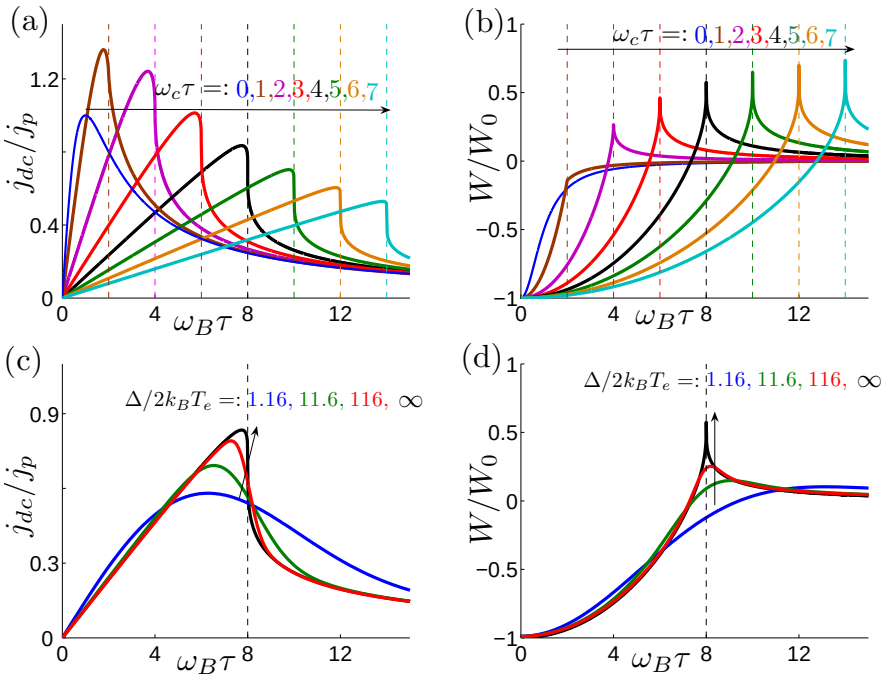

Figure 5.2: (a) VI characteristics at $T_e = 0$ K for $\omega_c\tau =: 0, 1, 2, 3, 4, 5, 6, 7$. The separatrices $\omega_B = 2\omega_c$ for different ω_c are marked with dashed lines. (b) The average miniband energy of the electrons as a function of dc bias at $T_e = 0$ K for the same magnetic field values ω_c. (c) VI characteristics for $\omega_c\tau = 4$ at different temperatures $\Delta/2k_BT_e =: 1.16, 11.6, 116$ and $T_e = 0$ K. (d) The average miniband energy for $\omega_c\tau = 4$ at the same temperatures.

miniband energy of the electrons, calculated numerically by using Eq. (2.57), shows interesting features due to the pendulum dynamics. Fig. 5.2 (b) shows that the miniband energy peaks strongly in the vicinity of the separatrix $\omega_B = 2\omega_c$, because the electron trajectories stick a very long time near the Brillouin zone boundary corresponding to the hyperbolic point of the pendulum. We also studied the temperature dependence using Eqs. (2.56), (2.57) and (2.32). Figs. 5.2 (c) and (d) show that the abrupt changes of the current density and average miniband energy as a function of ω_B smooth away as the temperature is increased. For $\Delta = 60$ meV, the temperature dependent parameters $\Delta/2k_BT_e = 1.16$, $\Delta/2k_BT_e = 11.6$ and $\Delta/2k_BT_e = 116$ used in Figs. 5.2 (c), (d) correspond to temperatures $T_e = 300$ K, $T_e = 30$ K and $T_e = 3$ K, respectively.

We now turn to the consideration of weak signal ($\beta \ll 1$) response in the limit of low temperature and low carrier density. The dynamics of the miniband electrons in the presence of time-dependent electric field $E(t) = E_{dc} + E_\omega \cos\omega t$ and constant magnetic field $\mathbf{B} = (0, 0, B_z)$ can be solved

analytically only in particular limits. In the limit $B_z \to 0$, we obtain the usual Bloch gain and more generally the Tucker relations, which we considered in Section 2.4.2. By using a perturbation theory with respect to parameter $\omega_c/\omega_B \ll 1$, it is also possible to calculate the corrections caused by a weak magnetic field. It turns out that weak magnetic field does not essentially change the gain profiles or the VI characteristics. On the other hand, in the opposite limit of strong magnetic field $\omega_B \ll \omega_c$ the dynamics of the miniband electrons is equivalent with a simple harmonic oscillator, and therefore the steady-state time-dependent current is given by

$$\begin{aligned} j_x(t) &= j_p \frac{2\omega_B\tau}{1+\omega_c^2\tau^2} + j_p\left[\frac{\omega\tau}{1+(\omega+\omega_c)^2\tau^2} + \frac{\omega\tau}{1+(\omega_c-\omega)^2\tau^2}\right]\beta\cos\omega t \\ &\quad + j_p\left[\frac{\omega(\omega+\omega_c)\tau^2}{1+(\omega+\omega_c)^2\tau^2} - \frac{\omega(\omega_c-\omega)\tau^2}{1+(\omega_c-\omega)^2\tau^2}\right]\beta\sin\omega t. \end{aligned} \tag{5.20}$$

We see that the cyclotron absorption in this limit is described by a standard Lorentzian shaped profile with resonant frequency ω_c.

Although these analytic limits gives us some insights about the electron dynamics, the most interesting results occur in the cases where the electric and magnetic field quanta are comparable to each other. This situation was studied in Paper IX by numerically solving the dissipative dynamics using Eq. (2.40) and (2.58). We find that the response to a weak ac field shows clear signatures of the different types of ballistic oscillations described in Section 5.1.1. The different types of gain profiles are shown in Paper IX in Fig. 1. In these calculations the magnetic field was fixed and the electric field was varied in such a way that the electrons perform several cycles of oscillations between the scattering events $\Omega\tau > 1$. If $\omega_c \gg \omega_B$, we obtained the Lorentzian absorption profile in excellent agreement with Eq. (5.20) [Paper IX Fig. 1 (c)]. In this case the real part of the dynamic conductivity is always positive and an amplification of probe field is not possible. By increasing the electric field E_{dc} the situation changes dramatically, so that high-frequency gain can now appear due to nonlinear cyclotron oscillations [Paper IX Fig. 1 (d), (e)]. The characteristic shape of the cyclotron gain profile can be seen also in Fig. 5.3. It is an inverse of the usual dispersive Bloch gain profile in the sense that the maximum values of the absorption occur at frequencies smaller than the resonant frequency, whereas the gain takes place at frequencies somewhat above the resonant frequency. In this gain profile the frequency of the nonlinear cyclotron oscillations Ω determines the resonant frequency of the crossover from absorption to gain. In the vicinity of separatrix in the cyclotron-like regime, replicas of the inverted dispersive gain profile appear at odd harmonics of Ω corresponding to the anharmonicity of the ballistic oscillations discussed in Section 5.1.1 [Paper IX Fig. 1 (e)]. If E_{dc} is further increased above the threshold $\omega_B > 2\omega_c$, we reach the Bloch-like regime, where we always have a dispersive Bloch gain profile with

a crossover frequency Ω [Paper IX Fig. 1 (f)]. Replicas of this gain profile now can appear at both even and odd harmonics of Ω, because in this regime all harmonics are present in the ballistic oscillations.

Our results show that both the cyclotron gain and the Bloch-like gain have such attractive properties as wide tunability and extremely large magnitudes of the gain, which can be utilized in an operation of THz oscillators and amplifiers. The gain profiles in both regimes of motion are easily tunable by changing magnetic and electric fields as discussed in Paper IX. On the other hand, the magnitudes of the Bloch-like gain and cyclotron gain, already in rather weak electric and magnetic fields ($\omega_c\tau \gtrsim 2$, $\omega_B\tau \gtrsim 3.6$) are approximately an order of magnitude larger than the usual Bloch gain at $\mathbf{B} = \mathbf{0}$. Such kind of magnitudes of the fields have been used in a number of experiments [45, 47, 48, 120, 156]. The maximum THz gain at low temperature takes place in the vicinity of the separatrix, where we estimate for moderate doping $N_0 = 10^{16}$ cm^{-3} unprecedented values $\alpha \approx 500$ cm^{-1}.

Although the response to the ac field results from complicated nonlinear electron dynamics, we identified in Paper IX an important role of the separatrix in the origin of large THz gain. In the vicinity of the separatrix, the electron trajectories stick a long time near the Brillouin zone boundary, which can be seen as a strong increase of average miniband energy of the electrons [Fig. 5.2 (b)] and enhancement of THz gain. Because the electrons have negative effective mass in the upper part of the miniband, we expect that the proposed oscillators bear analogies to the Kroemer's suggestion of negative mass amplifier [24] and cyclotron resonance lasers [159]. A more detailed description of the similarities and differences of these devices requires further analysis.

We emphasize that in the cyclotron-like regime the SL operates in the monotonously increasing part of the VI characteristic. Therefore, the cyclotron gain is inherently stable with respect to the space-charge fluctuations and also the boundary conditions, defined by the contacts attached to the SL, are not expected to play an important role in the device performance. On the other hand, in the Bloch-like regime the gain always extends to the low frequencies due to the operation in the NDC state. This means that the formation of electric domains has to be suppressed for example by using the methods described in Chapter 3.

As was discussed in the Chapter 1, semiconductor laser sources, QCLs, already exists at terahertz frequencies but the main problem is the maximal operation temperature. Thus, in addition to the stability and magnitude of the gain, a central issue from the applied perspective is the temperature dependence of the peak gain. It is easy to see that the steady-state time-dependent current [Eq. (2.40)] in SLs depends on the temperature via the equilibrium distribution $f_{eq}(\mathbf{k})$, which in the case of moderate carrier densities depends on a temperature-dependent parameter $\Delta/2k_BT_e$ [see Eq.(2.32)].

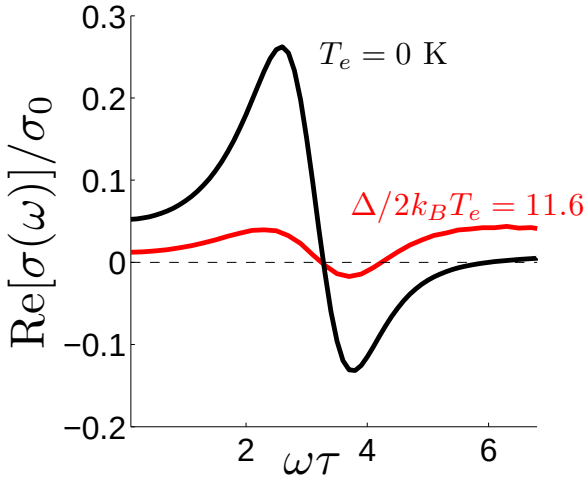

Figure 5.3: Cyclotron gain profiles at different temperatures for $\omega_B\tau = 6.3$ and $\omega_c\tau = 4$.

Although the approach based on Eq. (2.40) is very efficient at low temperatures, it becomes quite slow for calculation of the time-dependent current at high-temperatures. Therefore, we studied the gain at different temperatures by directly solving numerically a discretized Boltzmann equation (2.35) [160]. We observed that the parameter $\Delta/2k_BT_e$ affects the gain profiles differently depending on the regime of the oscillations. Figure 5.3 shows the cyclotron gain profile for electric and magnetic fields $\omega_B\tau = 6.3$ and $\omega_c\tau = 4$ and temperature-dependent parameter $\Delta/2k_BT_e = 11.6$ ($\Delta = 60$ meV, $T_e \approx 30$ K) [160]. The magnitude of the peak gain already at this temperature is approximately of the same order as in the case of usual Bloch gain at $\mathbf{B} = \mathbf{0}$. Similarly, we obtain for different magnitudes of the electric and magnetic fields that the cyclotron gain always decreases quickly with increasing temperature. On the other hand, in the Bloch-like regime enhancement of THz gain with applied magnetic field is obtained also at room temperature.

To understand why the cyclotron gain is more sensitive to the temperature than the Bloch gain, we study the ballistic electron trajectories at constant electric and magnetic fields. The effect of finite temperature is essentially to increase the kinetic energy of the electrons. If we assume that the initial inplane-momenta of the electrons are in an interval determined by $0 \leq \hbar^2 k_y^2/2m \lesssim k_BT_e$, we get from equation (5.4) that the "pendulum energies" are between

$$|\frac{\omega_B}{2\omega_c} - \sqrt{\frac{k_BT_e}{\Delta}}| \lesssim \frac{\Omega_0}{\omega_c} \lesssim \frac{\omega_B}{2\omega_c} + \sqrt{\frac{k_BT_e}{\Delta}}. \tag{5.21}$$

Now in order that the electrons perform nonlinear cyclotron oscillations

resulting in cyclotron gain, the electric field has to be sufficiently strong $\omega_B/2\omega_c \gtrsim 0.75$. On the other hand, sufficient majority of the electrons perform cyclotron oscillations only if $\frac{\omega_B}{2\omega_c} + \sqrt{\frac{k_B T_e}{\Delta}} \lesssim 1$. These two conditions result in upper limit for the temperature as

$$k_B T_e \lesssim \Delta/16. \tag{5.22}$$

This rough estimate agrees nicely with the maximal operation temperature of the cyclotron oscillator obtained from the numerical simulations. Therefore, we can now understand the sensitive dependence of the cyclotron gain on temperature. Namely, if the temperature is increased above the threshold value determined by inequality (5.22), sufficient part of the electrons perform Bloch-like oscillations due to thermal excitations. Now, the phases of the oscillating electrons in the mixture of Bloch and cyclotron oscillations are not synchronized, and the high-frequency gain vanishes. The inequality (5.22) can be rewritten as $T_e \lesssim \frac{\Delta}{1.4 \text{ meV}}$ K, which shows that room temperature operation of the cyclotron oscillator requires very wide SL miniband. It is not realistic to assume that the scattering in such system could be modelled with a relaxation time approximation. In contrast to cyclotron-like regime of motion, the Bloch-like oscillations far from the separatrix $\omega_B \gg 2\omega_c$ depend less sensitively on the thermal quasimomentum distribution, and sufficient majority of the electrons in standard SLs perform Bloch oscillations also at room temperature.

We have also made preliminary investigations of the large amplitude $E_\omega \gtrsim E_{cr}$ electron dynamics in crossed fields. Although we have found that for particularly chosen E_{dc} and B_z the cyclotron gain in conditions of PDC can still exist for $E_\omega > 2E_{cr}$, the electron trajectories in the vicinity of separatrix are typically very sensitive to E_ω. In the absence of scattering the electron dynamics can even become chaotic, and further work is still required to understand how this affects the operation of the devices.

5.2 Stark-cyclotron resonances & stable THz gain

In Paper IX we also discussed the possibility to obtain stable Bloch gain in the tilted magnetic field configuration $\mathbf{B} = (B_x, 0, B_z)$. In this case the ballistic electron dynamics in the presence of time-dependent electric field

$E(t) = E_{dc} + E_\omega \cos\omega t$ is described by equations

$$\begin{aligned}
\hbar\frac{dk_x}{dt} &= eE(t) + ev_yB_z = eE_{dc} + eE_\omega\cos\omega t + eB_z\frac{\hbar k_y}{m}, \\
\hbar\frac{dk_y}{dt} &= -ev_xB_z + ev_zB_x = -eB_z\frac{\Delta d}{2\hbar}\sin k_xd + eB_x\frac{\hbar k_z}{m}, \\
\hbar\frac{dk_z}{dt} &= -ev_yB_x = -eB_x\frac{\hbar k_y}{m}.
\end{aligned} \tag{5.23}$$

Similarly as in the case of crossed field, we proceed by first analyzing the ballistic oscillations in the case of static fields ($E_\omega = 0$), and then utilize the acquired insights in the analysis of the VI characteristics and small-signal absorption and gain.

In the tilted fields configuration, the electrons perform cyclotron oscillations in the plane perpendicular to the SL axis with the frequency $\omega_{c\perp} = eB_x/m$, and these in-plane cyclotron oscillations are coupled to the Bloch oscillations via the perpendicular magnetic field component ω_c [46, 47, 48]. It can be shown with a straightforward calculation using Eqs. (5.23) that the ballistic electron dynamics in the case of static electric field ($E_\omega = 0$) is equivalent with a simple harmonic oscillator driven by a time-dependent plane wave [47]

$$\frac{d^2k_z}{dt^2} + \omega_{c\perp}^2k_z = -\frac{\omega_{c\perp}\omega_c\sqrt{\mu}}{d}\sin\left[\frac{B_z}{B_x}k_zd - \omega_Bt - \phi\right], \tag{5.24}$$

where $\phi = k_x(0)d + \frac{B_z}{B_x}k_z(0)d$. The other components of the quasimomentum are then determined by equations

$$k_xd = \omega_Bt - \frac{\omega_c}{\omega_{c\perp}}\frac{k_zd}{\sqrt{\mu}} + k_x(0)d + \frac{\omega_c}{\omega_{c\perp}}\frac{k_z(0)d}{\sqrt{\mu}} \tag{5.25}$$

$$k_y = -\frac{1}{\omega_{c\perp}}\frac{dk_z}{dt}. \tag{5.26}$$

The harmonic oscillator driven by a time-dependent plane wave (5.24) is a well-known model system for chaotic dynamics [47]. It has attracted a lot of attention, because the transition to chaos in this system does not occur by gradual destruction of stable orbits in parameter space in accordance with a so-called Kolmogorov-Arnold-Moser (KAM) theorem [47, 161, 162, 163]. Instead, the non-KAM chaos in this system switches on and off abruptly at Stark-cyclotron resonances $\omega_B = n\omega_{c\perp}$ ($n = 0, 1, 2, 3...$). The onset of chaos is characterized by unbounded electron trajectories, which propagate through infinite stochastic web patterns in the phase-space [47]. Although stochastic webs are not formed in the case of Stark-cyclotron resonances $\omega_B = r\omega_{c\perp}$, where r is rational but not integer, the finite electron orbits still exhibit a resonant extension along x-axis [162]. The transient coupled cyclotron and

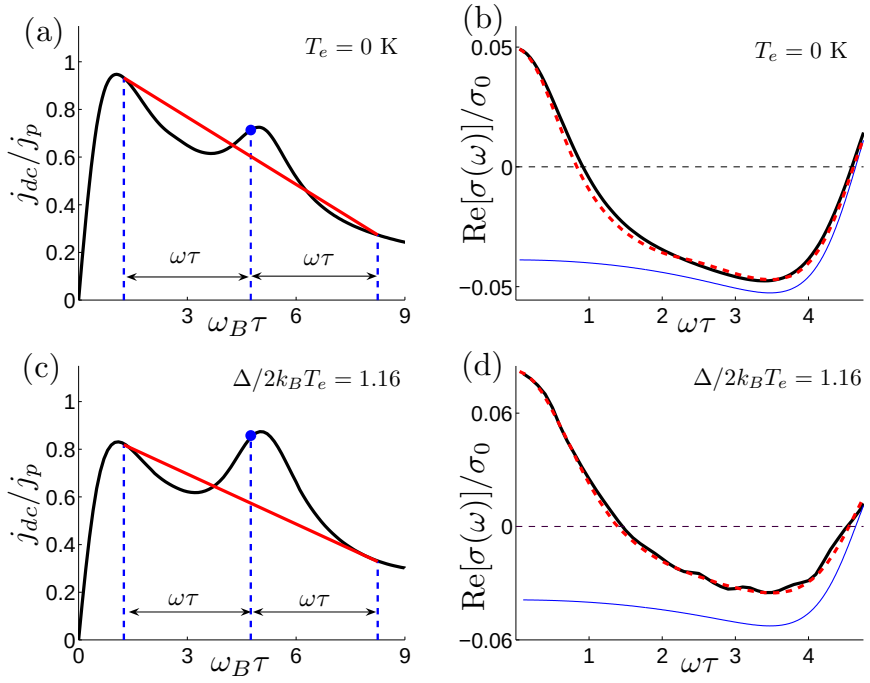

Figure 5.4: (a),(c) VI characteristics for $\omega_c\tau = 2$ and $\omega_{c\perp}\tau = 5$ at different temperatures. (b),(d) Gain profiles at different temperatures for the same magnetic field and dc bias $\omega_B\tau = 4.75$ (thick black line). The dashed (red) line shows the approximation obtained with a Tucker formula. The thin (blue) line indicates the usual Bloch gain profile at $\mathbf{B} = \mathbf{0}$.

Bloch oscillations in tilted magnetic field configuration were recently experimentally observed [48]. The complementary quantum mechanical picture to the delocalized semiclassical electron trajectories in tilted magnetic field have also been developed [47, 164]. There, a spatially extended character of the wave-functions, termed as magnetic-field-induced minibands [164], was obtained due to the Stark-cyclotron resonances.

In the presence of scattering, the delocalization of the electrons at Stark-cyclotron resonances results in a strong increase of dc current, which can be seen as additional resonant structures in the VI characteristics [47, 161, 162, 163]. Figs. 5.4 (a) and (c) demonstrate such additional structure for a particular magnetic field at temperatures $T_e = 0$ K and $T_e = 300$ K ($\Delta/2k_BT_e = 1.16$), respectively. We find that these structures in the VI characteristics can be utilized in a similar way as the photon-assisted peaks in dc-ac driven SLs discussed in Section 3.2. Namely, by choosing the working point at the PDC part of the peak, we find that the gain profile close to the Bloch frequency $\omega \approx \omega_B$ has the usual shape of the dispersive Bloch gain, whereas the dynamical conductivity at low frequencies is now positive

[Fig. 5.4 (b),(d)]. Importantly, the gain has a smooth temperature dependence and significant magnitudes can still be obtained at room temperature [Fig. 5.4 (d)]. The gain profiles at both temperatures can be well approximated by a Tucker formula [Eq. (3.5)], in which $j_{dc}(eE_{dc}d)$ is now the current density calculated in the presence of the magnetic field. The VI characteristic and gain profile shown in Figs. 5.4 (a) and (b) were calculated using the path-integral approach based on Eq. (2.40). At large temperature $\Delta/2k_BT_e = 1.16$ the results [Figs. 5.4 (c) and (d)] were obtained by numerically solving the discretized Boltzmann equation [160].

Recently, an alternative approach to obtain high-frequency gain in tilted magnetic field configuration in SLs was proposed by M. T. Greenaway *et al.* [38]. There, the authors predicted, using a drift-diffusion model, that sub-THz generation can be obtained in SLs due to the magnetic-field-induced multiple propagating charge domains. Such device would essentially be a new type of Gunn oscillator [32]. We emphasize that although the operation in the PDC part of the VI characteristic guarantees electric stability against *small* space-charge fluctuations, it does not necessarily mean that the space-charge domains are absent for all boundary conditions. If there is a strong mismatch in the conductivity at the boundary between the SL and the contact, the electric field changes abruptly at the interface, and the linear stability analysis becomes unreliable. Therefore, the SL in tilted magnetic field can probably operate as a Bloch oscillator or as a Gunn oscillator depending on the boundary conditions. In contrast to the Bloch oscillator with modulated bias, discussed in Section 3.4, here also heavily doped SLs can be used to obtain larger magnitudes of gain and smooth boundaries between SLs and contacts.

It should be mentioned that the Stark-cyclotron resonances can occur also if magnetic field is applied parallel to the SL direction $\mathbf{B} = (B_x, 0, 0)$. In this case the ballistic cyclotron and Bloch oscillations are decoupled, but in the presence of scattering resonant peaks can still appear in the (B_x, j_{dc})-characteristics at the Stark-cyclotron resonances $\omega_B = n\omega_{c\perp}$ [165]. In the quantum mechanical picture the Stark-cyclotron resonances correspond to isoenergetic states in the Landau-Stark ladder ($\hbar\omega_B = n\hbar\omega_{c\perp}$), which allow elastic scattering-assisted transitions between the states. In subsequent experiments it has been found that, in addition to these elastic scattering processes, also the inelastic scattering from optical phonons plays an important role in the resonant current enhancements [161, 164, 166, 167]. The variations of the current in this configuration of the fields are, however, too small to induce clear structures in the VI characteristics.

Chapter 6

Conclusions and perspectives

We have predicted several new possibilities to obtain stable THz gain in SLs. The energy which is converted to high-frequency radiation can either come from the dc bias (Bloch and cyclotron amplifiers/oscillators) or from ac pump field (parametric amplifiers/oscillators). The amplifiers have different attractive features. The Bloch and cyclotron oscillators and amplifiers are continuously tunable using electric and magnetic fields. The usual inversionless Bloch gain at $\mathbf{B} = \mathbf{0}$ (and in tilted magnetic field) has smooth temperature dependence resulting in reasonable magnitudes also at room temperature. On the other hand the nonlinear Bloch-like oscillations and cyclotron-like oscillations in crossed fields result in very large gain at low temperatures, but the gain decreases quickly with increasing temperature. The parametric amplifiers operating at room temperature can provide reasonably large phase-sensitive gain at low order harmonics and half-harmonics.

The central results of this thesis are related to the physical mechanisms of high-frequency gain and electrical stability of the SL amplifiers. We have shown that the amplifiers discussed above can operate in conditions, where the SL is stable against small space-charge fluctuations. The key idea to achieve this stability is put the operation point in the PDC part of the VI characteristic. Hence the low-frequency dynamical conductivity is positive while the high-frequency dynamical conductivity can still be negative providing the desirable THz gain. The high-frequency gain is achieved either due to Bloch oscillations (Bloch gain), cyclotron oscillations (cyclotron gain) or oscillations of specific energy-dependent parameter at twice the frequency of the signal (parametric gain), whereas the stability can be obtained either due to photon-assisted transport (Bloch gain in dc-ac driven SL), free-electron absorption (Bloch oscillator with modulated bias and parametric amplifiers) or Stark-cyclotron resonances (Bloch gain in tilted magnetic field).

In several approaches (Bloch gain in dc-ac driven SL, Bloch oscillator with modulated bias and Bloch gain in tilted magnetic field) we have demonstrated the possibility of stable high-frequency gain with the help of resonance struc-

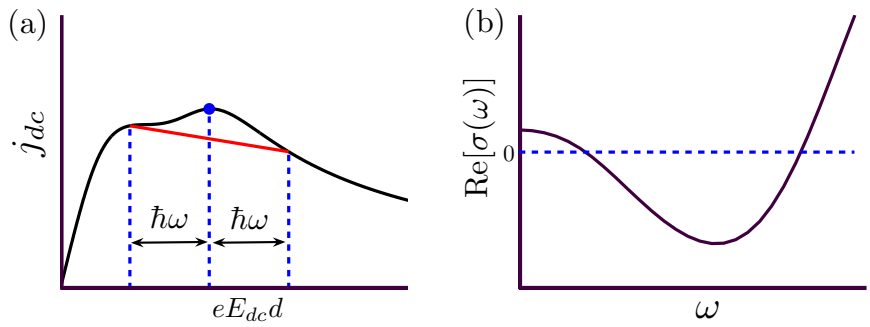

Figure 6.1: (a) Schematic VI characteristic with smooth structures providing stable high-frequency gain. (b) Gain profile obtained using the Tucker formula at the operation point marked in the VI characteristic.

tures in the VI characteristic (for schematic illustration of the basic idea, see Fig. 1.2). As pointed out by Kroemer [100], the PDC in this kind of situation occurs only in a relatively narrow range of electric field values [Fig. 1.2 (a)] and therefore for typical boundary conditions much of the contact-to-SL transition region remains in the NDC regime with "unknown – but almost certainly undesirable – consequences". We underline that the electric and magnetic fields allow precise control of the modifications of the VI characteristic, and in principle the stable high-frequency gain can be obtained without the NDC regimes in the VI characteristic between the low field values and the operation point. This kind of situation is schematically illustrated in Fig. 6.1. The optimization of the contact design for all the proposed amplifiers requires more detailed modelling of the system and goes beyond the scope of this thesis. However, we emphasize the very high electric stability of the cyclotron gain (Section 5.1) and Bloch gain in ac driven SL (Section 3.3). In these cases the operation point can be chosen from the almost linearly increasing part of the VI characteristic [see Fig. 1 (b) in Paper IX and Fig. 3.2]. The parametric amplifiers driven by quasistatic pump field and Bloch oscillator with modulated bias can also operate in almost linearly increasing part of the VI characteristic, but in these cases the electric stability also requires that the pump frequency is large enough $\Omega\tau_d \gg 1$ to prevent a significant accumulation of the charges during the NDC portion of the pump period.

We have found that the nonlinear character of the dynamics of the miniband electrons in the presence of magnetic field can result in very strong response to a weak ac field (see Section 5 and Paper IX). Therefore, we expect also enhancement of the parametric gain in the presence of magnetic field. Moreover, the magnetic-field-induced effects can most likely be utilized in sensitive THz photon detectors.

Bibliography

[1] P. H. Siegel, IEEE Trans. Microwave Theory Tech. **50**, 910 (2002); B. Ferguson and X.-C. Zhang, Nat. Mater. **1**, 26 (2002); T. W. Crowe *et al.*, IEEE J. Solid-State Circuits **40**, 2104 (2005); M. Tonouchi, Nat. Photonics **1**, 97 (2007).

[2] B. S. Williams, Nat. Photonics **1**, 517 (2007).

[3] L. Esaki and R. Tsu, IBM J. Res. Dev. **14**, 61 (1970).

[4] R. Tsu, Microelectron. J. **38**, 959 (2007).

[5] L. Esaki and L. L. Chang, Phys. Rev. Lett. **33**, 495 (1974).

[6] L. L. Chang, L. Esaki and R. Tsu, Appl. Phys. Lett. **24**, 593 (1974).

[7] L. L. Chang and L. Esaki, Phys. Today **45**, 36 (1992).

[8] R. F. Kazarinov and R. A. Suris, Sov. Phys. Semicond. **5**, 707 (1971).

[9] J. Faist *et al.*, Science **264**, 553 (1994).

[10] R. Köhler *et al.*, Nature **417** 156 (2002); A. Wade *et al.*, Nat. Photonics **3**, 41 (2009).

[11] F. Bloch, Z. Phys. **52**, 555 (1928).

[12] C. Zener, Proc. R. Soc. London, Ser. A **145**, 523 (1934).

[13] P. Drude, Ann. Phys., Lpz **1**, 566 (1900); P. Drude, Ann. Phys., Lpz **3**, 369 (1900).

[14] K. Leo, Semicond. Sci. Technol. **13**, 249 (1998).

[15] J. Feldmann *et al.*, Phys. Rev. B **46**, 7252 (1992); K. Leo *et al.*, Solid State Commun. **84**, 943 (1992).

[16] C. Waschke *et al.*, Phys. Rev. Lett. **70**, 3319 (1993).

[17] T. Dekorsy *et al.*, Phys. Rev. B **50**, 8106 (1994).

[18] T. Dekorsy *et al.*, Phys. Rev. B **51**, 17275 (1995).

[19] S. A. Ktitorov, G. S. Simin and V. Ya. Sindalovskii, Sov. Phys. Solid State **13**, 1872 (1972).

[20] Historically the idea of Bloch oscillator was suggested by L. Esaki, W. E. Howard and R. Tsu (see Ref. [4]) already before the calculation of the Bloch gain profile in Ref. [19].

[21] C. Hilsum, Solid-State Electron. **21**, 5 (1978).

[22] H. Kroemer, Z. Phys. **134**, 435 (1953).

[23] W. Shockley, Bell. Syst. Tech. J. **33**, 799 (1954).

[24] H. Kroemer, Phys. Rev. **109**, 1856 (1958); H. Kroemer, Proc. IRE **47**, 397 (1959).

[25] B. K. Ridley and T. B. Watkins, Proc. Phys. Soc. (London) **78**, 293 (1961); C. Hilsum, Proc. IRE **50**, 185 (1962).

[26] B. K. Ridley, Proc. Phys. Soc. (London) **82**, 954 (1963).

[27] M. Büttiker and H. Thomas, Phys. Rev. Lett. **38**, 78 (1977); A. A. Ignatov and V. I. Shashkin, Sov. Phys. JETP **66**, 526 (1987).

[28] A. Wacker, Phys. Rep. **357**, 1 (2002).

[29] L. L. Bonilla and H. T. Grahn, Rep. Prog. Phys. **68**, 577 (2005).

[30] B. Rieder, *Semiclassical Transport in Semiconductor Superlattices with Boundaries*, Dissertation, University of Regensburg (2004).

[31] P. G. Savvidis *et al.*, Phys. Rev. Lett. **92**, 196802 (2004).

[32] J. B. Gunn, Solid State Commun. **1**, 88 (1963); J. B. Gunn, IBM J. Res. Dev. **8**, 141 (1964); H. Kroemer, Proc. IEEE **52**, 1736 (1964); J. B. Gunn, IBM J. Res. Dev. **10**, 310 (1966).

[33] H. W. Thim *et al.*, Appl. Phys. Lett. **7**, 167 (1965); D. E. McCumber and A.G. Chynoweth, IEEE Trans. Electron Devices **13**, 4 (1966); B. W. Hakki and S. Knight, IEEE Trans. Electron Devices **13**, 94 (1966); H. Kroemer, IEEE Trans. Electron Devices **14**, 476 (1967); B. W. Hakki, J. Appl. Phys. **38**, 808 (1967).

[34] A. Sibille *et al.*, Phys. Rev. B **39**, 6272 (1989).

[35] M. Hadjazi *et al.*, Electron. Lett. **29**, 648 (1993); J. F. Palmier *et al.*, Solid State Electron. **37**, 697 (1994); C. Minot *et al.*, Superlattices Microstruct. **23**, 1323 (1998); J. F. Palmier *et al.*, Superlattices Microstruct. **25**, 13 (1999).

[36] H. Le Person *et al.*, Appl. Phys. Lett. **60**, 2397 (1992).

[37] K. Hofbeck *et al.*, Phys. Lett. A **218**, 349 (1996); E. Schomburg *et al.*, Appl. Phys. Lett. **71**, 401 (1997); E. Schomburg *et al.*, Phys. Rev. B **58**, 4035 (1998); E. Schomburg *et al.*, Appl. Phys. Lett. **72**, 1498 (1998); E. Schomburg *et al.*, Appl. Phys. Lett. **74**, 2179 (1999); E. Schomburg *et al.*, Electron. Lett. **35**, 1491 (1999); H. Eisele *et al.*, Appl. Phys. Lett. **93**, 182105 (2008).

[38] M. T. Greenaway *et al.*, Phys. Rev. B **80**, 205318 (2009).

[39] E. Schomburg *et al.*, Phys. Rev. B **65**, 155320 (2002).

[40] A.-K. Jappsen *et al.*, J. Appl. Phys. **92**, 3137 (2002).

[41] R. Scheuerer *et al.*, Appl. Phys. Lett. **81**, 1515 (2002).

[42] C. P. Endres *et al.*, Review of Scientific Instruments **78**, 043106 (2007).

[43] F. Klappenberger *et al.*, Appl. Phys. Lett. **84**, 3924 (2004); K. F. Renk *et al.*, Phys. Rev. Lett. **95**, 126801 (2005).

[44] K. Unterrainer *et al.*, Phys. Rev. Lett. **76**, 2973 (1996).

[45] T. Bauer *et al.*, Phys. Rev. Lett. **88**, 086801 (2002); A. B. Hummel *et al.*, Phys. Status Solidi B **242**, 1175 (2005).

[46] F. G. Bass, V. V. Zorchenko and V. I. Shashora, JETP Lett. **31**, 314 (1980).

[47] T. M. Fromhold *et al.*, Phys. Rev. Lett. **87**, 046803 (2001); T. M. Fromhold *et al.*, Nature **428**, 726 (2004).

[48] Yu. A. Kosevich *et al.*, Phys. Rev. Lett. **96**, 137403 (2006); Yu. A. Kosevich *et al.*, Phys. Status Solidi B **243**, 2405 (2006).

[49] J. C. McGroddy and P. Gueret, Solid-State Electron. **14**, 1219 (1971).

[50] A. Wacker *et al.*, Phys. Status Solidi B **204**, 95 (1997).

[51] J. R. Tucker and M. F. Millea, Appl. Phys. Lett. **33**, 611 (1978); J. R. Tucker, IEEE J. Quantum Electron. **15**, 1234 (1979); J. R. Tucker and M. J. Feldman, Rev. Mod. Phys. **57**, 1055 (1985).

[52] A. Patane *et al.*, Phys. Rev. B **72**, 033312 (2005); A. Ignatov *et al.*, Appl. Phys. Lett. **88**, 032107 (2006).

[53] A. Dyson and B. K. Ridley, Phys. Rev. B **72**, 193301 (2005); A. Dyson and B. K. Ridley, J. Appl. Phys. **104**, 113709 (2008).

[54] M. Ben Dahan *et al.*, Phys. Rev. Lett. **76**, 4508 (1996).

[55] U. Peschel, T. Pertsch and F. Lederer, Opt. Lett. **23**, 1701 (1998); A. Kavokin *et al.*, Phys. Rev. B **61**, 4413 (2000); R. Sapienza *et al.*, Phys. Rev. Lett. **91**, 263902 (2003); H. Trompeter *et al.*, Phys. Rev. Lett. **96**, 053903 (2006).

[56] A. A. Ignatov, K. F. Renk and E. P. Dodin, Phys. Rev. Lett. **70**, 1996 (1993).

[57] R. Battesti *et al.*, Phys. Rev. Lett. **92**, 253001 (2004); P. Clade *et al.*, Phys. Rev. Lett. **96**, 033001 (2006); M. Cadoret *et al.*, Phys. Rev. Lett. **101**, 230801 (2008).

[58] I. Carusotto *et al.*, Phys. Rev. Lett. **95**, 093202 (2005); G. Ferrari *et al.*, Phys. Rev. Lett. **97**, 060402 (2006).

[59] M. Gustavsson *et al.*, Phys. Rev. Lett. **100**, 080404 (2008).

[60] O. Naaman, W. Teizer and R. C. Dynes, Phys. Rev. Lett. **87**, 097004 (2001); Y. Koval, M. V. Fistul and A. V. Ustinov, Phys. Rev. Lett. **93**, 087004 (2004); C. Falci, V. Bubanja and G. Schön, Z. Phys. B **85**, 451 (1991).

[61] H. Ott *et al.*, Phys. Rev. Lett. **92**, 160601 (2004); A. V. Ponomarov *et al.*, Phys. Rev. Lett. **96**, 050404 (2006).

[62] A. Wacker, Phys. Rev. B **66**, 085326 (2002); H. Willenberg, G. H. Döhler and J. Faist, Phys. Rev. B **67**, 085315 (2003); F. T. Vasko, Phys. Rev. B **69**, 205309 (2004).

[63] For theory, see H. M. James, Phys. Rev. **76**, 1611 (1949); G. H. Wannier, Phys. Rev. **117**, 432 (1960).

[64] For experiment, see E. E. Mendez, F. Agullo-Rueda and J. M. Hong, Phys. Rev. lett., **60**, 2426 (1988); P. Voisin *et al.*, Phys. Rev. Lett. **61**, 1639 (1988); E. E. Mendez and G. Bastard, Phys. Today **46**, 34 (1993).

[65] A. Wacker, Nature Phys. **3**, 298 (2007).

[66] R. Terazzi *et al.*, Nature Phys. **3**, 329 (2007); D. G. Revin *et al.*, Appl. Phys. Lett. **92**, 081110 (2008); T. Gresch *et al.*, Appl. Phys. Lett. **94**, 031102 (2009).

[67] K. K. Likharev, *Dynamics of Josephson Junctions and Circuits*, (Gordon and Breach, New York, 1986), Chapters 10 and 11; A. N. Vystavkin *et al.*, JETP Lett. **17**, 204 (1973); P. W. Forder and J. R. Waldram, J. Phys. D **14**, 1585 (1981).

[68] D. L. Smith and C. Mailhiot, Rev. Mod. Phys. **62**, 173 (1990).

[69] R. de L. Kronig and W. G. Penney, Proc. Roy. Soc. London, Ser. A **130**, 499 (1931).

[70] G. Bastard, Phys. Rev. B **24**, 5693 (1981); H.-S. Cho and P. R. Prucnal, Phys. Rev. B **36**, 3237 (1987).

[71] F. Bloch, Phys. Today **29**, 23 (1976).

[72] M. P. Marder, *Condensed Matter Physics*, New York: John Wiley & Sons, USA (2000).

[73] H. Kroemer, Am. J. Phys. **54**, 177 (1986).

[74] F.G. Bass and A. P. Tetervov, Phys. Rep. **140**, 237 (1986).

[75] M. Abramowitz and I. A. Stegun, *Handbook of Mathematical Functions With Formulas, Graphs and Mathematical Tables*, National Bureau of Standards, Washington, D.C. (1972).

[76] A. M. Bouchard and M. Luban, Phys. Rev. B **52**, 5105 (1995).

[77] D. H. Dunlap and V. M. Kenkre, Phys. Rev. B **34**, 3625 (1986); D. H. Dunlap and V. M. Kenkre, Phys. Lett. A **127**, 438 (1988); D. H. Dunlap and V. M. Kenkre, Phys. Rev. B **37**, 6622 (1988).

[78] M. Holthaus, Phys. Rev. Lett. **69**, 351 (1992).

[79] J. Wan, C. M. de Sterke and M. M. Dignam, Phys. Rev. B **70**, 125311 (2004).

[80] E. Schomburg, N. V. Demarina and K. F. Renk, Phys. Rev. B **67**, 155302 (2003); N. V. Demarina and K. F. Renk, Phys. Rev. B **71**, 035341 (2005).

[81] R. R. Gerhardts, Phys. Rev. B **48**, 9178 (1993); Yu. A. Romanov and E. V. Demidov, Phys. Solid State **41**, 1698 (1999).

[82] F. G. Bass, V. V. Zorchenko and V. I. Shashora, Sov. Phys. Semicond. **15**, 263 (1981).

[83] F. G. Bass and A. A. Bulgakov, *Kinetic and electrodynamic phenomena in classical and quantum semiconductor superlattices*, Nova Science Publishers Inc., New York (1997).

[84] R. G. Chambers, Proc. Phys. Soc., London, Sect. A **65**, 458 (1952); H. Budd, Phys. Rev. **127**, 4 (1962); C. MacCallum, Phys. Rev. **132**, 930 (1963).

[85] K. Pyragas, Sov. Phys. Solid State **28**, 1387 (1986).

[86] A. Sibille *et al.*, Phys. Rev. Lett. **64**, 52 (1990).

[87] F. Beltram *et al.*, Phys. Rev. Lett. **64**, 3167 (1990).

[88] H. T. Grahn *et al.*, Phys. Rev. B **43**, 12094 (1991).

[89] E. Schomburg *et al.*, Proc. 23rd Int. Conf. Phys. Semicond., Vol. **3**, 1679 (1996).

[90] T. Feil *et al.*, Appl. Phys. Lett. **87**, 212112 (2005).

[91] W. Pan *et al.*, Appl. Phys. Lett. **92**, 052104 (2008).

[92] G. Brozak *et al.*, Phys. Rev. Lett. **64**, 3163 (1990).

[93] A. A. Ignatov and Yu. A. Romanov, Sov. Phys. Solid State **17**, 2216 (1975); A. A. Ignatov and Yu. A. Romanov, Phys. Status Solidi B **73**, 327 (1976).

[94] Yu. A. Romanov, V. P. Bovin and L. K. Orlov, Sov. Phys. Semicond. **12**, 987 (1978).

[95] T. Hyart, K. N. Alekseev and S. Denisov, *Coherent control of photon-assisted transport in tunneling systems* (unpublished).

[96] It was shown in Ref. [28] that in the case of monochromatic field the Tucker relations exist in SLs operating in sequential tunneling and miniband conduction regimes. For polychromatic field the existence of Tucker relations in both regimes was pointed out in Papers VI and VII.

[97] C. A. Hamilton and S. Shapiro, Phys. Rev. B **2**, 4494 (1970).

[98] V. V. Pavlovich and E. M. Epshtein, Sov. Phys. Semicond. **10**, 1196 (1976).

[99] A. A. Ignatov *et al.*, Z. Phys. B **98**, 187 (1995).

[100] H. Kroemer, arXiv:cond-mat/0009311 (2000).

[101] P. K. Tien and J. P. Gordon, Phys. Rev. **129**, 647 (1963).

[102] For review of the photon-assisted transport in semiconductor nanostructures, see G. Platero and R. Aguado, Phys. Rep. **395**, 1 (2004).

[103] B. J. Keay and C. Aversa, Phys. Rev. B **54**, R2284 (1996).

[104] H. Kroemer, arXiv:cond-mat/0007482 (2000).

[105] T. Hyart, J. Mattas and K. N. Alekseev, *Electron bunches in semiconductor superlattices: A link between ballistic and dissipative dynamics*, (unpublished).

[106] A. A. Ignatov *et al.*, Ann. Phys. **3**, 137 (1994); E. Schomburg *et al.*, Appl. Phys. Lett. **68**, 1096 (1996); S. Winnerl *et al.*, Superlattices Microstruct. **21**, 91 (1997); S. Winnerl *et al.*, Phys. Rev B **56**, 10303 (1997); S. Winnerl *et al.*, Phys. Status Solidi B **204**, 58 (1997); E. Schomburg *et al.*, Physica E **7**, 814 (2000).

[107] F. G. Bass and E. A. Rubinshtein, Sov. Phys. Solid State **19**, 800 (1977); A. A. Ignatov and Yu. A. Romanov, Radiophysics and Quantum Electronics **21**, 90 (1978); A. A. Ignatov and V. I. Shashkin, Phys. Status Solidi B **110**, K117 (1982); A. A. Ignatov and V. I. Shashkin, Phys. Lett. **94A**, 169 (1983).

[108] P. S. S. Guimaraes *et al.*, Phys. Rev. Lett. **70**, 3792 (1993); B. J. Keay *et al.*, Phys. Rev. Lett. **75**, 4098 (1995); B. J. Keay *et al.*, Phys. Rev. Lett. **75**, 4102 (1995); S. Zeuner *et al.*, Phys. Rev. B **53**, R1717 (1996); S. Zeuner *et al.*, Appl. Phys. Lett. **69**, 2689 (1996).

[109] A. Wacker *et al.*, Phys. Rev. B **56**, 13268 (1997).

[110] K. N. Alekseev, M. V. Erementchouk and F. V. Kusmartsev, Europhys. Lett. **47**, 595 (1999); K. Seeger, Appl. Phys. Lett. **76**, 82 (2000).

[111] Yu. K. Pozhela and H. J. Karlin, Proc. IEEE **53**, 1788 (1965); W. Schneider and K. Seeger, Appl. Phys. Lett. **8**, 133 (1966); E. Dupont *et al.*, Phys. Rev. Lett. **74**, 3596 (1995); A. Hache, J. E. Sipe and H. M. van Driel, IEEE J. Quantum Electron. **34**, 1144 (1998); J. M. Fraser *et al.* Appl. Phys. Lett. **74**, 2014 (1999); M. Schiavoni et al., Phys. Rev. Lett. **90**, 094101 (2003); R. Gommers et al., Phys. Rev. Lett. **94**, 143001 (2005); R. Gommers, S. Denisov and F. Renzoni, Phys. Rev. Lett. **96**, 240604 (2006); R. Gommers, S. Bergamini and F. Renzoni, Phys. Rev. Lett. **95**, 073003 (2005).

[112] P. Reimann, Phys. Rep. **361**, 57 (2002).

[113] S. Flach, O. Yevtushenko and Y. Zolotaryuk, Phys. Rev. Lett. **84**, 2358 (2000); O. Yevtushenko *et al.*, Europhys. Lett. **54**, 141 (2001); E. Neumann and A. Pikovsky, Eur. Phys. J. B **26**, 219 (2002); S. Flach and S. Denisov, Acta Phys. Pol. B **35**, 1437 (2004).

[114] A. A. Ignatov, E. P. Dodin and V. I. Shashkin, Mod. Phys. Lett. B **5**, 1087 (1991).

[115] T. Hyart *et al.*, Int. J. Mod. Phys. B **23**, 4459 (2009).

[116] R. Scheuerer, *Domänendynamik in Halbleiter-Übergittern*, Dissertation, University of Regensburg (2002).

[117] J. A. Copeland, Proc. IEEE **54**, 1479 (1966); J. A. Copeland, J. Appl. Phys. **38**, 3096 (1967).

[118] J. Mattas, *Numerical simulations related to the electrical stability of superlattice amplifiers* (personal communication).

[119] A. Wacker and A.-P. Jauho, Phys. Rev. Lett. **80**, 369 (1998).

[120] T. Feil, C. Gerl and W. Wegscheider, Phys. Rev. B **73**, 125301 (2006); T. Feil *et al.*, Physica E **32**, 301 (2006).

[121] A. A. Ignatov *et al.*, Superlattices Microstruct. **22**, 15 (1997); A. A. Ignatov and A-.P. Jauho, J. Appl. Phys. **85**, 3643 (1999).

[122] Y. Shimada *et al.*, Phys. Rev. Lett. **90**, 046806 (2003); N. Sekine and K. Hirakawa, Phys. Rev. Lett. **94**, 057408 (2005).

[123] R. Ferreira *et al.*, Appl. Phys. Express **2**, 062101 (2009).

[124] A. Lisauskas *et al.*, Appl. Phys. Lett. **93**, 021122 (2008).

[125] P. Shiktorov *et al.*, Acta Phys. Pol. A **113**, 913 (2008).

[126] A. Zhang, D. Wang and M. M. Dignam, Appl. Phys. Lett. **86**, 171110 (2005); D. Wang *et al.*, Phys. Rev. B **77**, 115307 (2008).

[127] T. Kurosawa and S. Nagahashi, J. Phys. Soc. Jpn. **45**, 707 (1978); T. Feil *et al.*, Phys. Status Solidi C **1**, 2111 (2004).

[128] E. S. Daniel *et al.*, IEEE Trans. Electron Devices **50**, 2434 (2003); H. Xu *et al.*, Phys. Rev. B **79**, 245318 (2009).

[129] Yu. A. Romanov, L. G. Mourokh and N. J. M. Horing, J. Appl. Phys. **93**, 4696 (2003); G. M. Shmelev, I. I. Maglevanny and E. M. Epshtein, J. Phys. A: Math. Theor. **41**, 075002 (2008); M. L. Orlov, Yu. A. Romanov, and L. K. Orlov, Microelectron. J. **36**, 396 (2005).

[130] D. A. Ryndyk et al., Phys. Rev. B **67**, 033305 (2003).

[131] A. A. Andronov *et al.*, Semiconductors **37**, 360 (2003); A. A. Andronov *et al.*, Semiconductors **43**, 228 (2009).

[132] L. K. Orlov and Yu. A. Romanov, Sov. Phys. Solid State **19**, 421 (1977).

[133] This interesting connection was noticed by S. Winnerl (personal communication).

[134] R. Scheuerer *et al.*, Physica E **22**, 797 (2004).

[135] For details of numerical calculations, see J. Mattas, *On the Electrical Stability of Superlattice Amplifiers*, M. Sc. Thesis, University of Oulu, 2007. We used the Einstein relation for the diffusion coefficient and included a notch in the doping profile to ensure that sufficient fluctuations for the initiation of domain formation always exist. Similar notch was also used in reference: S. I. Domrachev and A. A. Kuznetsov, Tech. Phys. **44**, 544 (1999).

[136] A. Lisauskas *et al.*, Appl. Phys. Lett. **86**, 102103 (2005).

[137] H. Kroemer, International Solid-State Circuits Conference, Digest of Tehcnical Papers, Vol. III, 86 (1960); V. V. Migulin, *Basic Theory of Oscillations* (Mir, Moscow, 1983).

[138] A. V. Shorokhov and K. N. Alekseev, Int. J. Mod. Phys. B **23**, 4448 (2009).

[139] Eqs. (4.11)-(4.13) have been derived earlier using a so-called asymptotic saddle point method. See A. V. Shorokhov and K. N. Alekseev, Physica E **33**, 284 (2006).

[140] Yu. A. Romanov, J. Yu. Romanova, and L. G. Mourokh, J. Appl. Phys. **99**, 013707 (2006).

[141] J. M. Manley and H. E. Rowe, Proc. IRE **44**, 904 (1956).

[142] R. Tsu and L. Esaki, Appl. Phys. Lett. **19**, 246 (1971).

[143] V. V. Pavlovich and E. M. Epshtein, Sov. Phys. Solid State **18**, 863 (1976).

[144] V. V. Pavlovich, Sov. Phys. Solid State **19**, 54 (1977).

[145] Yu. A. Romanov, Radiophysics and Quantum Electronics **23**, 421 (1980).

[146] M. J. Feldman, P. T. Parrish and R. Y. Chiao, J. Appl. Phys. **46**, 4031 (1975); R. Movshovich *et al.*, Phys. Rev. Lett. **67**, 1411 (1991).

[147] L. K. Orlov and Yu. A. Romanov, Radiophysics and Quantum Electronics **23**, 942 (1980); L. K. Orlov and Yu. A. Romanov, Radiophysics and Quantum Electronics **25**, 413 (1982); L. K. Orlov and Yu. A. Romanov, Radiophysics and Quantum Electronics **25**, 506 (1982).

[148] J. Grenzer *et al.*, Ann. Phys. **4**, 265 (1995); E. Schomburg *et al.*, IEEE J. Selected Topics Quantum Electron. **2**, 724 (1996).

[149] S. Winnerl *et al.*, Appl. Phys. Lett. **77**, 1259 (2000).

[150] R. Scheuerer *et al.*, Appl. Phys. Lett. **82**, 2826 (2003); M. Haeussler *et al.*, Electron. Lett. **39**, 628 (2003).

[151] F. Klappenberger *et al.*, Eur. Phys. J. B **39**, 483 (2004).

[152] A. Rogl *et al.*, Int. J. Infrared Millim. Waves **29**, 906 (2008).

[153] V. M. Polyanovskii, Sov. Phys. Semicond. **14**, 718 (1980).

[154] D. Miller and B. Laikhtman, Phys. Rev. B **52**, 12191 (1995); A. B. Hummel *et al.*, J. Phys.: Condens. Matter **18**, 2487 (2006).

[155] Yu. A. Kosevich, Phys. Rev. B **63**, 205313 (2001).

[156] A. Sibille *et al.*, Europhys. Lett. **13**, 279 (1990); J. F. Palmier *et al.*, Semicond. Sci. Technol. **7**, B283 (1992); F. Aristone *et al.*, Physica B **184**, 246 (1993); H. J. Hutchinson *et al.*, J. Appl. Phys. **75**, 320 (1994); F. Aristone *et al.*, Solid-State Electron. **37**, 1015 (1994).

[157] M. Orlita *et al.*, Phys. Rev. B **74**, 125312 (2006).

[158] E. H. Cannon *et al.*, Phys. Rev. Lett. **85**, 1302 (2000); A. G. Balanov *et al.*, Phys. Rev. E **77**, 026209 (2008).

[159] For reviews, see Y. L. Ivanov, Opt. Quantum Electron. **23**, S253 (1991); E. Gornik, K. Unterrainer and C. Kremser, Opt. Quantum Electron. **23**, S267 (1991); A. A. Andronov, IEEE Trans. on Plasma Science **27**, 303 (1999).

[160] J. Mattas and T. Hyart, *Temperature dependencies of the cyclotron and Bloch gain obtained by numerically solving the Boltzmann equation.* The gain profile shown in Fig. 5.3 was calculated by removing a transient of 15τ from the beginning of the simulation, assuming that $f(\mathbf{k}, t)$ vanishes outside the range $-6 < k_y d/\sqrt{\mu} < 6$ and using step sizes $\delta k_x d = 0.02$, $\delta k_y d/\sqrt{\mu} = 0.02$ and $\delta t/\tau = 2 \cdot 10^{-4}$. The results shown in Figs. 5.4

(c) and (d) were obtained by removing transient of 10τ from the beginning of the simulation, assuming that $f(\mathbf{k}, t)$ vanishes outside the range $\{(k_y, k_z)| -5 < k_y d/\sqrt{\mu} < 5, -5 < k_z d/\sqrt{\mu} < 5\}$ and using step sizes $\delta k_x d = 0.05$, $\delta k_y d/\sqrt{\mu} = 0.05$, $\delta k_z d/\sqrt{\mu} = 0.05$ and $\delta t/\tau = 10^{-3}$.

[161] A. Patane and M. Fromhold, Phil. Trans. R. Soc. A **364**, 3477 (2006).

[162] S. P. Stapleton *et al.*, Physica D **199**, 166 (2004).

[163] T. M. Fromhold *et al.*, Acta Phys. Pol. A **109**, 43 (2006).

[164] D. Fowler *et al.*, Phys. Rev. B **76**, 245303 (2007).

[165] L. Canali *et al.*, Phys. Rev. Lett. **76**, 3618 (1996); L. Canali *et al.*, Superlattices Microstruct. **22**, 155 (1997).

[166] A. Patane *et al.*, Phys. Rev. Lett. **93**, 146801 (2004); D. Fowler *et al.*, Appl. Phys. Lett. **88**, 052111 (2006).

[167] R. S. Deacon, R. J. Nicholas and P. A. Shields, Phys. Rev. B **74**, 121306 (2006).